Agglomeration and Defluidisation Behaviour of High-Sodium, High-Sulphur South Australian Lignite under Fluidised Bed Gasification Conditions

Daniel Peter McCullough

Thesis submitted for the degree of

Doctorate of Philosophy

School of Chemical Engineering

The University of Adelaide

January 2007

CHAPTER 1

INTRODUCTION

1.1 Background

One of the most contentious and pressing concerns facing the world today is the issue of global warming. Accumulation of gases in the atmosphere due to man-made emissions, including CO_2, CH_4 and N_2O, are seen as the major cause of global warming. These gases act to trap heat produced from solar radiation within the earth's atmosphere, hence the term 'greenhouse gas'. Many industries in Australia are now investigating measures to reduce greenhouse gas emissions in anticipation of increasingly strict government regulations on emissions coming into effect in the future.

Electricity generation is a major contributor to greenhouse gas production in Australia, contributing approximately 50% of all energy-related emissions (at 1998; Trewin, 2001). The significant level of emissions from electricity generation is due largely to the reliance of the Australian electricity industry on coal combustion. Coal accounts for approximately 90% of the fuel used for electricity generation in Australia, of which approximately one third is brown coal, or lignite (Trewin, 2001).

Conventional coal combustion processes have inherently low thermal efficiencies, averaging 35% for black coal combustion and only 29% for lignite (Trewin, 2001). The low thermal efficiencies result in correspondingly high levels of greenhouse gas emissions,

at 0.93 t/MWh for black coal and 1.23 t/MWh for lignite (Trewin, 2001). Thus, significant reductions in greenhouse gas emissions in Australia can be achieved by addressing the emissions resulting from coal combustion processes, in particular those utilising lignite.

Significant lignite deposits exist in South-Eastern Australia. A number of brown coal deposits are contained in the Latrobe Valley in Victoria, supplying a low-cost, high-quality fuel source for use in the many pulverised fuel-fired combustion plants in the region. South Australia also contains a number of lignite deposits, although the typically high salt content of these coals renders them unsuitable for use in high temperature coal combustion processes. With the current exception of these low quality coal reserves, the lignite deposits in South-Eastern Australia are capable of providing a fuel source for many future generations.

Current trends indicate that peak demand of electricity in South-Eastern Australia will increasingly outstrip supply in years to come. In order to meet demand, expansion of lignite reserves is necessary. The continued use of conventional technology to achieve this expansion is hampered, however, by the aforementioned concerns over greenhouse gas emissions (McIntosh, 2000). Therefore, development of alternative technologies is required to make expansion of these coal supplies possible, while minimising adverse impacts on the environment.

Gasification is an alternative technology for cleaner, more efficient coal utilisation. Gasification typically involves reacting coal with steam and air/oxygen to form a gas rich in hydrogen and carbon monoxide. The gas produced can be used directly for electricity generation, or alternatively for purposes including hydrogen generation for fuel cells, supply of town gas, or as a reducing gas for chemical processing. Gasification also presents an opportunity for the use of lignite containing high salt and ash contents.

1.2 Fluidised Bed Gasification

Fluidised bed gasification possesses a number of advantages over conventional combustion technology. Gasification allows operation at significantly lower temperatures compared to

pulverised fuel combustion plants. Reducing operating temperature may improve fouling problems associated with low melting point ash. The Integrated Gasification Combined Cycle (IGCC) process offers significant thermal efficiency improvement over conventional technology with suitably prepared coal (e.g. drying to reduce the high moisture content of brown coal; Tomita and Ohtsuka, 2004). Fluidised bed technology also allows for more precise control over emissions, such as via addition of dolomite to the bed to control sulphurous gas emission.

Agglomeration and defluidisation are major inhibitors to the use of fluidised bed technology. Agglomeration is generally caused when bed temperature exceeds a critical temperature, sometimes referred to as the 'sintering point' (Siegell, 1984). Beyond the sintering point, bed particles enter a softened or sticky state. This reduces relative movement between particles and results in particle growth. Under worst-case conditions, the bed ceases to fluidise effectively, or 'defluidises'. Controlling agglomeration and defluidisation is thus critical for any commercial fluidised bed process.

In fluidised bed coal processes, agglomeration and defluidisation arises due to the reactions and transformations of inorganic components in the coal structure. Inorganic content of Victorian lignite deposits are low, and previous studies under combustion conditions (e.g. He, 1998; Vuthaluru, 1999b; Bhattacharya et al., 1999) have shown that agglomeration and defluidisation can be controlled when using such coal in fluidised bed environments. South Australian lignite on the other hand possesses high ash content, with high levels of sodium and sulphur. These species are known to form low melting point sodium-calcium-sulphur eutectics under combustion conditions, which create the sticky phase necessary for agglomeration to occur (Manzoori, 1990).

Only a limited number of studies have been performed to investigate the inorganic transformations of South Australian lignite under fluidised bed gasification conditions. One of the most extensive fundamental studies was performed by Kosminski (2001) to analyse the behaviour of sodium, silicon and aluminosilicate species when subjected to a gasification environment. It was shown that sodium bound to the organic coal structure decomposes to sodium carbonate, which in turn reacts with quartz to form sodium disilicate glass. This reaction is facilitated by steam, which lowers the melting point of

sodium carbonate below its typical melting point in air (i.e. 851°C). Sodium disilicate has a eutectic temperature of approximately 790°C (Kracek, 1939), sufficient to cause liquid phase formation in the ash under normal gasification conditions. Thus, sodium disilicate was identified as a key component likely to contribute to agglomeration and defluidisation during fluidised bed gasification of high sodium lignite.

The conclusions developed by Kosminski (2001) were based on experiments performed in a small-scale tubular furnace under intimately controlled conditions. Coal composition was also modified to assess the behaviour of specific interactions taking place within the coal matter, such as sodium chloride with quartz. The actual implications of these inorganic interactions on fluidised bed gasifier operation are yet to be fully investigated.

1.3 Scope and Structure of Thesis

The purpose of this investigation is to gain an improved understanding of the operational implications of inorganic transformations in South Australian lignite when subjected to a fluidised bed gasification environment. The desired outcomes of this study include:

- determination of the viability of fluidised bed gasification for utilisation of high-sodium, high-sulphur lignite; and
- development of control methods for minimising the problems of agglomeration and defluidisation.

Chapter 2 presents the literature review of current knowledge in the field. Characteristics of inorganic matter in low-rank coal are identified. Inorganic reactions and transformations under different reaction environments – oxidising, reducing, and pyrolysis – are investigated to identify possible ash components contributing to agglomeration. Mechanisms of agglomeration and defluidisation for a variety of different systems are also examined. The literature review suggests that agglomeration and defluidisation will impact on gasification of high-sodium lignite, and that operating parameters including air/fuel ratio, steam/air ratio, and bed temperature all contribute to agglomeration and defluidisation.

Chapter 3 presents details of the experimental program. The experimental apparatus used in the study – a spouted bed gasifier – is described. The properties of the studied coal – from the Lochiel coal deposit in South Australia – are presented, including preparation conducted prior to gasification. Experimental procedures are explained, as are the conditions for each set of experiments performed. Analytical methods used to examine experimental samples are presented, and the limitations of the experimental program are discussed.

Chapter 4 reports on the investigation into the physical mechanisms of agglomeration and defluidisation during fluidised bed gasification of Lochiel coal. Three sets of experiments are investigated, which span the extremes of gasifier operation, from 'low' steam, 'medium' steam, and 'high' steam gasification conditions. Process monitoring and visual observations are interpreted, and runs in which agglomeration and defluidisation occurred are distinguished from stable runs. A measure of extent of agglomeration is developed, and measured against relevant gasification operating parameters including bed temperature, superficial gas velocity, and air/fuel and steam/fuel ratios.

Chapter 5 presents the inorganic chemistry behind the occurrence of agglomeration and defluidisation. Samples are collected from each experiment, including bed char, cyclone dust, ash deposits and agglomerates, and subjected to elemental and mineralogical analysis to elucidate the reactions contributing to agglomeration. The chemical structure of agglomerates is also analysed to identify the critical species involved with agglomerate formation.

Chapter 6 presents Lochiel gasification tests conducted in the gasifier Process Development Unit (PDU) operated by the CRC for Clean Power from Lignite. The results arising from these tests are compared and contrasted with those from the spouted bed gasification experiments. This analysis allows conclusions to be derived regarding mechanisms of agglomeration and defluidisation during gasification of high-sodium, high-ash lignite.

Chapter 7 combines the results of Chapters 4, 5 and 6 to determine the mechanisms of agglomeration and defluidisation during gasification of lignite. The gasifier operating

conditions susceptible to agglomeration and defluidisation are identified, and possible control methods are suggested.

Chapter 8 summarises the implications for gasifier operation of results produced by the present study. Recommendations for future investigations into agglomeration and defluidisation during gasification of low-quality lignite are discussed.

CHAPTER 2

LITERATURE REVIEW

2.1 Introduction

The aim of the literature review presented in the following sections is to provide a critical assessment of existing knowledge in the field of fluidised bed gasification, in particular regarding the agglomeration and defluidisation behaviour of Australian lignite. This assessment will provide a basis for determining the direction of the current study. The following areas are to be addressed with this review:

- characteristics of low-rank coal, including identification of typical inorganic species;
- fluidisation and the gasification process;
- ash formation and inorganic matter transformations of low-rank coal; and
- mechanisms of agglomeration and defluidisation.

2.2 Lignite and Inorganic Matter

2.2.1 Introduction

Coal is a carbonaceous, heterogeneous product of organic and inorganic matter. Coal is formed via the process of ‘coalification’, which involves bodies of dead vegetation being naturally subjected to elevated pressure and temperature conditions over extended periods in the presence of water (Francis, 1961).

Organic matter, as the name implies, originates from the parent plant matter and other fungal and algal influences (Warne, 1982b). The organic matter in coal is the portion that enables its use as a fuel, and is composed of carbon, hydrogen, oxygen, nitrogen, and sulphur elements. Of these elements, carbon and oxygen form the majority of the coal structure, with hydrogen, sulphur and nitrogen comprising the remainder. Sulphur and nitrogen are typically only present in minor amounts in Victorian brown coal (Schafer, 1991), while sulphur is comparatively high in South Australian low-rank coal (ETSA, 1988).

Most of the oxygen in low-rank coal is present in carboxyl functional groups, and in phenolic hydroxyl groups to a lesser extent (CSIRO, 1971; Schafer, 1991). These functional groups are able to take part in ion exchange processes. Ion exchange involves displacement of hydrogen atoms with cations in carboxylate functional groups bound to the coal structure. These cations are referred to as 'organically bound' elements. Some of the carboxyl functional groups remain in carboxylic acid form (–COOH), resulting in an elevated acidity of lignite (Burns et al., 1962; Durie and Swaine, 1971).

Inorganic matter, also known as mineral matter, represents the impurities in coal. Inorganic matter is essentially any material not classified as organic (Gluskoter et al., 1981; Warne, 1982b). Compositions and modes of association of inorganic matter in coal are many and varied, and differ from coal to coal, even within the same seam (Brockway and Higgins, 1991). The inorganic matter portion of a coal significantly influences its use as a fuel, as it affects all aspects of the coal industry from mining to utilisation (Warne, 1982b).

Inorganic matter forms the 'ash content' of coal, and is the portion of material remaining following consumption of the organic material via combustion. Victorian brown coal possesses characteristically low ash contents, at 1 to 4%wt dry basis (d.b.) (Wibberley, 1982; Gloe and Holdgate, 1991). South Australian lignite typically contains high contents of ash, ranging from 10 to 35%wt d.b. (Wibberley, 1982; ETSA, 1988).

2.2.2 Classes of Inorganic Matter

Inorganic matter can be divided into two separate areas of classification: 'Inorganics,' and 'Minerals.' Each class of inorganic matter has a different mode of association with the coal structure, and hence behaves differently when the coal is heated.

Inorganics, also known as 'Inherent mineral matter,' describe the inorganic constituents originally associated with the vegetation from which the coal originated (Francis, 1961; Kiss and King, 1977, 1979; Wall et al., 1975; Warne, 1982b; Brockway et al., 1991). Inorganics are elements absorbed by plants during their growth, and include organically bound cations and elemental inclusions in the coal structure. Inorganics cannot be separated from the coal by physical means, and their relative compositions depend to a large extent on the type of plants contributing to the formation of the coal seam (Warne, 1982b). Inorganics comprise a significant percentage of the ash in lignite, exceeding 50% in some cases (Readett and Quast, 1987; Brockway et al., 1991; Gloe and Holdgate, 1991).

Minerals, also known as 'Adventitious mineral matter,' are mineral species that are present as discrete inclusions in the coal (Francis, 1961; Kiss and King, 1977, 1979; Wall et al., 1975; Warne, 1982b; Brockway et al., 1991). The mineral types associated with any particular coal depend largely on the environmental conditions under which the coal was formed. Mechanisms of mineral inclusion in coal include natural deposition over time, and contact of the coal seam with solutions containing dissolved salts (Warne, 1982b). Minerals can also enter the coal structure during the mining phase, which can include a variety of different materials, from overburden to parts of railway sleepers (Grant and Weymouth, 1962; Dixon et al., 1964). Minerals are not intimately associated with the coal structure, and can thus be separated from the coal by physical means (e.g. flotation). Minerals are the major form of inorganic matter present in black coal (Francis, 1961; Warne, 1982b; Readett and Quast, 1987; Brockway et al., 1991).

2.2.3 Inorganic Species in Lignite

2.2.3.1 Minerals

Table 2.1 summarises the typical mineral forms of major elements present in lignite. Silicon-based minerals contribute the majority of ash forming constituents in lignite. Quartz is the most predominant of these minerals in both Victorian and South Australian

lignite (Kemezys and Taylor, 1964; Durie and Swaine, 1971; Murray, 1973). Clays, or aluminosilicates, are also common in such lignite. The most notable clay inclusion is kaolinite, while others include montmorillonite, illite, chlorite, muscovite and biotite (Kemezys and Taylor, 1964; Durie and Swaine, 1971; Murray, 1973; Readett and Quast, 1987; Brockway et al., 1991). Other silicates that may be found in Australian coals are the feldspars, including plagioclase and orthoclase, which are generally found in clay-rich layers of seams (Kemezys and Taylor, 1964).

Table 2.1. Elemental Constituents in Coal Minerals (adapted from Thiessen, 1945).

Inorganic Constituent	Mineral Forms in Coal
Silicon	Quartz (sand), silicates
Aluminium	Clays (combined with silica)
Calcium	Lime, carbonate, sulphate, sulphide, silicates
Magnesium	Carbonate, silicates
Sodium and Potassium	Silicates, carbonate, chloride
Iron	Pyrite and marcasite (sulphides)
Sulphur	Sulphides, sulphates

Sulphur can be present in both organic and inorganic forms (Attar, 1978; Calkins, 1994). Inorganic sulphur is mostly present as sulphide minerals in freshly mined lignite, although South Australian coal does contain some of the sulphate mineral gypsum (Durie and Swaine, 1971; Readett and Quast, 1987). Of the sulphide minerals, pyrite and marcasite (two different crystalline forms of FeS_2) are the most abundant, with traces of sphalerite and galena also possible (Brown and Swaine, 1964; Kemezys and Taylor, 1964; Tsai, 1982). In both Victorian and South Australian lignite, marcasite tends to be the predominant sulphide present (Kemezys and Taylor, 1964; Durie and Swaine, 1971; Readett and Quast, 1987).

Carbonate minerals are not present in any significant amounts in as-mined Victorian and South Australian low-rank coal. The acidity of lignite due to carboxylic acid groups in the coal structure results in decomposition of carbonate minerals through ion exchange (Durie and Swaine, 1971). However, the carbonate mineral siderite has been shown to occur in sediments within some lignite seams (Kiss and King, 1977).

Traces of other minerals, in addition to those listed above, may be present in lignite, although are not present in quantities sufficient to significantly contribute to inorganic

interactions in the ash. Examples of the more common trace minerals include fluorapatite ($Ca_5(PO_4)_3(F,OH)$) and zircon ($ZrSiO_4$) (Kemezys and Taylor, 1964).

2.2.3.2 Inorganics

Organically bound inorganics in Victorian and South Australian lignite include calcium, magnesium, sodium, iron and aluminium (Durie, 1961; Burns et al., 1962; Brown and Swaine, 1964; Durie, 1971; Schafer, 1977; Readett and Quast, 1987; Brockway et al., 1991). In Victorian lignite, typically all of the calcium and magnesium, and most of the sodium, are in organically bound form (Brockway et al., 1991). South Australian lignite contains these organically bound inorganics, but also contains a significant proportion of water-soluble elements (Readett and Quast, 1987).

Water-soluble species are present as free ions in the inherent moisture of coal. The presence of these species is due to the saline environments under which the coals were formed (Readett and Quast, 1987). These species mainly include sodium and chlorine in Victorian and South Australian low-rank coal (Edgcombe, 1956; Durie, 1961; Hodges et al., 1983), although in Victorian coal are present only in small quantities (Brockway et al., 1991). South Australian coal also contains dissolved sulphate salts in the inherent moisture, which are combined as sodium, calcium and magnesium sulphates (Wall et al., 1975; Readett and Quast, 1987; Calkins, 1994).

2.3 Fluidised bed Gasification

2.3.1 Fluidisation Principles

A fluidised bed is a body of solid particles that attains a liquid-like state via an upward flow of fluid. This state is achieved as each particle in the bed is in a constant balance with gravity, buoyancy and drag forces (Gluckman et al., 1975; Basu, 1982; Manzoori, 1990; Kunii and Levenspiel, 1991). Other cohesive forces may also act in the bed, including van der Waals forces, liquid bridging, and sintering, depending on particle size and other process conditions (Seville et al., 2000).

Different fluidisation regimes exist, which depend primarily on the particle characteristics. Geldart (1973) showed that fluidisation behaviour differs depending on the density

difference between solid and gas, and the mean particle size. Four different particle classifications were developed, labelled from A to D, and are graphically presented in Figure 2.1.

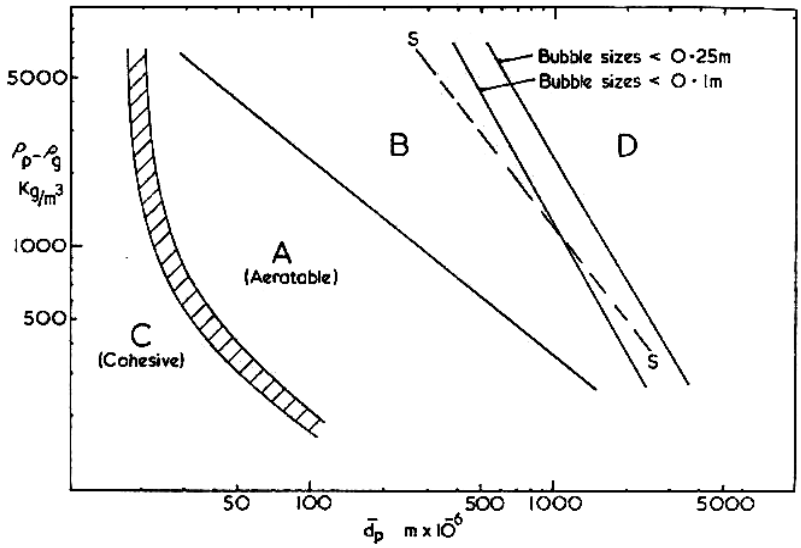

Figure 2.1. Powder classification diagram (Geldart et al., 1984).

Descriptions of the Geldart groups are summarised in Table 2.2. The most difficult to fluidise of the Geldart groups are from Group C, which are comprised of very fine particles (Geldart, 1973; Kunii and Levenspiel, 1991). The fine size of these particles enhances the magnitude of van der Waals forces, making them cohesive and inhibiting inter-particle movement (Geldart, 1973). Group A particles tend to fluidise easily, with a smooth expansion of the bed from minimum fluidisation to bubbling velocity (Geldart, 1973). Group B particles are the most common particle type, with bubbling observed at or slightly above minimum fluidisation (Geldart, 1973). Finally, Group D particles are the most coarse or dense particles, and show stable spouting behaviour (Geldart, 1973).

Coal is classified as a Group D particle owing to its typical particle size and density. In order to effectively fluidise coal, two main options are available. One option involves adding a Group B material such as silica to the bed to facilitate stable fluidisation and mixing in the bed. Another method is to utilise the stable spouting abilities of coal in a spouted bed reactor configuration.

Table 2.2. Geldart group classifications (Geldart, 1973; Kunii and Levenspiel, 1991).

Group	Description of Particles	Inherent Behaviour
A	Small mean size and/or low particle density e.g. catalysts	Considerable bed expansion before bubbling
B	Most materials in mean size and density ranges e.g. sand	Bubbling occurs at or slightly above minimum fluidisation velocity
C	Cohesive, or very fine powders e.g. flour, starch, face powder	Normal fluidisation extremely difficult – interparticle forces
D	Large and/or very dense particles e.g. gasifying coals	Deep beds difficult to fluidise – erratic behaviour

2.3.2 Spouted Bed Fluidisation

A schematic of a spouted bed reactor is shown in Figure 2.2. Two main regions of flow are present, which include the 'spout' and the 'annulus'. The spout involves an upward movement of particles in lean phase flow, and the annulus region involves downward movement of particles in relatively dense solids flow (Altwicker and Konduri, 1992). This creates a circulating motion of the particles, with particles exiting from the top of the bed through the spout and re-entering the spout at the bottom of the bed.

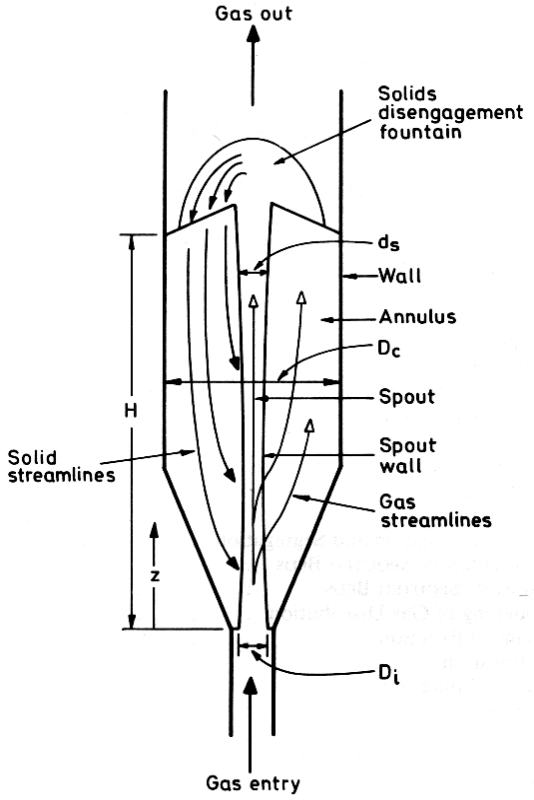

Figure 2.2. Schematic of a spouted bed indicating different phases of flow (Bridgwater, 1985).

Temperature distribution in a spouted bed is not uniform throughout the bed, as shown in Figure 2.3. In the spouted bed gasifier, the minimum temperature is located directly above the gas inlet. The maximum temperature is reached rapidly, and coincides with the location of the combustion flame. Bed temperature gradually decreases from the combustion zone towards the freeboard in the reactor. In comparison, the temperature profile of a bubbling bed is more uniform (Figure 2.3). While a uniform temperature distribution allows greater operational control to be achieved than compared to a bed with a highly variable temperature distribution, the spouted bed remains an appropriate choice for coal gasification owing to its fluidisation compatibility with pure char beds.

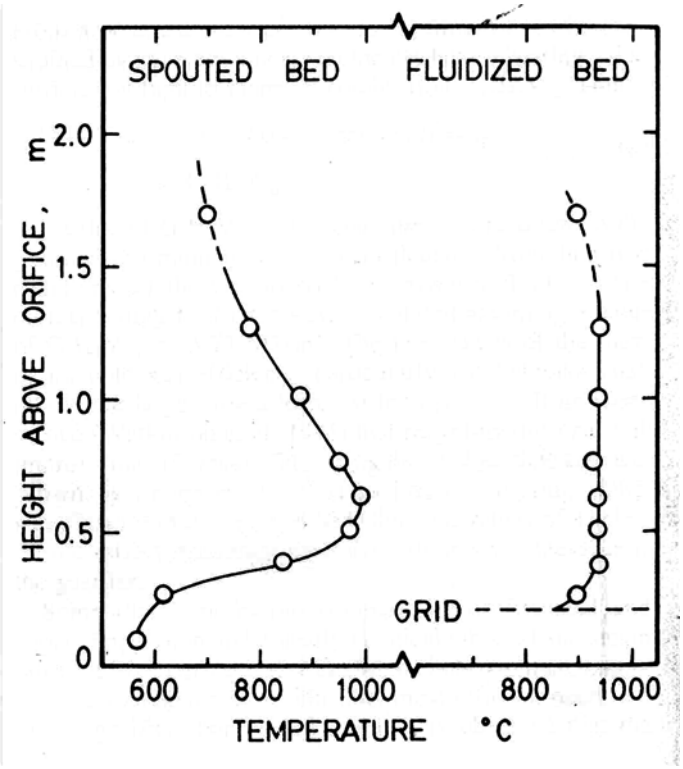

Figure 2.3. Comparison of axial temperature profiles of spouted and fluidised bed gasifiers (Watkinson et al., 1983).

2.3.3 Minimum Spouting Velocity

The minimum fluidisation velocity is the critical gas velocity that separates fixed bed and fluidised bed modes of operation. Below this velocity, the bed fails to fluidise effectively, if at all. For a spouted bed, the equivalent velocity is referred to as the minimum spouting velocity, and is the limiting velocity required for stable spouting to be achieved (Altwicker and Konduri, 1992).

Correlations exist for the calculation of minimum spouting velocity of a spouted bed. Equation 2.1 shows the formulae developed by Mathur and Gishler (1955), which has been successfully applied to much of the spouted bed data in the literature (Altwicker and Konduri, 1992). Minimum spouting velocity depends not only on particle diameter, and density difference between particle and fluid, but also on the weight of the bed.

$$U_{ms} = \left(\frac{d_p}{D_c}\right)\left(\frac{d_i}{D_c}\right)^{1/3}\left(\frac{\rho_p - \rho_f}{\rho_f}(2gH)\right)^{1/2} \tag{2.1}$$

where d_p = particle diameter;
d_i = inlet diameter;
D_c = cylindrical diameter;
ρ_p = particle density;
ρ_f = fluid density;
g = gravitational acceleration;
H = static bed height.

The correlation of Mathur and Gishler applies only to ambient conditions. As temperature increases from ambient conditions in a spouted bed, the minimum spouting velocity decreases due to the effect of viscous forces (Altwicker and Konduri, 1992; He, 1998). This decrease in minimum velocity with increasing temperature only applies up to a temperature that is dependent on the sintering characteristics of the bed particles. Particle sintering results in a linear rise of minimum spouting velocity with further temperature increase (Siegell, 1984; Manzoori, 1990; He, 1998).

Trends for variation of minimum spouting velocity with bed temperature are illustrated in Figure 2.4 (He, 1998). The minimum spouting velocity for a bed of silica sand is seen to decrease from approximately 24 cm/s at ambient conditions to 14 cm/s at 700°C. No increase in minimum spouting velocity is observed within this temperature range, with negligible silica sintering rate below 700°C. Sand coated in ash from Lochiel coal ('low-mineral' deposit) shows a minimum spouting velocity rise at approximately 560°C, while the minimum superficial velocity of sand coated in Bowmans ash shows a rise at approximately 490°C. He (1998) attributed the difference between the minimum particle sintering temperature of the two latter runs to a higher proportion of sodium in the Bowmans ash, which contained 15.0 wt% Na, compared to 9.6 wt% in low-mineral Lochiel ash. These trends clearly show the effect of particle coating composition on sintering behaviour.

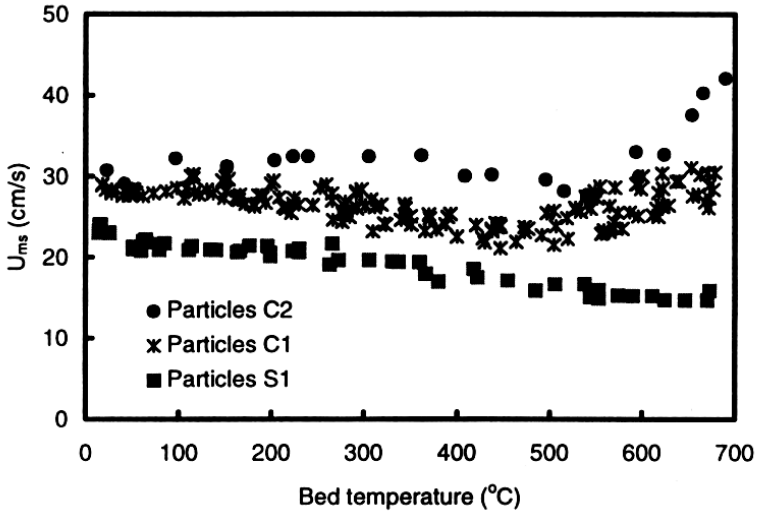

Figure 2.4. Variation of minimum spouting velocity with bed temperature (He 1998). Particles S1 = silica sand (0.85 – 1.0mm diameter, sphericity 0.72); C1 = silica sand coated with ash from South Australian Bowmans coal; C2 = silica sand coated with ash from South Australian Lochiel coal ('low-mineral' deposit).

Minimum spouting velocity can be measured experimentally by charging the bed with a known mass of particles, raising the velocity until the bed begins to spout, and then decreasing the velocity until the bed collapses (He, 1998; Vuthaluru, 1999c). The point at which the bed collapses is specified as the minimum spouting velocity.

2.3.4 Gasification

Gasification is the partial oxidation of a solid fuel, with the desired product from the process being a gas composed primarily of carbon monoxide and hydrogen (CSIRO, 1969; Ward, 1984). This gas can be used for a variety of different purposes in industry, for example as a fuel gas, a reducing agent, or a raw material for chemical synthesis (CSIRO, 1969). Table 2.3 gives the basic reactions involved in the gasification of coal. Two of the primary gasification reactions, namely the water-gas shift and Boudouard reactions, are endothermic, indicating that heat must be supplied for the reactions to occur. Steam and air is primarily used as the fluidising medium in fluidised bed gasification reactors. Combustion occurs at the gas inlet, supplying heat to drive the gasification reactions (Yang and Keairns, 2000). Thus, a gasifier bed is comprised of two different reaction regions: a combustion zone above the gas inlet, and a reducing zone occurring in the upper region of the bed.

Table 2.3. Coal gasification reactions (Peters, 1976).

Primary Reactions	**Equation**	**ΔH^o_{rxn} (kJ/mol)**
Water-gas reaction	$C_{solid} + H_2O_{steam} \rightarrow CO + H_2$	131.3
Boudouard reaction	$C_{solid} + CO_2 \rightarrow 2CO$	172.3
Partial combustion	$C_{solid} + 0.5O_2 \rightarrow CO$	-110.5
Hydrogasification	$C_{solid} + 2H_2 \rightarrow CH_4$	-74.9
Secondary Reactions	**Equation**	**ΔH^o_{rxn}**
Shift reaction	$CO + H_2O_{steam} \rightarrow H_2 + CO_2$	-41.0
Methanation	$3H_2 + CO \rightarrow CH_4 + H_2O_{steam}$	-206.2

2.3.5 Gasifier Process Control

Control of a fluidised bed gasifier is complicated by the presence of both combustion and gasification zones, along with the various reactions that they produce. An excess of air will result in a decrease of CO and H_2 yield owing to high levels of combustion. An oversupply of steam may also decrease the yield of CO via the shift reaction, but may also quench the bed and reduce the efficiency of the process. In addition to this, the amount of gas entering the reactor must be at a velocity sufficiently above the minimum fluidising velocity of the bed to ensure fluidisation proceeds effectively. Bed temperature has a major impact on gasifier operation, both in terms of reaction rate of the gasification process, and also on the behaviour of ash from the coal. The dependency of these variables on the other operating parameters in the gasifier highlight the difficulties associated with gasifier control.

In general, gasifier control is achieved by operating against ratios between coal feed, air, and steam rates. These ratios are ideally set to give optimum gas yield and process efficiency. The air/fuel mass ratio must be maintained below the stoichiometric level for complete combustion to occur, but be sufficient to generate heat for the endothermic gasification reactions to take place. Similarly, the steam/fuel ratio should be maintained so that the water-gas shift reaction may proceed with as much steam conversion from the fluidising gas as possible, particularly for an efficient gasification process (CSIRO, 1969).

A number of studies have been conducted into fluidised bed gasification of Western Canadian coal in spouted bed and fluidised bed reactors (Foong et al., 1980; Foong et al., 1981; Watkinson et al., 1983). The systems studied show that the optimum values of the aforementioned ratios, with respect to the gas yield and gas quality produced, were approximately 0.2 and 2 for steam/fuel and air/fuel ratios, respectively. The optimum

values of these ratios vary however, depending on the coal used and the reactor design (Watkinson et al., 1983). A summary of the various operating parameters used in the literature for various coal gasification systems is shown in Table 2.4.

Table 2.4. Literature values of typical gasifier operating parameters.

Literature	Gasifier type	Coal type	Coal size (mm)	Air/fuel (wt/wt)	Steam/fuel (wt/wt)
Foong et al. (1980)	Spouted bed	Bituminous, sub-bituminous	1.2-3.4	2	0.1-0.4
Foong et al. (1981)	Spouted bed	Bituminous, sub-bituminous	1.0-3.36	1.8	0.2
Watkinson et al. (1983)	Spouted and Bubbling bed	Bituminous, sub-bituminous & reject coal (55% ash)	1.19-3.36	2.56-3.54	0.13-0.49
Kikuchi et al. (1985)	Spouted bed	Bituminous	<3.0	Not specified	Not specified
Sue-A-Quan et al. (1995)	Spouted bed	Bituminous, sub-bituminous	1-3	2.0-5.2	0.19-0.84
Bhattacharya (1997)	Bubbling bed	Low-rank	Not specified	1.67 (1 bar) 2.36-3.86 (10 bar)	0.3 (1 bar) 0.7-1.9 (10 bar)
Lim et al. (2000)	Circulating fluidised bed	Low-rank	Not specified	2-2.5	<0.2
Overall range	-	-	<3.4	1.67-5.2	0.1-1.9

Ash formation presents separate issues for efficient gasifier operation. The bed must be operated at such a temperature to give sufficient gas output from the reactor, but also at a temperature that avoids severe agglomeration of the bed. This requires that the ash be in a suitable state to allow its removal from the reactor, but does not contribute to excess sintering of the ash (Jéquier et al., 1960; CSIRO, 1969).

Ash removal to avoid build-up in the bed has been carried out in some systems by utilising the agglomeration process to advantage. By allowing controlled agglomeration, ash particles grow in size and move towards the bottom of the bed. The agglomerates can then be removed at the distributor plate level (Jéquier et al., 1960; Yerushalmi et al., 1975; Schad and Hafke, 1983; U.S. Department of Energy, 1986; Kunii and Levenspiel, 1991). This process is known as the Godel phenomenon (Yerushalmi et al., 1975). Alternatively, agglomeration can be avoided altogether by operating the bed below the temperature at which the ash begins to soften or become molten, although this could have an adverse effect on the efficiency of the process (Yerushalmi et al., 1975). Operating at lower than optimum efficiency may be unavoidable in systems using high-sodium low-rank coal

however, as excessive liquid ash may potentially form even below optimum temperatures. Thus, knowledge of the behaviour of gasifier ash is critical in determining agglomeration and defluidisation control methods.

2.4 Ash Formation and Inorganic Transformations

2.4.1 Physical Ash Formation Mechanisms

A number of physical and chemical processes occur when coal enters the gasification environment. Heat causes any remaining surface or inherent moisture to evaporate. Dissolved salts subsequently crystallise throughout the coal structure. Devolatilisation occurs, as weaker chemical bonds between organic and inorganic species are broken. Transformations and interactions also occur between inorganic species, resulting in ash formation.

Inorganic matter is expressed from coal in a variety of different forms via the following mechanisms:

- liberation of mineral grains due to char fragmentation or exposure due to receding char surface (Benson et al., 1995);
- coalescence of inorganic matter inside char particles, which may accumulate and coalesce as molten droplets on the char surface (Loehden et al., 1989; Manzoori, 1990; Benson et al., 1995); and
- vaporisation of inorganic species (Benson et al., 1995).

Molten ash droplets forming on the char surface tend to become detached due to the low affinity of ash for char (Benson et al., 1995). The molten ash subsequently deposits on solid mineral particles or other surfaces within the reactor (Loehden et al., 1989).

Manzoori (1990) found that deposition of sulphate-rich ash onto silica bed material under combustion conditions causes particles to cohere, and hence initiates agglomeration. Under gasification conditions pure char beds are used, which may limit agglomeration caused by deposition. However, liberation of mineral grains from gasifier char may still provide sites onto which ash can deposit.

Gaseous environment type has a significant impact on the mode of ash formation. Manzoori (1990) showed that sulphate-rich ash coalesces only on the char surface under combustion conditions, with no evidence of sulphate formation within char grains. Kosminski (2001) subsequently found that silicate-rich ash forms evenly throughout the char grain when placed under gasification conditions, and that ash becomes exposed as the char surface recedes. The latter finding indicates that coalescence of inorganic matter throughout the char grain occurs regardless of gas environment, and that ash components react to form different species depending on the gas composition surrounding the char particles.

Ash forming evenly throughout the char grain has implications for agglomeration and defluidisation. Kosminski (2001) suggested that increasing carbon conversion of a gasifier would result in greater amounts of ash being released into the bed. With more ash available to deposit on other surfaces in the bed – including solid mineral particles – this would result in a greater potential for agglomeration and defluidisation to occur. Thus, the requirement to maximise carbon conversion, and hence efficiency, of a gasification reactor without effective ash removal may in fact increase the likelihood of agglomeration and defluidisation occurring.

2.4.2 Thermodynamic Equilibrium Calculations

Thermodynamic equilibrium calculations are a useful tool to predict the likely inorganic products forming in a given reaction system. Such calculations are based on minimising Gibbs' free energy of each component in the specified inorganic mixture, and allow the products and their state (i.e. solid, liquid or gas) to be predicted. Limitations of thermodynamic equilibrium calculations include the accuracy of the thermochemical data on which they are based, and the assumption that the system reaches equilibrium (Mojtahedi and Backman, 1989b). Despite these limitations, thermodynamic predictions can complement analysis of experimental work, enabling identification of species that may contribute to molten ash formation under certain conditions.

Thermodynamic equilibrium calculations can be performed with full specification of reaction system parameters, including:

- initial inorganic composition
- temperature

- pressure
- gas phase composition

The following sections summarise the compounds expected to form in lignite containing high sodium, chlorine and sulphur contents under a variety of different reaction environments.

2.4.2.1 Primary transformation products

Sodium carbonate (Na_2CO_3) is the preferred sodium form in systems of low sulphur content (Kosminski and Manzoori, 1990; Kosminski, 2000a). For steam gasification (excluding oxygen) of a high-sulphur coal, organically bound sodium forms solid sodium carbonate up to 750°C (Kosminski, 2000a). Between 750°C and 900°C, sodium carbonate is predicted to exist in liquid form, and above 900°C sodium hydroxide and metallic sodium are the preferred sodium forms (Kosminski and Manzoori, 1990; Kosminski, 2000a).

Organically bound calcium is predicted to form $CaCO_3$ at low temperature, and CaO above 800°C (Kosminski and Manzoori, 1990). Magnesium is also favoured to form MgO.

2.4.2.2 Sulphur-based reaction products

Sulphur reaction products differ greatly depending on the amount of sulphur initially present in the system, and whether the reaction environment contains oxygen. In an oxidising environment with high levels of sulphur, sodium and calcium sulphates are favoured to form. These products are predicted to form a liquid phase above 650°C (Kosminski and Manzoori, 1990). In a low oxygen system, sulphur is favoured to form sulphide species such as H_2S, FeS, CaS and Na_2S, although Na_2S is not experimentally detected in actual gasification systems (Kosminski, 2001).

Sulphur has a marked influence on calcium product formation, and is predicted to react preferentially with calcium where both sodium and calcium are present (Kosminski and Manzoori, 1990). Calcium sulphide, CaS, is the most stable form of calcium in a reducing environment (Kosminski and Manzoori, 1990).

2.4.2.3 Silica-based reaction products

Sodium is favoured to react with silica in the coal under reducing conditions (Kosminski and Manzoori, 1990; Kosminski, 2000a). The composition of silicates, as well as their states, is determined by the amount of silica specified in the starting system.

Low silica in the system (i.e. <1 wt%) results in organically bound sodium forming solid sodium silicates and aluminosilicates at all temperatures up to 1000°C, with some gaseous elemental sodium at higher temperatures (Kosminski and Manzoori, 1990; Kosminski, 2000a). No sodium disilicate ($Na_2Si_2O_5$) is formed in such a system, and no liquid phase is present.

Normal silica content in the system (i.e. 3.5 wt%) results in sodium silicate (Na_2SiO_3) and sodium disilicate forming the preferred constituents. At 750°C, sodium disilicate is predicted to be completely in liquid phase, and is the preferred component over sodium silicate up to approximately 900°C (Kosminski and Manzoori, 1990; Kosminski, 2001). Only above 900°C is sodium silicate predicted as the dominant sodium form of the two silicates.

High silica content in the system (i.e. 5 wt%) significantly increases the amount of liquid silicate phase present. At 750°C, less than 5% of the total sodium is present as a solid phase, with 70% present as liquid sodium disilicate. At 1000°C, the system is entirely liquid, with liquid sodium disilicate still the dominant phase at just under 70% total sodium in the system. Where aluminium is present from species such as clay, preferred compounds become solid albite ($NaAlSi_3O_8$) and nepheline ($NaAlSiO_4$) above 700°C, which remain in solid form up to 1000°C (Kosminski and Manzoori, 1990; Kosminski, 2001).

Sodium chloride is thermodynamically favoured over silicate and aluminosilicate compounds, melting at approximately 800°C and almost completely vaporising by approximately 900°C (Kosminski and Manzoori, 1990). However, sodium chloride formation is suppressed and sodium silicate formation is promoted under conditions where silicon content is much greater than chlorine content, or when steam is present in the reaction environment. Steam also increases the release of chlorine as gaseous HCl (Kosminski and Manzoori, 1990; Kosminski, 2001). Potassium competes with sodium to form KCl, which is present completely as a liquid phase above 700°C, forming a gas phase

above 1000°C (Kosminski and Manzoori, 1990; Kosminski, 2001). Potassium chloride is a more stable species than NaCl, and as such is thermodynamically favoured. Excess potassium in the system also results in the formation of K_2CO_3 and KOH.

2.4.2.4 Alkaline earth metals (Ca and Mg)

Even with the addition of silicon, both solid CaS and calcium silicates are predicted to form.

In a system of equimolar amounts of sodium, calcium and silicon, solid calcium and sodium silicates are favoured to form in competing reactions (Kosminski and Manzoori, 1990). At higher silicon contents, liquid sodium silicates form alongside both solid and liquid calcium silicates, indicating the presence of liquid sodium silicates reduces the melting point of calcium silicates (Kosminski and Manzoori, 1990). When magnesium is added to the mixture, liquid diopside ($CaMgSi_2O_6$) becomes the dominant silicate phase. Increasing the excess of calcium in the system results in less silicon being available for liquid sodium silicate formation, and instead solid merwinite ($Ca_3MgSi_2O_8$) is favoured to form, which is a more stable compound than sodium silicate (Kosminski and Manzoori, 1990).

Spinel ($MgAl_2O_4$) and MgO are the favoured magnesium species in a reducing environment. Spinel in particular is the most stable species when organically bound aluminium is present. If sufficient amounts of other elements are present, magnesium silicates and calcium magnesium silicates are also formed. $CaMgSi_2O_6$ is the most stable of these species, even more so than spinel and MgO (Kosminski and Manzoori, 1990; Kosminski, 2001). Forsterite (Mg_2SiO_4) may form when silica is present in the system, which is favoured to form a liquid phase above 950°C. If greater than stoichiometric amounts of silica are present, then $MgSiO_3$ also forms. This is in liquid form above 750°C. However, adding sodium to the system results in all magnesium being present in liquid silicate form above 950°C.

2.4.2.5 Iron

Iron is limited in the forms it may take in a reducing atmosphere. Iron sulphide (FeS) is the most stable of these species (Kosminski and Manzoori, 1990). However, sub-stoichiometric sulphur results in iron oxide formation. If excess chlorine is present in the

system, gaseous $FeCl_2$ forms. Limited reactions with silica may take place as well, with fayalite (Fe_2SiO_4) formed in a system containing silicon.

2.4.2.6 Aluminium

As mentioned previously, spinel is the most stable aluminium species that may form. In addition, sodium and calcium aluminosilicates are also favoured to form when aluminium is added to a system containing Ca, Na and Si. In cases where sodium and aluminium are present with low silicon contents, solid sodium aluminosilicates are favoured over liquid silicates in the temperature range 700° to 1000°C (Kosminski and Manzoori, 1990). This indicates that aluminium has an impact in reducing the formation of liquid phases within the ash, and hence may decrease the likelihood of agglomeration and defluidisation occurring within the bed.

2.4.2.7 Silicon

Silica (SiO_2) is the major species that results from the presence of silicon, in addition to the species discussed in the preceding sections. Silica forms a liquid phase in situations where other liquid silicates are in the system, or otherwise is present in solid form.

2.4.3 Chemical transformations of inorganic matter during gasification

Many studies have been conducted investigating the behaviour of various coal constituents under gasification conditions. The results of these studies are presented in the following sections, the reactions distinguished by inorganic-based and mineral-based transformations.

2.4.3.1 Inorganics-based transformations

Carbonates form from carboxylate groups (i.e. organically bound elements) in the coal structure. The carboxylate groups containing exchangeable cations decompose during heating between approximately 400°C and 600°C (Murray, 1973; Schafer, 1979a,b; Kosminski and Manzoori, 1990). Decomposition results initially in carbonate formation of the organically bound cations, which may then undergo further transformation depending on temperature and the metal cation (Murray, 1973). Calcium and magnesium carbonates form oxides of the respective elements, with carbon dioxide release, above 600°C. Sodium remains stable in carbonate form. Some volatilisation of sodium carbonate does occur at

temperatures above 600°C, although not to a significant extent (Murray, 1973). Organically bound iron decomposes to iron carbonate, which then reduces to iron oxides such as magnetite (Fe_3O_4), and possibly metallic iron and iron carbide (Murray, 1973; Attar, 1978). Iron oxide in the form FeO also can react further with sulphur to form iron sulphide under reducing conditions, which occurs below 1200°C (Attar, 1978).

Kosminski (2001) demonstrated in crucible furnace experiments that the melting point of sodium carbonate is decreased by addition of steam to the reaction environment. Pure sodium carbonate has a melting point of approximately 850°C in air, which is predicted to decrease to as low as 750°C in a steam atmosphere (Kosminski, 2001). This finding has important implications for a fluidised bed gasifier, as the steam in the fluidising gas may increase the agglomeration and defluidisation tendency of coal containing high sodium content. The results of Kosminski have yet to be confirmed in a fluidised bed environment.

Organically bound calcium and magnesium form sulphates of the respective elements in the presence of oxygen (Manzoori, 1990), as evidenced by the presence of water soluble forms of calcium and magnesium in ash from the combustion of South Australian lignite (Kosminski and Manzoori, 1990). Organically bound calcium forms mostly calcium sulphate by reaction with sulphur dioxide (Kosminski, 2001), with calcium only partially present in oxide form in the ash (Manzoori and Agarwal, 1992). Magnesium, on the other hand, predominantly forms an oxide, and only partially forms sulphate (Manzoori and Agarwal, 1992).

The dominant product of sodium in the presence of sulphur and oxygen is sodium sulphate (Manzoori, 1990; Manzoori and Agarwal, 1992). This species can be formed by reaction of sulphur dioxide with vaporised sodium in chloride or hydroxide form (see Equations 2.2 and 2.3) to form sodium sulphate (Halstead and Raask, 1969). The presence of calcium and magnesium sulphates in the inherent moisture of the coal can also be a source of sodium sulphate formation via the mechanisms shown in Equations 2.4 and 2.5 (Wall et al., 1975). During combustion of South Australian lignite, the formation of these sulphate species is observed to result in molten ash composed of sodium, calcium and magnesium, with solid species such as metal oxides, silica and aluminosilicates embedded in the matrix (Manzoori, 1990; Manzoori and Agarwal, 1992).

$$2NaCl_{(g)} + H_2O + SO_2 + 0.5O_2 \rightarrow Na_2SO_{4\,(g)} + 2HCl \quad (2.2)$$

$$2NaOH_{(g)} + SO_2 + 0.5O_2 \rightarrow Na_2SO_{4\,(g)} + H_2O \quad (2.3)$$

$$CaSO_4 + 2NaCl + H_2O \rightarrow Na_2SO_4 + 2HCl + CaO \quad (2.4)$$

$$MgSO_4 + 2NaCl + H_2O \rightarrow Na_2SO_4 + 2HCl + MgO \quad (2.5)$$

Calcium volatilisation, in the form of hydroxide, is found to occur at a significantly lower rate than organically bound sodium volatilisation (Mody et al., 2000). This is due to the respective valencies of the elements; the 2+ valency of calcium effectively implies that two bonds with the coal structure must be broken for calcium volatilisation to occur, in comparison to one bond for the 1+ valency of sodium (Mody et al., 2000). Pyrolysis experiments by Mody et al. (2000) show that organically bound sodium in sodium exchanged Victorian lignite begins to become volatilised above 500°C, the process approximately 70 to 80% complete at 900°C.

Sodium chloride undergoes significant volatilisation at temperatures above 600°C at a significantly greater rate than that of organically bound sodium (Murray, 1973; Mody et al., 2000). Sodium chloride vaporisation is minimally affected by reducing gas composition (Kosminski, 2000a), with much of the sodium species in the vapour phase existing in chloride form above 800°C (Kosminski, 2000a; Mody et al., 2000). Chlorine is released disproportionately from sodium during heating at almost double the rate of sodium (Brinsmead and Kear, 1956; Edgecombe, 1956; Kosminski and Manzoori, 1990; Manzoori, 1990; Mody and Li, 2000), indicating a mechanism other than direct volatilisation of sodium chloride is occurring (Brinsmead and Kear, 1956). One mechanism contributing to this dissociation of sodium and chlorine is a simple reaction between sodium chloride and hydrogen in the coal, as in Equation 2.6 (Brinsmead and Kear, 1956; Halstead and Raask, 1969).

$$NaCl_{(l)} + 0.5H_2 \rightarrow Na_{(g)} + HCl \quad (2.6)$$

Chlorine is predominantly released as HCl at temperatures around 200°C (Hodges et al., 1983). This is reflected by chlorine in ash from combustion reactors being present only in trace amounts (Kosminski and Manzoori, 1990; Vassilev et al., 2000), the remainder therefore released as volatiles. Kosminski (2001) suggests that approximately half of the

sodium present as sodium chloride undergoes direct vaporisation, while the remainder of sodium reacts with carboxylic acid groups attached to the coal structure to form sodium carbonate.

Addition of moisture to a system of silica and sodium chloride may lead to sodium silicate formation, as in Equation 2.7. Moisture also results in dissociation of sodium and chlorine with the formation of sodium hydroxide, as in Equation 2.8 (Brinsmead and Kear, 1956; Halstead and Raask, 1969). These reactions result in the majority of chlorine in the coal evolving as hydrogen chloride during heating (Hodges and Richards, 1989).

$$2NaCl_{(l)} + SiO_{2\,(s)} + H_2O \rightarrow Na_2SiO_{3\,(l)} + 2HCl \quad (2.7)$$

$$NaCl_{(g)} + H_2O \rightarrow NaOH_{(g)} + HCl \quad (2.8)$$

The effect of moisture on sodium reactions is significant. Brinsmead and Kear (1956) found that using humidified air to heat a sodium chloride-impregnated carbon particle resulted in a decrease in the rate of sodium evolution while increasing the rate of chlorine release when compared to results for dry air. Increasing reactor pressure also has the effect of decreasing sodium release from char due to the vapour pressure of sodium chloride increasing (Mojtahedi and Backman, 1989a,b; Kosminski and Manzoori, 1990; Mojtahedi et al., 1990). Morey and Ingerson (1938) also found that increasing steam pressure results in a lowering of sodium disilicate melting point temperature, decreasing by almost 150°C for a pressure increase of 2000 psig (approximately 140 bar).

Aside from HCl volatilisation in a gasifier, other forms of chloride in the gas include iron, calcium, magnesium and potassium chlorides (Kosminski and Manzoori, 1990). Deposits found at the gas cooler section of a High-Temperature Winkler gasification process by Kosminski and Manzoori (1990) were shown to contain significant amounts of ammonium chloride, with sodium, magnesium and calcium chlorides also being detected in smaller amounts. Readett and Quast (1987) obtained similar results from analysis of deposits from gasification tests using South Australian coal, finding that chlorides of sodium and ammonium were major mineral species present, with sulphur dioxide and various silicates also detected.

2.4.3.2 Mineral-based transformations

Silicon and Aluminium

Minerals present in the coal also undergo various reactions and transformation upon entering a fluidised bed environment. Table 2.5 shows the more significant transformation products obtained from decomposition of typical minerals in low-rank coal. Figure 2.5 summarises the transformations – both physical and chemical – undergone by inorganic matter as a coal particle is heated (Warne, 1982a).

Table 2.5. Inorganic transformations of common coal minerals in air (Warne, 1982a).

NOTE: This table is included on page 28 of the print copy of the thesis held in the University of Adelaide Library.

.

NOTE: This figure is included on page 28 of the print copy of the thesis held in the University of Adelaide Library

Figure 2.5. Mineral matter transformations during combustion (Warne, 1982a).

When coal enters the fluidised bed environment, clays first decompose, losing their water of hydration by 350°C (Murray, 1973; Warne, 1982a). Clays such as illite and montmorillonite decompose to aluminosilicates and water (Warne, 1982a), while kaolinite additionally has aluminates and silica as its decomposition products (Warne, 1982a). Equation 2.9 gives the basic mechanism for the dehydration of kaolin clay (Wall et al., 1975)

$$Al_2O_3 \cdot 2SiO_2 \cdot 2H_2O \rightarrow Al_2O_3 \cdot 2SiO_2 + 2H_2O \quad (2.9)$$

Decomposition of clay results in aluminosilicate formation, which can subsequently react with other metal compounds in the ash to form high melting point compounds (Wall et al., 1975; Kosminski, 2001). Wall et al. (1975) shows that the presence of kaolin clay results in a decrease, or even elimination, of molten ash formation due to reaction of sodium chloride with silica and aluminosilicate products from the clay. This reaction, as shown in Equation 2.10 (Wall et al., 1975), forms a high melting point sodium aluminosilicate, while also removing NaCl from taking part in further reactions such as forming sodium silicates and sulphates (Wall et al., 1975).

$$Al_2O_3 \cdot 2SiO_2 + 2NaCl + H_2O \rightarrow Na_2O \cdot Al_2O_3 \cdot 2SiO_2 + HCl \quad (2.10)$$

Quartz, or silica, is essentially unchanged during heating due to its high melting point (Murray, 1973; Warne, 1982a). It may react with other species however, such as with sodium to produce sodium silicates (Wall et al., 1975; Kosminski, 2001). Sodium compounds, including chloride and sulphate, react with silica to form sodium silicates, which can have melting temperatures as low as 635°C (Wall et al., 1975). Due to their relatively low melting points, sodium silicates can contribute to agglomeration in fluidised-bed combustors (Wall et al., 1975; Kosminski, 2001). Equations 2.11 and 2.12 show possible reactions that may take place between silica and sodium salts.

$$3SiO_2 + 2NaCl + H_2O \rightarrow Na_2O \cdot 3SiO_2 + 2HCl \quad (2.11)$$

$$3SiO_2 + Na_2SO_4 \rightarrow Na_2O \cdot 3SiO_2 + SO_2 + 0.5O_2 \quad (2.12)$$

Kosminski (2001) found that liquid sodium carbonate reacts with silica in a liquid-solid reaction to form sodium silicate compounds. These silicates then become liquid regardless of the gas atmosphere at a temperature of 850°C, or at a lower temperature when steam is present. Conversely, sodium chloride also reacts with silica, such as by the mechanism in Equation 2.11, yet occurs at a much lower rate of reaction than that of sodium carbonate. He therefore concluded that sodium chloride in the coal might actually react with the coal

structure to form sodium carbonate, which can then react with silica in subsequent reactions.

Kosminski and Manzoori (1990) demonstrated the occurrence of reactions between aluminium oxide and silicate compounds in South Australian lignite. Analysed ash samples from combustion experiments showed the formation of water and acid soluble silicon species occurred, implying sodium silicate formation (Kosminski and Manzoori, 1990; Poeze and Zhang, 2000). Acid soluble aluminium (i.e. in exchangeable cation form; Kosminski and Manzoori, 1990) was found to transform into acid insoluble form, confirming reactions between aluminium and silicates were taking place to form complex silicates and aluminosilicates (Kosminski and Manzoori, 1990).

Ash samples obtained by Kosminski and Manzoori (1990) from the High Temperature Winkler gasification of South Australian lignite were found to contain significant amounts of silica, sodium silicates and aluminosilicates, with minor amounts of calcium, magnesium and iron silicates. The sodium silicates in particular were found to be the predominate species in ash agglomerates, with imbedded particles of silica and aluminosilicates. Evidence of solid silica dissolving in the molten silicate mixture was also found, which ultimately adds to the amount of molten ash formed during gasification.

Kosminski (2001) performed experiments on modified Lochiel coal to examine the effect of gasification on silica and sodium transformations. It was found that two forms of silicate are formed from reaction with sodium carbonate from organically bound sodium. These silicate products include sodium metasilicate (Na_2SiO_3) and sodium disilicate ($Na_2Si_2O_5$). Equations 2.13 to 2.15 show the proposed mechanisms for their formation (Kosminski, 2001).

$$Na_2CO_3 + SiO_2 \rightarrow Na_2SiO_3 + CO_2 \quad (2.13)$$

$$Na_2SiO_3 + SiO_2 \rightarrow Na_2Si_2O_5 \quad (2.14)$$

$$Na_2CO_3 + 2SiO_2 \rightarrow Na_2Si_2O_5 + CO_2 \quad (2.15)$$

Kosminski (2001) found that sodium metasilicate is the initial silicate to form at 650°C, while sodium disilicate forms at higher temperatures. Sodium disilicate formation is also

promoted over sodium metasilicate in a steam atmosphere. Melting of disilicate was also found to occur within the operating temperature range of normal gasifier operation, which indicates this species may have an effect on agglomeration. In the same experiments, sodium chloride was also found to react extensively with kaolin clay, forming sodium aluminosilicates, although the melting temperature of these species was found to be higher than those of the silicates. Thus, the formation of silicates are more likely to contribute to agglomeration during fluidised-bed operation than aluminosilicates.

Another important finding by Kosminski (2001) is that solid silica was found to dissolve in the molten sodium silicate mixture, similar to the preceding findings by Kosminski and Manzoori (1990). Silica dissolving in the sodium disilicate phase results in an increase in the amount of liquid phase forming. Kracek (1939) developed a binary phase diagram of sodium and silicon mixtures, which shows that a sodium disilicate-quartz eutectic forms at a composition of approximately 74.2% SiO_2. This mixture possesses a eutectic temperature of 789°C, which is within the range of typical gasifier operating temperatures. This result is a significant finding by Kosminski (2001) for fluidised bed gasification of high-sodium lignite. With steam in the gas mixture, sodium carbonate may become liquid at lower temperatures than normal. Liquid sodium carbonate may then facilitate sodium-silicon reactions to form liquid sodium disilicate, which in turn may dissolve added quartz in the coal to increase melt phase formation (Kosminski, 2001). This mechanism may increase the severity of agglomeration and defluidisation behaviour of Australian lignite under fluidised bed gasification conditions, in comparison to fluidised bed combustion conditions. This mechanism also has yet to be tested in a fluidised bed environment.

With a molten sodium silicate phase formed, this phase can then react further with oxides of other elements, such as with CaO, to form more complex silicates (e.g. Wall et al., 1975). Equations 2.16 and 2.17 indicate some of the complex silicates possibly formed in a gasifier.

$$Na_2O.3SiO2 + 3SiO_2 + 3CaO \rightarrow Na_2O.3CaO.6SiO_2 \quad (2.16)$$

$$Na_2O.3SiO2 + 2CaO \rightarrow Na_2O.2CaO.3SiO_2 \quad (2.17)$$

Iron and Sulphur

Sulphur products resulting from the pyrolysis of coal, depend largely on the initial form of sulphur in the coal. During gasification, sulphur in the gas phase is composed mainly of H_2S, CS_2, CH_3SH and COS, with SO_x formation also possible in the presence of oxygen (Attar, 1978; Calkins, 1985; Hodges and Richards, 1989). Organic sulphur is oxidised directly to SO_2 by diffusion of oxygen into the coal particle (Halstead and Raask, 1969), as given by Equation 2.18. By the same mechanism, sulphur present in inorganic forms, such as in pyrite (FeS_2), transforms to sulphur dioxide after sulphur dissociates from the iron. This release of sulphur dioxide into an oxidising system leads to reactions with other inorganic components, such as sodium and calcium, to form sulphates (Halstead and Raask, 1969; Manzoori, 1990). However, sulphates are essentially absent from gasification coal ash due to H_2S being the dominant form of organic sulphur to form in a gasifier (Attar and Dupuis, 1981; Attar, 1985), with sulphide products being the main form of sulphur under these conditions (Benson et al., 1995; Vuthaluru et al., 1998).

$$0.5S_2 + O_2 \rightarrow SO_2 \qquad (2.18)$$

Anthony et al. (1989) investigated the solid wastes from a circulating fluidised bed combustor, sampling at various points in the reactor. It was found that the highest proportion of sulphides, primarily in the form of calcium sulphide, coincided with the largest amounts of unburnt carbon in the waste. The unburnt carbon present indicates that reducing conditions existed in certain parts of the process, which is particularly relevant to gasification. It also confirms that sulphides, rather than sulphates, are the most stable sulphur forms under reducing conditions.

Calkins (1985) conducted pyrolysis experiments on bituminous coal (containing 1.5% organic and 3.3% pyritic sulphur), and found that the major gaseous sulphur groups emitted from the coal during pyrolysis were H_2S, COS, SO_2, CS_2 and CH_3SH. Tests on the same coal with most of the pyrite removed gave similar results, except with SO_2 and CS_2 in negligible amounts. This indicates that inorganic sulphur is largely responsible for SO_2 and CS_2 sulphur compounds, while the organic sulphur is responsible for decomposition into the other sulphur gases.

Pyritic sulphur compounds, which include pyrite and marcasite, decompose under pyrolysis conditions to form FeS and sulphur. Murray (1973) reports that pyrite (FeS_2) loses half its sulphur in the temperature range 400 to 450°C in Victorian lignite during pyrolysis (i.e. to form FeS). The resultant FeS further loses its sulphur to form metallic iron or iron oxide (Halstead and Raask, 1969). However, Attar (1978) found that FeS is thermodynamically stable under pyrolysis conditions, and as such the further reduction of FeS is a much slower rate process than the initial reduction of FeS_2 (Attar, 1978).

The process of decomposition of pyrite compounds initially involves a transformation from FeS_2 to FeS with a loss of sulphur, (Halstead and Raask, 1969; Mason, 1992; Vuthaluru et al., 1998), as in Equation 2.19 (Halstead and Raask, 1969). This process has been shown to take place in 0.5 seconds at 1100°C (Halstead and Raask, 1969) and at even faster rates at higher temperatures (e.g. 20 milliseconds at 1500°C; Vuthaluru et al., 1998). A second stage of the process then occurs, as in Equation 2.20 (Halstead and Raask, 1969), which involves the further loss of sulphur from FeS to give metallic iron; compared to the initial stage, this is a relatively slower process (Halstead and Raask, 1969). Finally, the metallic iron oxidises to FeO, with Fe_2O_3 (Halstead and Raask, 1969; Warne, 1982a; Mason, 1992; Vuthaluru et al., 1998) and possibly Fe_3O_4 (Warne, 1982a; Kosminski, 2001) forming as final products, as in Equation 2.21 (Halstead and Raask, 1969).

$$FeS_{2\,(s)} \rightarrow FeS_{\,(s)} + 0.5S_{2\,(g)} \qquad (2.19)$$

$$FeS_{\,(l)} \rightarrow Fe + 0.5S_2 \qquad (2.20)$$

$$Fe + 0.5O_2 \rightarrow FeO \rightarrow Fe_2O_3 \text{ etc.} \qquad (2.21)$$

The presence of iron oxides during ash formation can lead to the formation of high melting point compounds with silica and sodium under oxidising conditions. Wall et al. (1975) gives the reaction between iron oxides and sodium silicate as in Equation 2.22, where the product formed, acmite, has a high melting point of approximately 955°C (Wall et al., 1975). This increase in melting point temperature from reaction of sodium silicate with iron oxide can contribute to a decrease in the potential for agglomeration to occur during fluidised-bed combustion of a coal with significant amounts of sodium present.

$$Fe_2O_3 + Na_2O_3{\cdot}3SiO_2 + SiO_2 \rightarrow Na_2O{\cdot}Fe_2O_3{\cdot}4SiO_2 \qquad (2.22)$$

Various studies relating to high rank coals have shown that the iron content of the eutectic system FeO/Fe_2O_3-Al_2O_3-SiO_2 is important in controlling the ash melting temperature under reducing conditions, with iron acting as a fluxing agent (Kolodney et al., 1976; Mason and Patel, 1980; Huffman et al., 1981; Federer and Lauf, 1985; Dawson and Brown, 1992). The fluxing behaviour of iron is related to iron valency, where Fe^{3+} acts to polymerise the ash matrix, whereas Fe^{2+} depolymerises the network (Varshneya, 1993); the reducing conditions of the gasifier reduce iron to Fe^{2+} form, where it then causes the ash to melt at lower temperatures compared to oxidising conditions. However, the presence of high amounts of sulphur leads to the formation of FeS, forming the FeO-FeS eutectic, which then has a larger influence on the melting point of the ash (Kolodney et al., 1976; Huffman et al., 1981). Kolodney et al. (1976) found evidence of FeS in ash agglomerates, confirming that FeS has an effect on ash melting temperature. This demonstrates the effect that the sulphur content of coals can potentially have on ash melting temperature, and so may significantly contribute to the agglomeration and deposition behaviour of a coal under gasification conditions.

It should be noted that the melting point of the Fe oxide-Al_2O_3-SiO_2 system is approximately 1400 to 1500°C (Huffman et al., 1981; Federer and Lauf, 1985), which is much higher than normal fluidised bed gasification operating temperatures. As such, this eutectic system alone would not be expected to affect agglomeration or deposition during gasification. However, experiments by Federer and Lauf (1985) showed that the addition of 37 wt% Na_2O to the ash matrix lowered its melting point temperature to approximately 850°C, indicating that reactions between sodium, silica and alumina can lead to the formation of low melting point mixtures.

Pyritic sulphur (pyrite and marcasite) is shown to react almost completely with hydrogen to produce H_2S, as in Equation 2.23 (Attar, 1978), which can further reduce to Fe and H_2S, as in Equation 2.24 (Attar, 1978). However, Equation 2.23 is the more significant of these two reactions, occurring at a rapid rate above 500°C (Attar, 1978). Equation 2.24 occurs much slower due to the stability of FeS under reducing conditions (Attar, 1978).

$$FeS_2 + H_2 \rightarrow FeS + H_2S \qquad (2.23)$$

$$FeS + H_2 \rightarrow Fe + H_2S \quad (2.24)$$

The H_2S formed can react with other vapour species to produce other sulphur volatiles (Attar, 1978), such as in Equations 2.25 and 2.26. The major sulphur species in the gas phase at temperatures above 800°C are therefore H_2S and CS_2, due to the secondary reaction of COS with H_2S after its formation (Attar, 1978). The hydrogen sulphide also reacts with metallic carbonates and oxides to form sulphides of the respective metals. This is true for iron and other divalent metal compounds such as those with calcium and magnesium (Attar, 1978), and the basic reaction mechanisms are shown in Equations 2.27 and 2.28, where M denotes any divalent metal ion.

$$H_2S + CO_2 \leftrightarrow COS + H_2O \quad (2.25)$$

$$H_2S + COS \rightarrow CS_2 + H_2O \quad (2.26)$$

$$MO + H_2S \rightarrow MS + H_2O \quad (2.27)$$

$$MCO_3 + H_2S \rightarrow MS + H_2O + CO_2 \quad (2.28)$$

2.5 Agglomeration and Defluidisation

2.5.1 Introduction

Agglomeration and defluidisation are related operational problems that have been identified in fluidised bed processes run at elevated temperature. Defluidisation is a condition caused by the minimum fluidising velocity increasing above the actual superficial velocity in the bed (Gluckman et al., 1975; Basu, 1982; Siegell, 1984). Agglomeration on the other hand is a result of sticky particles cohering to form a larger mass. Many authors attribute particle growth from agglomeration as the direct cause of defluidisation (Langston and Stephens, 1960; Siegell, 1984; Seville et al., 1998), while others have found defluidisation to occur as a result of interactions between sticky particles interrupting stable fluidisation, with large agglomerates forming once the bed has slumped (Gluckman et al., 1975; Basu, 1982; Manzoori, 1990). It is clear that the exact mechanisms of agglomeration and defluidisation are still not well understood.

2.5.2 Sintering

The basis for agglomeration of particles in a fluidised bed is the process known as 'sintering'. Sintering is a time-dependent process involving the transport of mass from a dense to a less dense area of a material, resulting in the formation of a neck between particles at their point of contact (Liss et al., 1983; Siegell, 1984; Seville et al., 2000). These inter-particle bonds facilitate material transport between adjacent particles, resulting in the formation of a single larger mass. The transport of mass for bond formation between particles is thought to occur through the action of four possible mechanisms in different proportions of influence (Kuczynski, 1949; Siegell, 1984; Marinov et al., 1992). These mechanisms include:

- surface diffusion;
- volume diffusion;
- viscous flow; and
- vaporisation.

Surface diffusion is the initial adhesion of solid particles through sufficient contact time under high temperatures. The motion of charged atoms in adjacent particles to the contact zone causes surface diffusion to progress. This type of sintering requires the lowest activation energy of all the sintering mechanisms (Siegell, 1984). Volume diffusion is an extension of surface diffusion, and is the merging of bonding particles into a single particle. Viscous flow, also known as liquid sintering (Siegell, 1984), involves the contribution of a liquid, or molten phase, especially as a coating on solid particles. In the case of adjacent coated particles in contact with one another, surface tension effects result in the flow of material between the coatings, resulting in bond formation (Smith, 1956; Siegell, 1984; Seville et al., 1998). Viscous flow is a more rapid process than diffusion sintering, as it involves the shifting of entire lattice planes to the bonding region between adjacent particles rather than movement of single atoms through the contact area (Siegell, 1984). Finally, vaporisation sintering is the action of differences in partial pressures causing the bonding of particles.

The sintering mechanisms have various levels of influence depending on the characteristics of the bonding material. For example, iron particles or other metallic material sinter mainly through the surface and volume diffusion mechanisms (Siegell, 1984; Mikami et al., 1996),

while glass beads sinter most rapidly under the viscous flow mechanism (Siegell, 1984; Seville et al., 1998). In the case of coal and other similar fuel types, viscous flow is the dominant contributor to sintering (Siegell, 1984; Manzoori, 1990; Ergudenler and Ghaly, 1993a,b; Mansaray and Ghaly, 1997; Natarajan et al., 1998), as the ash from coal is typically based on silicate glass chemistry. Other sintering mechanisms may also have an effect on agglomeration during fluidised bed coal processing, such as diffusion sintering between solid metallic species in the inorganic matter, which may result in sintering at temperatures lower than that required for liquid phase formation in the ash (Siegell, 1984). However, viscous flow is expected to be the main contributor to sintering during low-rank coal gasification, particularly with the formation of low melting point silicate mixtures.

Experiments conducted by He (1998) appeared to contradict the viscous flow assumption for sintering of low-rank coal ash. Ash samples from Australian lignite were placed in a laboratory-scale furnace and heated under combustion conditions, with samples from the furnace providing no evidence of sintering when subjected to temperatures similar to, and significantly above, those found under agglomerating fluidised-bed conditions. These results cannot necessarily be applied to the behaviour observed during actual fluidised-bed combustion however, as air would mainly interact only with ash particles on the surface of crucible, and the experiments also ignore the effect of char particle temperature, which may be significantly greater than temperatures actually measured in fluidised bed combustors.

As sintering is a time-dependent process, it will proceed most effectively in situations where sufficient time is available for mass transfer to occur between contacting particles without interruption to bond formation. Because of this time dependency, agglomeration is seen as a rate-dependent process, which is a balance between the rate of bond formation due to sintering and the rate of bond destruction due to particle collisions. In other words, agglomeration will proceed when the rate of cohesion of particles is greater than the rate of bond destruction, resulting in particle growth (Siegell, 1984; Manzoori, 1990; Seville et al., 1998). The growth of particles is undesirable, as it results in an increase in the minimum fluidisation velocity of the bed. When the minimum fluidisation velocity increases to a level above the operating fluidising velocity, defluidisation of the bed occurs (Manzoori, 1990; Siegell, 1984). Thus, in situations where velocity is close to the minimum fluidisation velocity, the relative particle momentum may be sufficiently low to allow

bonds to form between colliding particles. The same scenario applies to a reactor configuration such as a spouted bed, in which particles in the annulus region around the spout are in continuous contact for as long as they remain in the annulus, providing good opportunity for bond formation.

2.5.2.1 Initial Sintering Temperature

In a fluidised bed, the minimum fluidising velocity maintains a relatively constant value (decreasing by a minor amount) as bed temperature increases until a characteristic temperature is reached (He, 1998). This characteristic temperature is known as the 'Initial sintering temperature', which is defined as the temperature beyond which the minimum fluidisation velocity begins to increase sharply with increasing temperature (Basu, 1982; Basu and Sarka, 1983; Siegell, 1984), as shown in Figure 2.6. This sharp increase is known as the 'High-temperature defluidisation limit', and the velocity in the bed must be maintained above this level to avoid bed defluidisation (Gluckman et al., 1975; Basu, 1982; Siegell, 1984).

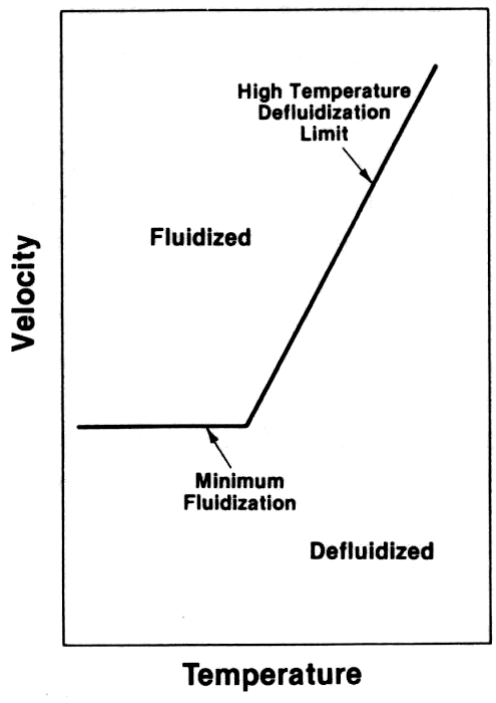

Figure 2.6. Typical minimum fluidisation limit for high temperature operation of a fluidised bed (Siegell, 1984).

In effect, the initial sintering temperature is the point at which sintering begins to affect fluidisation in a fluidised bed reactor due to excessive sintering taking place in the bed.

While defluidisation results by falling below this operating limit, it has been shown to be a reversible process. Fluidisation has been shown to recommence from a defluidised state by increasing the fluidisation velocity or decreasing the temperature (Gluckman et al., 1975; Basu, 1982), although the use of South Australian lignite under combustion conditions has yielded cases where defluidisation could not be resumed at all after defluidisation (Manzoori, 1990; He, 1998).

Measurement of the initial sintering temperature has been attempted using a number of different methods and techniques. The ASTM method (ASTM, 1994) is the standard method for measuring coal ash fusibility, the point at which the ash begins to soften. The technique involves creating a small triangular ash cone, placing it in a furnace, and visually observing its melting behaviour with increasing temperature. The characteristic temperature points include the initial deformation temperature (IT), softening temperature (ST), hemispherical temperature (HT), and fluid temperature (FT), and are demonstrated in Figure 2.7. While the initial deformation temperature is defined to measure the onset of sintering, the objective nature of the test has lead numerous authors to find that the test is unsuitable for determination of the initial sintering point of coal ash (e.g. Barnhart and Williams, 1956; Stallmann and Neavel, 1980; Natarajan et al., 1998; He, 1999), and is found to over-predict the initial sintering point by as much as 400^{o}C.

NOTE: This figure is included on page 39 of the print copy of the thesis held in the University of Adelaide Library.

Figure 2.7. The ASTM ash fusion prediction method (ASTM, 1994).

Another method of measuring the onset of sintering of coal ash is by using a dilatometer technique (Smith, 1956; Basu and Sarka, 1983; Siegell, 1984). This technique measures the expansion and contraction of a coal ash sample as temperature is increased, and operates on the principle that thermal expansion causes the size of the sample to increase and sintering causes the particles to flow together and decrease the sample size. The point at which expansion equals contraction is deemed to be the initial sintering point (Smith,

1956). The initial sintering temperatures obtained by this method correspond well with the onset of defluidisation in actual fluidised bed operations (Smith, 1956; Basu and Sarka, 1983; Siegell, 1984). A dilatometer curve is constructed from the technique, an example shown in Figure 2.8.

NOTE: This figure is included on page 40 of the print copy of the thesis held in the University of Adelaide Library.

Figure 2.8. Typical dilatometer curves – copper shot in oxidising atmosphere (Gluckman et al., 1975).

He (1999) investigated a similar technique for initial sintering temperature measurement, using thermo-mechanical analysis (TMA) to measure the expansion and contraction of ash samples. This technique involves heating a small sample of ash in an equipment that is able to measure small changes in sample height as it is heated, allowing data to be logged directly to a computer file. This method is more accurate than the dilatometer method due to the greater sensitivity afforded by TMA technology.

The initial sintering temperature of coal ash may also be determined by measuring the compressive strength of specially prepared ash pellets (Barnhart and Williams, 1956; Hupa et al., 1989). This technique operates on the principle that the compressive strength of ash increases with temperature until the sintering point is reached, where the strength then begins to decrease. This method was shown to be suitable for observing the change in sintering behaviour with chemical composition of fly ash (Hupa et al., 1989).

Stallmann and Neavel (1980) define an alternate method of measuring the sintering temperature of coal ash. The technique involves sieving coal ash particles to a uniform size of 100 mesh (0.149 mm), placing samples in platinum crucibles and heating at various temperatures. The resulting samples are then sieved again to 100 mesh in order to collect

any agglomerates formed. The percentages of agglomerates formed are then plotted against temperature in order to show the severity of agglomeration occurring with temperature. The point at which the resultant curve touches the temperature axis is defined as the initial sintering point. This method has several drawbacks however, such as inaccuracies introduced with the breakage of agglomerates upon sieving.

2.5.3 Agglomeration and Defluidisation Mechanisms

Various authors have examined the mechanisms of agglomeration during fluidised bed processing of various fuels including coal, peat and biomass (Langston and Stephens, 1960; Gluckman et al., 1975; Yerushalmi et al., 1975; Siegell, 1984; Manzoori, 1990; Ergudenler and Ghaly, 1993a,b; Mansaray and Ghaly, 1997; Natarajan et al., 1998). These processes generally involve the use of inert bed material such as silica sand to aid in fluidisation and heat transfer. The following mechanism applies to agglomeration processes that make use of inert bed material:

- Inorganic transformations result in the formation of eutectic compositions inside char particles as they are heated.
- The eutectic mixture becomes molten as the temperature reaches its melting point, and forms a molten ash coating on the surface of the char particles.
- Collisions between inert bed material and char particles result in the transfer of molten ash from the char to the bed material due to a greater affinity of the ash for the bed material (Benson et al., 1995).
- Collisions between coated bed particles result in the formation of bonds between particles, as viscous and surface tension effects cause the molten ash to flow.

Yerushalmi et al. (1975) and Kolodney et al. (1976) investigated the gasification of high rank coal (i.e. bituminous and anthracite) in beds of pure coal, finding a similar agglomeration mechanism to the one involving inert bed material. However, as there are no bed particles for deposition to occur on, the mechanism involves molten ash becoming detached from the coke particle surface and merging with other ash particles. Continued merging of ash results in particle growth, and hence agglomeration proceeds. This process is termed ‘the Godel phenomenon’ (Yerushalmi et al., 1975). As the agglomerates continue to grow, they eventually move towards the bottom of the bed, and provisions can be made in the reactor to allow the heavy agglomerates to fall out of the bed into an ash collector.

In this case agglomeration is actually advantageous to the process, as it enables bed ash content to be controlled, thus avoiding defluidisation caused by agglomeration.

Defluidisation is defined as loss in quality of fluidisation during fluidised-bed operation (McLaughlin, 1999). It can result in bed behaviour from decreased fluidised activity, to a complete loss of fluidisation with channelling through the bed (Gluckman et al., 1975; Basu, 1982; Siegell, 1984; Manzoori, 1990; He, 1998; McLaughlin, 1999). It has been shown to be both an instantaneous process, where a sharp change of state from fluidised to defluidised occurs (Basu, 1982; Siegell, 1984; Manzoori, 1990), and a gradual process, where it occurs over a longer period of time before eventually defluidising (Gransden et al., 1970; He, 1998). It is apparent therefore that defluidisation is not a well-understood phenomenon.

Although particle growth via agglomeration has the potential to result in defluidisation if not managed correctly, agglomeration is not necessarily a requirement for defluidisation to occur. Defluidisation of fluidised beds has been found to occur in instances with no noticeable signs of agglomeration (Gransden et al., 1970; Manzoori, 1990; He, 1998). Thus, the cohesive interactions occurring between particles may only need to be sufficiently large to alter the force balance on fluidised particles and cause defluidisation (Manzoori, 1990).

Gransden et al. (1970) found that the reduction of iron ore pellets in high temperature fluidisation resulted in ‘nodules’ of iron compounds accumulating on the surface of particles. As defluidisation was only found to occur when nodules were present, it was concluded that they were the cause of defluidisation. While agglomerates were not observed to form in beds, the nodules were sufficient to create adhesive surfaces that could inhibit particle movement, thereby upsetting the balance of forces in the bed.

Siegell (1984) conducted fluidisation tests on particles under high temperatures, and observed the defluidisation process using high-speed photography. At a constant gas velocity the bed temperature was increased, and observations of the fluidisation characteristics were recorded. As the temperature was increased towards the defluidisation limit, particles were seen to collide with each other and cohere, while agglomerates were broken by collision with other particles and agglomerates. Increasing the temperature was

found to increase the size and rate of agglomerates formed, which was attributed to the rate of sintering being increased. When the temperature was increased above the high temperature limit, the bed began to decrease in activity, and "seemed as if it now had to overcome some sort of heavy weight which was placed on top of it" (Siegell, 1984). At the point of defluidisation, the bed collapsed and the fluidising gas began to channel through the bed. The occurrence of defluidisation in this instance was extremely fast, taking place within seconds, while agglomerates were only detected in the bed at temperatures immediately below the high temperature defluidisation limit. In this case, the process of defluidisation was practically instantaneous.

As mentioned in preceding sections, the process of defluidisation is reversible under certain conditions. Gluckman et al. (1975) reported on agglomeration and defluidisation problems in a fluidised bed iron ore reduction process. It was found that for any particular bed temperature, there existed a point where the bed would slump into a defluidised state. It was found that the bed could be re-fluidised again by increasing the fluidisation velocity if not left in the slumped state for an extended period of time. If the bed remained defluidised for too long, sintering progressed to such an extent that the bonds would not break even when exposed to high velocities. Other authors (e.g. Basu, 1982; Siegell, 1984) obtained similar results in coal combustion processes. Further results by Gransden et al. (1970) showed that the static bed height of a defluidised bed was greater than that of the original bed. By increasing the fluidisation velocity, the bed could only be re-fluidised for a short period of time before defluidising again, with an even greater static bed height than before. This was thought to indicate that the defluidised bed had a greater voidage than could be overcome by the fluidising velocity, and further re-fluidisation only served to increase the voidage until defluidisation occurred again.

He (1998) observed two different types of defluidisation when conducting spouted bed combustion experiments under constant temperature conditions with South Australian lignites. He termed these defluidisation types 'partial' and 'total' defluidisation. In using low-mineral Lochiel coal, partial defluidisation was observed, characterised by a gradual loss in pressure drop across the bed over time before stabilising at a constant value. This behaviour can be seen in Figure 2.9. Tests with Bowmans and high-mineral Lochiel coal exhibited total defluidisation behaviour, as in Figure 2.10, where again the pressure drop gradually decreased with time, but was accompanied by a sudden loss of pressure drop and

defluidisation after a certain amount of time. In this case, the bed could not be re-fluidised, even after only being in the slumped position for a short period of time, due to the particles adhering to the wall surrounding the gas inlet. As such, the gas could only pass up the centre of the bed, and was unable to agitate any of the particles to re-fluidise the bed. As this differs from the general assumption that a bed can be re-fluidised if brought above the high temperature defluidisation limit, this shows the effect that bed hydrodynamics can have on defluidisation behaviour.

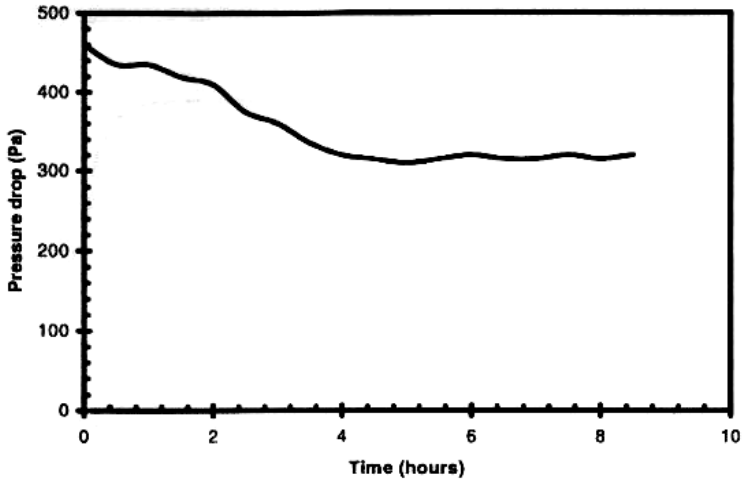

Figure 2.9. Partial defluidisation during FBC with low-mineral Lochiel coal (He, 1998).

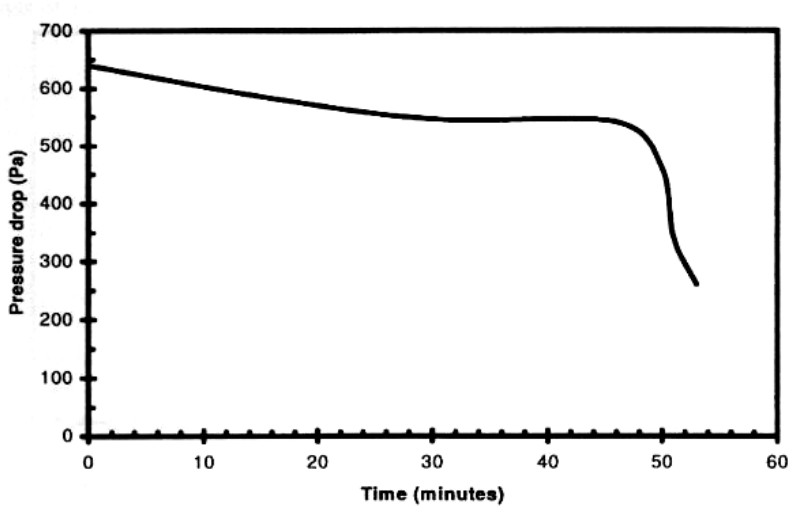

Figure 2.10. Total defluidisation during FBC with Lochiel and Bowmans coal (He, 1998).

Defluidisation has been shown to occur because of a change in Geldart group behaviour owing to the formation of a liquid phase. McLaughlin (1999) conducted cold experimental modelling studies to examine the effect of liquid on fluidisation behaviour of particles. The controlled addition of liquid to a fluidised bed of non-porous, spherical particles was found to change the behaviour of the fluidised-bed in terms of the Geldart classification system. The particles, in the initial dry state, were found to exhibit Geldart B behaviour, with the addition of a liquid phase causing the transition to group A behaviour. Increasing the proportion of liquid in the bed eventually lead to the observation of group C behaviour, while increasing the viscosity or surface tension of the liquids used was found to enhance these transitions. This effect was attributed to an increase in the magnitude of interparticle forces present in the bed resulting from liquid bonds forming between particles. This was dependent on the surface tension and viscosity of the liquid used. The transitions between Geldart classifications were found to be enhanced using liquids of higher viscosities and surface tensions. This effect has important implications in the gasification of coal, as the presence of molten ash in a bed will change particle behaviour as well as causing bonding and forming agglomerates.

Stable fluidisation, and hence defluidisation, can be detected during fluidised bed operation by monitoring the total pressure drop across the bed and the bulk bed temperature (Gluckman et al., 1975; Siegell, 1984; Atakul and Ekinci, 1989; Manzoori, 1990). A loss of pressure drop across the bed indicates defluidisation behaviour has commenced due to the gas forming channels through the bed, leading to uninhibited gas flow. A rapid rise in bed bulk temperature also indicates the occurrence of defluidisation, due to a combination of a more closely packed bed and the creation of hot spots in the slumped bed. Figure 2.11 shows a typical temperature and pressure profile of a defluidising bed. Note that the pressure drop fluctuations change from a regular pattern to a more erratic one as the point of defluidisation is reached.

NOTE: This figure is included on page 46 of the print copy of the thesis held in the University of Adelaide Library.

Figure 2.11. Pressure drop and temperature profiles of an agglomerating fluidised-bed (Gluckman et al., 1975).

While the above investigations examine the agglomeration response in gasifying and combusting various different fuels, very little work has been carried out on agglomeration and defluidisation under fluidised bed gasification of high-sodium, high-sulphur low-rank coal. Kosminski and Manzoori (1990) collected ash from the bottom of a High Temperature Winkler gasifier in which South Australian lignite was gasified, and found that a significant proportion of the ash was present as ash agglomerates up to 6 cm in diameter. Examination of the agglomerates found that they consisted of a molten glassy silicate phase containing sodium, with embedded silica and aluminosilicate particles from the coal in the silicate phase. This indicates that a liquid silicate phase is forming in the bed during gasification and resulting in agglomeration of the inorganic matter in the coal via viscous flow sintering. However, aside from this work there has been no extensive investigation into agglomeration of low-rank coal under gasification conditions. Thus, agglomeration and defluidisation must be evaluated for such a system in order to determine the likelihood of future use of such fuel for electricity generation.

2.5.4 Operational Factors Affecting Agglomeration and Defluidisation

The operational methods used to control fluidised-bed combustion and gasification processes can significantly influence the fluidisation behaviour of a bed, particularly the agglomeration propensity of the fuel used. Successful operation of a large-scale fluidised bed therefore requires the balancing of a number of different factors, which can be achieved by an extensive mapping of principal operating conditions (Matsen, 1996).

Temperature and Fluidising Velocity

The combined effects of bed temperature and fluidising velocity have been shown by many researchers to have the greatest impact on agglomeration tendencies of fluidised bed particles (Kuczynski, 1949; Mason and Patel, 1980; Siegell, 1984; Manzoori, 1990; Ergudenler and Ghaly, 1993a,b). Temperature determines whether the material being fluidised is above its initial sintering temperature, as well as determining the rate of bond formation between particles due to sintering. Fluidisation velocity, on the other hand, determines whether the particles have sufficient momentum to break bonds that have formed in agglomerates, so that the bed can remain in a fluidised state. The relationship between temperature and velocity has been discussed in preceding sections, and is shown by the high temperature defluidisation limit in Figure 2.6.

Bed Composition

The ash content and particle coating thickness are related, in that the more ash that is present in the bed, the thicker the coatings on bed material and other solid particles in the bed. As molten ash is considered the main cause of viscous flow sintering in fluidised bed operations (e.g. Siegell, 1984; Manzoori, 1990), then obviously the greater the ash content of the bed, the higher the propensity for agglomeration.

Langston and Stephens (1960) investigated agglomeration of iron in a fluidised-bed iron ore reduction process. It was found that agglomerate size formation could be controlled by controlling bed temperature, fluidising gas velocity, and particle size; the temperature controls the adhesiveness of particle surfaces, fluidising velocity controls the particle momentum (and hence bond formation and breakage) while the particle size controls the area available for particle contact, as well as the velocity range that can be used to maintain fluidisation.

For agglomeration or defluidisation to occur, Manzoori (1990) and Manzoori and Agarwal (1994) concluded that the system temperature has to exceed the sintering temperature of the bed particle coating, and a minimum coating thickness must be deposited on the bed material. This indicates the existence of a critical molten ash content of the bed, below which agglomeration will not occur (Manzoori, 1990; Manzoori and Agarwal, 1994). Apte and Fein (1981) support this view, finding that the extent of agglomeration is proportional

to the amount of molten ash formed in the system. They also found that the rate of heating of the bed affects agglomeration. It was found that by influencing the rate of heating, the formation of molten phase could be controlled, and hence agglomeration could be avoided.

Hsieh and Roberts (1985) studied agglomeration propensities of low-rank American coals, and found the level of carbon conversion during gasification had a significant effect on agglomeration. Agglomeration was found to only occur above approximately 80% conversion, where the percentage of ash agglomerates existing tends to increase linearly to 100% carbon conversion. At 100% conversion, pure ash was essentially present, and the bed was fully agglomerated. This indicates that the concentration of ash in the bed at any one time has a substantial impact on the agglomeration behaviour of a coal in a gasifier. The presence of inert bed material or other additives could therefore actually aid in reducing defluidisation caused by agglomeration by diluting the ash content of the bed (Hsieh and Roberts, 1985).

Vuthaluru (1999a) investigated the effect of temperature on agglomeration in fluidised bed combustion, and found that it had a significant influence on the distribution of inorganics throughout the system. It was found that the proportion of low melting point compounds in bed particle coatings increased with increasing temperature, thereby decreasing the critical coating thickness and increasing the agglomeration propensity.

Coal composition is an important factor in the agglomeration and deposition behaviour occurring within a fluidised-bed gasifier. Vuthaluru (1999a) found that, under combustion conditions, the ash coatings on bed materials produced by two different low-rank coals had significant differences in characteristics. Further to this, Hodges and Richards (1989) found that the fate of different elements contained in coal, including sulphur, sodium, potassium, calcium, and magnesium, varied significantly depending on the sample of coal used.

Hsieh and Roberts (1985), investigating agglomeration of American low-rank coals under gasification conditions, found that the agglomeration temperature decreased with increasing sodium content, where the agglomeration temperature was defined as the point at which agglomerates formed 50% of the total bed weight (Stallmann and Neavel, 1980).

Natarajan et al. (1998) found that by changing the bed material from silica to lime, the initial agglomeration temperatures of various biomass fuels were increased under combustion conditions. However the temperatures of agglomeration were found to decrease with the same biomass materials with lime under gasification conditions, which may be due to the interaction of calcium with the ash produced. It was also noted that initial sintering temperatures for biomass were generally higher than those for lignite, which is primarily related to the differences in inorganic content of the different fuels.

Agglomeration studies have been performed involving the gasification of various types of biomass (Ergudenler and Ghaly, 1993a,b; Natarajan et al., 1998; Mansaray and Ghaly, 1997). In gasification processes with biomass, potassium is considered the major contributor to agglomeration behaviour encountered, due to the relatively large amounts of potassium present.

Particle size has been shown to have a significant impact on agglomeration and defluidisation. Atakul and Ekinci (1989) found, in fluidised-bed combustion experiments with Turkish lignites, that the temperature of agglomeration could be increased by increasing feed particle size, increasing fluidisation velocity and hence expanded bed height, and by decreasing the size of inert bed particle material. This corresponds to findings by Bhattacharya et al. (1999), which found that combustion tests using South Australian lignites could be prolonged by introducing fine material into the bed, which acts to "soak up" molten ash being produced and elutriate it from the bed.

The height of bed material is another operating variable affecting the agglomeration tendency of coal particles. A review by He (1996) found that static bed height was one of the main factors affecting defluidisation tendency in fluidised bed combustion of lignite. An increase in bed height was found to increase the minimum velocity for spouting to occur (in a spouted bed), and was also found to decrease the initial sintering temperature. Similarly, other authors (Seville et al., 1998; Siegell, 1984) have found that an increase in the bed height-to-diameter ratio tends to increase the propensity for agglomeration to occur. The reason for this effect may be due to the fact that as the height is increased, the particles in the lower section of the bed would be more closely packed and have lower relative movement. This would lead to greater interparticle interaction, such as increased

contact time between particles, and increased heat conductivity through the bed (resulting in increased bed temperatures), hence a greater tendency for agglomeration to occur.

Operating Environment

As mentioned in preceding sections, the operating environment has a significant effect on the various inorganic interactions that take place. As agglomeration, to a large extent, depends on the formation of low melting point species, it would be expected that the operating environment would have some affect on agglomeration tendency of a coal. The behaviour of some mineral species under reducing conditions, particularly in terms of melting, may also be different than those under oxidising conditions (Huffman et al., 1981; Kosminski, 1997, 1999, 2000a-c), which could aid in producing reactions between inorganics at lower temperatures.

Natarajan et al. (1998) investigated agglomeration tendencies of different agricultural residues, under both combustion and gasification conditions. It was found that the initial agglomeration temperatures of the fuels under gasification conditions were less that those found under combustion conditions. This was attributed to the differences in inorganic transformations during ash formation.

Hsieh and Roberts (1985) conducted scanning electron microscope analysis of a variety of ash samples, and found that the extent of sintering of American lignite ash was much greater under reducing than oxidising conditions. This sintering behaviour would certainly contribute to lower temperatures of agglomeration being experienced under the environment of a fluidised bed gasifier due to lower melting point eutectics being formed under gasification conditions compared to combustion.

Moisture content of the fluidising gas has also been found to affect agglomeration. Brinsmead and Kear (1956) found that increasing the moisture content of the air in combustion decreases the amount of sodium released as volatiles but increases the proportion of chlorine released. The increased concentration of sodium retained in the coal could therefore contribute to the increased formation of low melting point eutectics, increasing the eutectic concentration of the system and the potential for agglomeration to occur. However, Rehmat and Saxena (1980) investigated the gasification of high-rank coal and determined that increasing the amount of steam actually reduces the chance for ash to

form agglomerates. This effect of steam is deemed to be the case because steam reduces the maximum temperature that the particles are able to obtain, and hence enables the sintering temperature of the ash to be avoided. This suggests that oxygen is the main factor for agglomeration development, mainly because increasing it also increases the temperature of individual particles, while also suggesting that not every particle in the bed needs to attain the ash melting temperature to provide a nucleus for further agglomerate growth. This disagrees with work by Kosminski (2001) however, which suggests that steam reduces the melting point of sodium carbonate in the ash, facilitating reactions that form low-melting sodium disilicate.

Bed Hydrodynamics

The hydrodynamics of the bed can affect the agglomeration behaviour of coal particles, as it affects movement of particles through the bed. The amount of relative movement between particles can affect their agglomeration behaviour in a fluidised-bed, as the more contact time particles have, the more advanced bond formation will be (Seville et al., 1998). Particularly in large fluidised beds, regions may exist in the bed that encompass lower relative movement between particles (Matsen, 1996), which will contribute to agglomerate formation and an eventual defluidisation of the bed (Seville et al., 1998). It would therefore be expected that agglomeration, and hence defluidisation, would be most likely to occur towards the wall of a spouted bed reactor under agglomerating conditions, and this behaviour has been observed during combustion tests using various Australian lignites in spouted bed reactors (Manzoori, 1990; He, 1998; Vuthaluru, 1999c).

Different zones of relative movement exist in a fluidised bed due to the circulating mixing pattern, particularly in industrial scale equipment (Matsen, 1996). These different zones indicate that there will be areas of lower relative movement where particles are in contact for longer periods of time. In these sections of lower relative movement, flow will also be dense. In dense phase flow, bonds between particles will have longer to form under the viscous flow mechanism, and as such, agglomeration will be most problematic to operation in these regions.

Beds with different hydrodynamics, burning the same fuel, have also been shown to produce different output properties. Anthony et al. (1989) obtained samples from a pilot-scale CFBC rig and a full-scale plant, which both combusted high-sulphur-content (7%

sulphur) New Brunswick coal. It was found that in the solid residues obtained from tests, while being mostly similar in chemical properties, the pilot-scale plant residue contained significantly higher calcium sulphide contents (4.1 to 4.7 wt% CaS) than those of the full-scale rig (0.45 to 0.60 wt% CaS). This suggests that analysis of residue from laboratory-scale fluidised bed reactors would benefit from comparison with samples from other gasification rigs to ensure that conclusions reached are applicable to a wide range of cases.

Bhattacharya et al. (1999) found in pilot plant combustion experiments with Australian lignites, that the impact of agglomeration on defluidisation was significantly less than for laboratory-scale combustion experiments with the same coals. While no evidence of formation of agglomerates was found during the pilot plant runs, results from laboratory-scale tests (e.g. Manzoori, 1990; He, 1998; Vuthaluru, 1999a) indicate that some defluidisation behaviour may be experienced during combustion of these coals. This demonstrates that caution must be taken when applying results obtained from small-scale experiments to industrial applications.

Watkinson et al. (1983) conducted a comparison of coal gasification in fluidised and spouted beds, and found that, while results for most coals tested were relatively similar for a given coal between reactors, some coals did produce different gas yields, gas qualities and thermal efficiencies between reactors. The reactor configuration could therefore have a significant impact on the agglomeration behaviour of a bed, although it should be noted that in their experiments, Watkinson et al. (1983) found that gasification of one particular low-rank coal lead to severe agglomeration and defluidisation behaviour regardless of the reactor type.

2.5.5 Control Methods

Various methods to control agglomeration and defluidisation have been developed by numerous researchers, with varying degrees of success. Vuthaluru (1999b-d) investigated the effects of agglomeration control methods during fluid bed combustion, including alternative bed materials (sillimanite, bauxite, calcite and magnesite), mineral additives (clay, kaosil and bauxite), coal pre-treatment (water washing, aluminium and calcium pre-treatment) and coal blending (lignites with sub-bituminous coals in varying ratios). It was found that all methods were successful in extending the time of fluidised bed operation before defluidisation, except for the water washing pre-treatment, which was thought to

reduce sodium levels in the coal and remove clay particles. However, it must be noted that these methods only prolong the operating time of fluidised-bed operation, and do not completely prevent agglomeration or defluidisation from occurring.

By using the alternate bed materials described above, the ash coatings of bed material were enriched in the elements Al, Mg and Ca. These are found to increase the melting temperature of the eutectics formed and lead to a decrease in the agglomeration propensity. Similarly, Dawson and Brown (1992) found that the aluminosilicate material produced as a molten bonding phase was sourced from both clays and shales in the coal, and feldspars found in the fluidising sand, suggesting that the bed material also reacts with the melt to form a bonding phase. They also found that reactions between calcium oxides and aluminosilicate material decreases the viscosity of the molten phase, and contributes to defluidisation.

Tests on Lochiel coal in a circulating fluidised bed combustion pilot plant by Bhattacharya et al. (1999) showed poor solid circulation during the run after about 28 hours of operation, indicating agglomeration and defluidisation was taking place. With the introduction of additives to the bed, taking the form of various clay minerals and also calcium-based sorbents, operation could be extended to in excess of 120 hours with no noticeable agglomeration problems, depending on the additive used.

The methods, as mentioned above, for controlling agglomeration and defluidisation act only to prolong operation time, rather than eliminate the phenomena from occurring. Another option, the mechanical-thermal expression (MTE) dewatering of lignites (Huynh, 2000; Favas and Chaffee, 2000; Qi and Chaffee, 2000; Huynh et al., 2001), may be more effective in reducing agglomeration behaviour of Australian lignites, as it alters the inorganic matter content of the coal before it enters the reactor. By removing a significant proportion of the sodium content in the coal with the extracted water (Favas and Chaffee, 2001; Qi and Chaffee, 2001), the initial sintering point of the ash may potentially be significantly increased, thereby decreasing its propensity to agglomerate within the operating conditions. Another benefit of this method is that species, which vaporise readily during heating of the coal, are removed, thereby potentially reducing problems with deposition (Qi and Chaffee, 2001).

2.6 Conclusions and recommendations

The preceding literature review revealed deficiencies in the knowledge of agglomeration and defluidisation of low-rank coal under fluidised bed gasification conditions. The problems of agglomeration and defluidisation have been extensively investigated under combustion conditions (Manzoori, 1990; He, 1998; Vuthaluru, 1999a-d; Bhattacharya et al., 1999), while most of the work in gasification has focused on the behaviour of high-rank coal and alternate fuels (Yerushalmi et al., 1975; Kolodney et al., 1976; Foong et al., 1980, 1981; Sue-A-Quan et al., 1995). The differences between combustion and gasification processes, combined with those between low-rank coal and other fuel properties, indicate that a thorough investigation of agglomeration and defluidisation of low-rank coal under gasification conditions is necessary.

Kosminski (2001) conducted a comprehensive study on the reactions taking place between sodium, silicon and aluminium compounds in a gasification environment. This study is particularly relevant to the objectives of the current study, as sodium has been shown to be an important component in South Australian lignite, particularly as it has a large influence on the ash melting behaviour. Key findings from this work are that a gasification environment results in the formation of ash throughout the char grains, and steam reduces the melting point of sodium carbonate (produced from organically bound sodium), which in turn reacts with silica in the coal to form a low melting sodium disilicate eutectic. The mode of ash formation has implications on the carbon conversion in the bed, with increasing conversion resulting in more ash release into the bed. More importantly, the effect of steam on lowering the melting point of sodium compounds in the ash has major implications for agglomeration and defluidisation of low-rank coal in fluidised bed gasifier reactors. The findings of Kosminski were not applied to an actual fluidised bed environment however, so the full impact of these issues on gasifier operation is not yet known. Thus, the objectives of the current investigation should focus on application of the work by Kosminski (2001) to a fluidised bed gasifier in order to determine the agglomeration and defluidisation behaviour arising from gasification of high sodium, chlorine and sulphur content low-rank coal.

The current study should include the following elements:

- Gasification trials should be conducted in a rig similar to that used in the study performed by Manzoori (1990), namely a 77 mm I.D. spouted bed, in order to provide a basis for comparison of gasification with combustion.
- Conduct gasification trials with lignite from the South Australian Lochiel deposit in order for direct comparisons to be made between spouted bed gasification conditions, and work performed by Kosminski (2001) under tubular furnace conditions.
- The spouted bed gasification trials should be performed to investigate both the physical behaviour of the bed, and inorganic behaviour of the coal ash.
- Gasifier operating parameters of greatest importance for investigation include air-to-fuel ratio, steam-to-fuel ratio, steam concentration in the fluidising gas, bed temperature, and superficial velocity.
- Validation of the spouted bed gasification results should be conducted in a pilot scale gasification rig with the same lignite, namely Lochiel coal.

By accounting for these elements, confident conclusions can be reached regarding the viability of utilising high-sodium lignite for power generation purposes.

CHAPTER 3

EXPERIMENTAL

3.1 Introduction

The literature review of Chapter 2 revealed deficiencies in the knowledge of agglomeration and defluidisation of lignite under fluidised bed gasification conditions, particularly coal with high contents of sodium, chlorine and sulphur. The main deliverables arising from the review are to:

- Determine the mechanism of agglomeration and defluidisation of Australian lignite during fluidised bed gasification;
- Quantify the effect of salient gasifier operating parameters on agglomeration and defluidisation;
- Validate the findings of Kosminski (2001) in an actual fluidised bed gasification environment; and
- Devise solutions to minimise or eliminate agglomeration and defluidisation during gasification of Australian lignite.

The experimental program for this study has been designed to address these deliverables. The outcomes of this work will aid in the development of the fluidised bed gasification process proposed by the Cooperative Research Centre (CRC) for Clean Power from Lignite.

3.2 Experimental Apparatus

3.2.1 Introduction

Two different fluidised bed gasification systems were used in this experimental program. The majority of experiments were conducted in a 77 mm I.D. spouted bed gasifier, operated at atmospheric pressure. Results from these experiments were used to develop the conclusions arising from this study. Tests were also conducted by the CRC for Clean Power from Lignite using a 300 mm I.D. pressurised gasifier system – the Process Development Unit (PDU), which was leased from Herman Research Laboratory Ltd. (HRL). Results from these tests, as they relate to agglomeration and defluidisation behaviour, were analysed in order to validate the findings from spouted bed experiments. The following sections describe the details of each system, with particular attention paid to the spouted bed gasification system.

3.2.2 Spouted Bed Gasifier System

The spouted bed gasification system, depicted in Figure 3.1, was designed to fulfil the following requirements:

- Allow stable spouting of beds of pure char;
- Enable spouting of the bed during experiments to be physically observed;
- Provide flexibility for gasifying coal with gas consisting of up to 100% steam;
- Provide the ability to feed coal at a steady, user-defined rate while mitigating pyrolysis of coal in the feed line prior to entering the bed;
- Allow the coal hopper to be replenished during operation without releasing toxic gas into the laboratory environment;
- Enable bed material at the end of each experiment to be removed with minimal breakage of agglomerates;
- Minimise heat loss from the reactor during gasification;
- Provide the ability for external heating to be employed during start-up, independent of bed temperature;
- Ensure particulates and moisture in flue gas are removed to allow gas composition analysis to be conducted without damaging the gas analysis equipment;
- Enable bed temperature and pressure drop across the bed to be monitored on a laboratory PC.

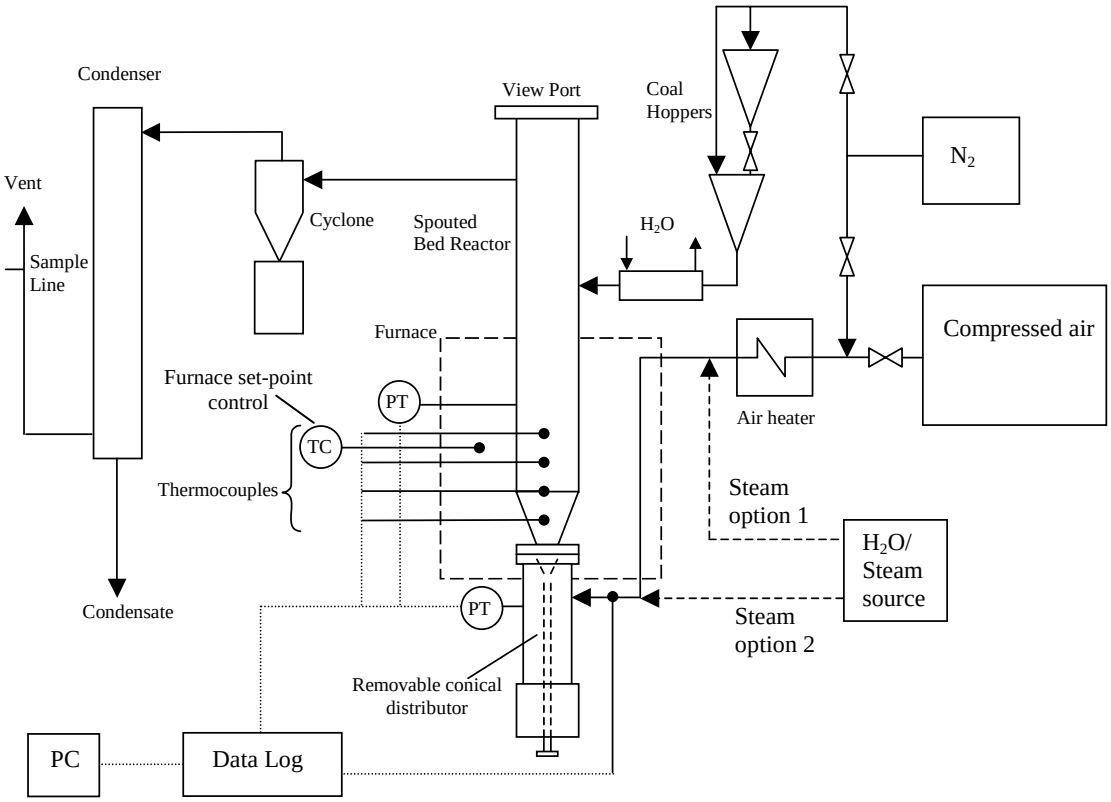

Figure 3.1 Spouted bed gasifier system

A more detailed layout of the main spouted bed reactor vessel, including temperature probe and pressure sensor locations, is shown in Figure 3.2. The fluidising gas mixture enters the vessel in a chamber below the conical section. This chamber houses the conical distributor, through which the fluidising gas passes into the bed. The lower chamber area also contains a removable “solids canister”, threaded to the base of the cylinder, which collects bed material upon removal of the conical distributor at the completion of experiments. The canister includes a tap at its base to allow for manual drainage of any condensate that may collect during start-up of each run.

The conical distributor, shown in Figure 3.3, provides a 10 mm-diameter gas inlet to the bed. The distributor is affixed to a partially porous stem, which screws into the base of the solids canister. The stem is adjustable to seal the conical distributor firmly against the bottom of the conical section at the base of the reactor vessel. The removable nature of the distributor facilitates bed material removal at the conclusion of experiments, particularly as agglomerate size may potentially approach that of the cylindrical diameter of the reactor. A patch of wire mesh covers the opening of the conical distributor to prevent material falling from the bed during operation.

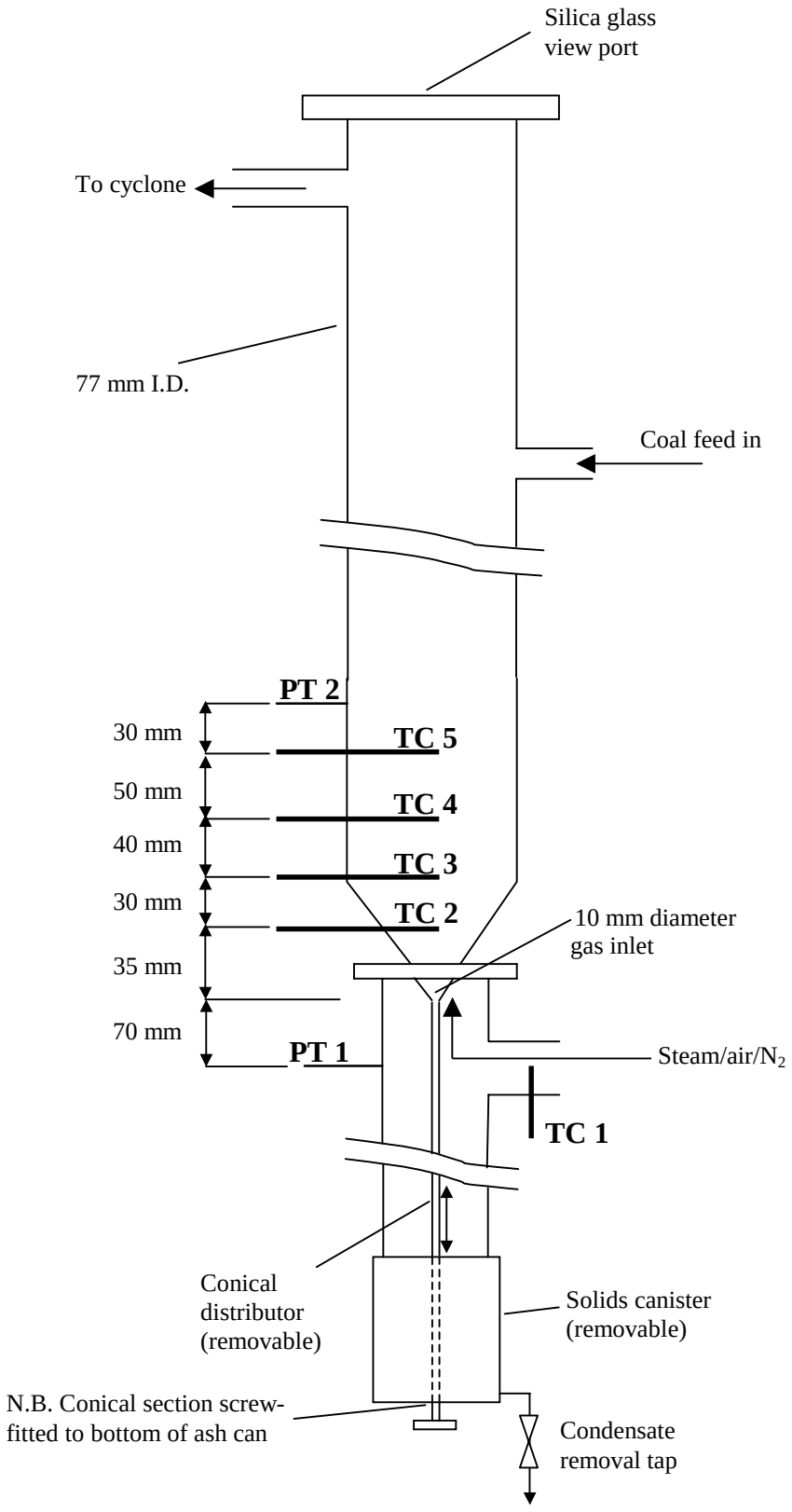

Figure 3.2 Spouted bed gasifier layout, including positioning of in-bed thermocouple sensors and pressure transmitter lines

Figure 3.3 Removable conical distributor

The majority of gasification reactions proceed in the reactor vessel. This section consists of a 55 mm high conical base (65 mm including removable distributor). The 10 mm diameter gas inlet expands to a 77 mm internal diameter cylindrical section. The cylindrical section extends upwards approximately 1.1 m to a high temperature glass view port, which enables the bed to be viewed while in operation. A coal feed port is located on the side of the cylindrical vessel, located approximately half way between the conical section and the view port. Another port is located towards the top of the cylindrical section, where gas and fine solids exit from the vessel to the downstream gas handling section.

3.2.3 Coal Feed System

Coal is fed into the top of the bed via a screw feeder arrangement. The coal feed exit is located at a height of approximately 550 mm above the entrance to the conical section. A variable speed motor, capable of 3000 RPM maximum speed, is connected to a 102:1 ratio gear. This enables a feed rate of air-dry Lochiel coal of up to 1.75 $kg.hr^{-1}$.

Coal is introduced to the screw feeder via a lock-hopper arrangement. The lower hopper is sealed during each experiment, and contains a Perspex viewing window on its side to enable visual monitoring of coal level. The upper hopper is used to introduce coal into the

lower hopper, which ensures that the system is always sealed to the laboratory atmosphere. Nitrogen flows at a constant rate through the top of the lower hopper, and can also be introduced to the upper hopper via a manual valve for the purposes of adding extra coal to the system. Nitrogen is used principally to provide a backpressure from the hoppers to ensure that steam does not condense in the feed line and cause blocking. The feed line is encased in a water jacket, which utilises mains water as the cooling medium. This ensures that coal does not become heated before entering the bed.

3.2.4 Gas supply

Process air is provided to the system via a CompAir BroomWade 6000E Series air compressor. A refrigerant dryer is used to remove any excess moisture and contaminants from the compressed air stream. High-purity nitrogen (Air Liquide) is supplied in cylinders. Flow rate of the gas supply to the reactor is controlled using variable-area flow meters.

Two sizes of variable-area flow meters were installed to account for the wide range of gas flow rates required for experiments, set up as in Figure 3.4. For flow rates from approximately 10 to 70 LPM, a 'Metric Size 18E' flow meter was used, with aluminium float. Smaller flow rates required a more sensitive flow meter, and a 'Metric Size 7' flow meter was used, also with aluminium float. The flow meter size is user-selectable by opening the valve at the foot of the desired flow meter, and ensuring the valve on the other flow meter was closed.

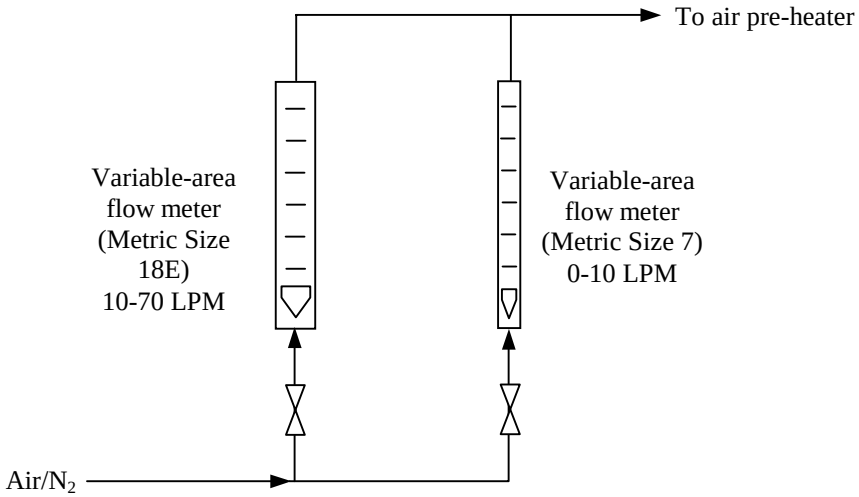

Figure 3.4. Variable-area flow meter system for gas flow measurement.

3.2.5 Steam Generation

Two selectable options are present for the generation of steam for experiments, as indicated in Figure 3.5. The mode used is dependent on the amount of steam required. Steam Option 1 enables steam flow rates between 1.5 and 20 $g.min^{-1}$ while Steam Option 2 is capable of providing flow rates as large as 95 $kg.hr^{-1}$ (1,580 $g.min^{-1}$).

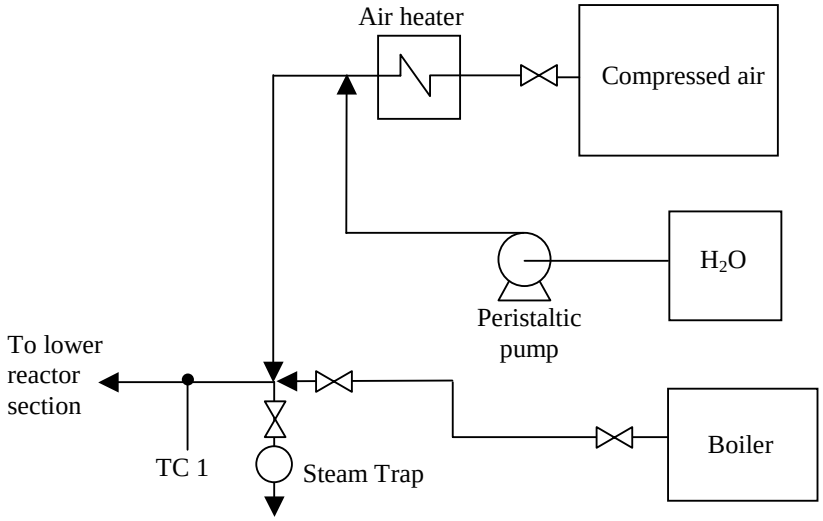

Figure 3.5. Steam generation section

Steam Option 1 consists of a Cole-Parmer Masterflex C/L peristaltic pump supplied with de-ionised water from a separate tank. The pump is calibrated to allow precise setting of water flow rate, and hence steam mass flow rate. Pumped water is injected into the hot air stream in the pipe section following the air pre-heater. The vaporised water-air mixture then passes through the electrical furnace and into the gas inlet.

Steam Option 2 provides a direct steam source from a Simons VS 300-60kW Automatic Electric Steam Boiler. Excess moisture in the steam is removed via a float-type steam trap. The remaining steam subsequently enters the air stream immediately at the gas inlet. The steam flow rate for Option 2 is calibrated by measuring the amount of condensate collected from the condenser section of the heated reactor prior to feeding coal.

3.2.6 Heating

External heating is used in order to aid in start-up and minimise heat loss from the reactor. An electrically heated furnace is constructed around the middle section of the reactor, as indicated in Figure 3.6.

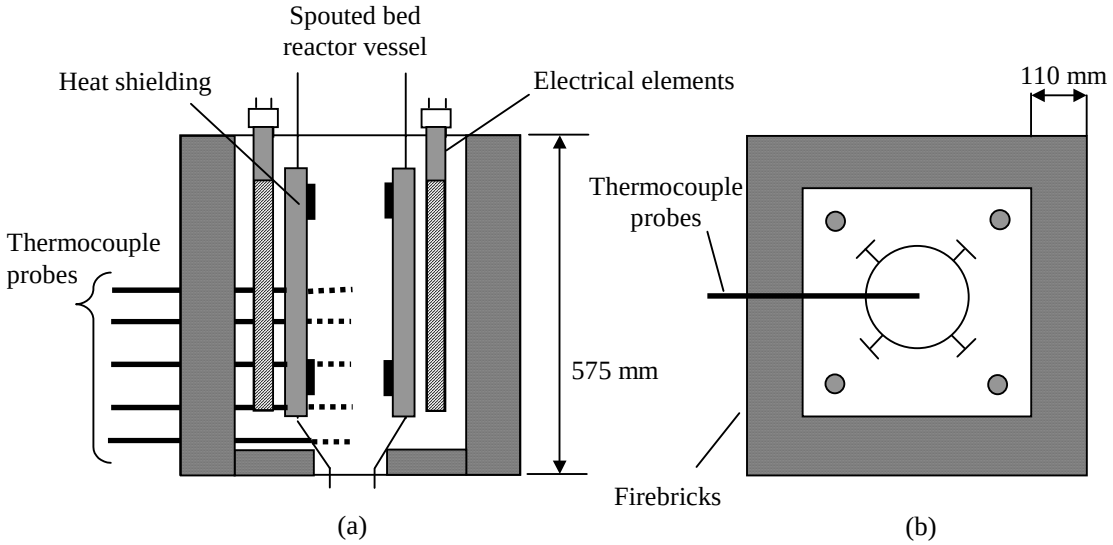

Figure 3.6. Electrical furnace arrangement. (a) Side view, (b) Top view.

The outer walls of the furnace consist of Thermal Ceramics insulating firebricks, creating a surrounding wall 110 mm thick and 575 mm in height. Two pairs of Kanthal Crusilite electrical heating elements are used to provide heating, which each have a nominal resistance of 6.0 Ohms. One pair acts as a control for the furnace, allowing a set-point temperature to be specified, while the other pair provides constant heating to the furnace. The elements are suspended vertically from the top plate of the furnace and situated in each of the four corners surrounding the reactor vessel. Elements in each pair are positioned on opposite corners of the furnace to provide balanced heating to the bed. Shielding prevents the creation of hot spots on the reactor wall due to radiation from the heating elements. Shields are in the form of vertical stainless steel strips, which are welded to the outside of the middle cylindrical section of the reactor.

The control elements are controlled with a Shimaden Microprocessor-based Auto-tuning PID controller, enabling the furnace temperature to be set and regulated with on/off action. A thermocouple connected to the Shimaden controller (‘Furnace set-point control’ in Figure 3.1) is inserted into the furnace to measure temperature and aid in set-point regulation. The control elements are able to raise the furnace temperature to approximately 500° to 600°C. Constant heating elements are used in order to provide extra heat for raising the temperature further.

Air or nitrogen is pre-heated with a Leister Electric Hot Air Tool type 5000. This allows temperature adjustment between 20 and 700°C, and automatically adjusts heating rate for changing airflow to provide a constant temperature output. The heated air/N_2 stream is passed through the electrical furnace before entering the bottom of the reactor vessel in order to provide extra heat to the stream.

3.2.7 Downstream Gas and Solids Handling

Gas from the reactor passes through a cyclone to remove much of the elutriated fine material, collecting in a threaded canister at its base. The gas exiting the cyclone enters a water-cooled condenser. The condenser consists of an arrangement as shown in Figure 3.7. It is a basic arrangement of a cylindrical vessel, 60 mm diameter and 900 mm in height, containing a spiral-wound tube facilitating the flow of mains water for cooling. Condensed steam is removed manually by opening a valve on a tube connected to the base of the condenser and collected in a container for appropriate disposal. The remaining gas passing out of the condenser is then safely expelled from the laboratory through a dedicated ventilation system, with the option to draw off a small amount of gas for further compositional analysis.

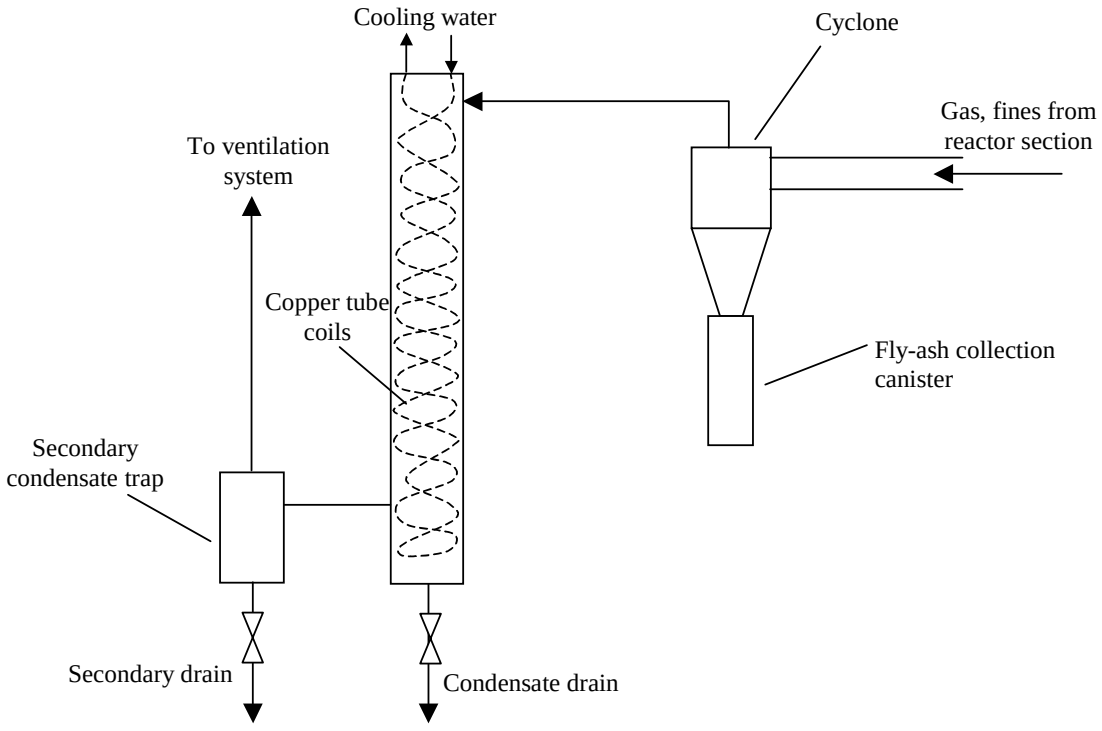

Figure 3.7. Downstream gas and solids handling.

3.2.8 Process Monitoring

Temperature is measured at various locations along the centreline of the reactor with 3.0 mm diameter Type-K thermocouples, with spacing as in Figure 3.2. Thermocouples are connected to a Shimaden KR20 Multiple Point Selector. This allows any of the temperatures measured by thermocouples TC1 to 5 to be selected and displayed on a Shimaden SD10 process display unit on the control panel, in °C.

Pressure drop is measured from 15 mm below the inlet to 190 mm above the inlet. The pressure line 'PT 1' is connected to a Wika Pressure Transmitter, which supplies a 4-20 mA reading to a Mann Industries PM350 Industrial Process Monitor. This displays the operating gauge pressure of the vessel in Pa. Both PT 1 and PT 2 are connected to an ABB Kent Deltapi K Series electronic transmitter, which similarly provides a 4 to 20 mA reading of the pressure drop across the bed. Again, the pressure in Pa is displayed on a separate PM350 unit.

The thermocouples and pressure drop leads are connected to a Pico Technology 8-channel data logger, Model TC-08. This is connected via serial port to a laboratory PC, and results are collected in real time using the supplied PicoLog software. This information is used in particular to determine whether agglomeration and defluidisation is occurring during operation, as indicated by a rapid increase in bed temperature corresponding to a decrease in pressure drop (Gluckman et al., 1975; Basu, 1982; Siegell, 1984; Manzoori, 1990). The state of fluidisation of the bed is also determined visually through the view port at the top of the vessel, which complements the PicoLog readings. Visual observation and online monitoring data provide an overall indication of whether defluidisation has occurred.

3.3 Experimental Procedure

The following sections present the Standard Operating Procedure (SOP) that was followed for each experiment conducted with the spouted bed gasifier.

3.3.1 Start-up

The reactor was first inspected to ensure that no material is present from previous runs, and all flanges were checked for loose fittings. Dried and sieved coal was inserted into the

hopper and sealed. All main air valves in the laboratory for non-operating rigs were closed, and the air compressor and refrigerant air dryer were both switched on. The main air valve to the system was opened to allow airflow through reactor. The air pressure was then adjusted to 1 atm. Nitrogen flow was also turned on at this time, with the valve at the coal hopper opened to allow nitrogen to purge the feed line. The cooling water was subsequently turned on before activating the hot air tool to pre-heat the air to approximately 700°C. The control elements in the electrical furnace were also engaged to begin heating of the reactor to the desired experiment temperature.

When the furnace temperature could no longer increase at a significant rate (at around 500 to 600°C), the constant heating elements were activated to provide extra heat to achieve the set point temperature of the furnace. Temperature in the reactor vessel was monitored during start-up using data logging software in order to determine when steady-state temperatures were attained.

Steam was introduced to the vessel upon reaching steady-state temperatures inside the reactor, with the steam production method depending on experimental requirements. For instance, in the case of steam requirements below 10 $g.min^{-1}$ the peristaltic pump was switched on at the required water flow rate. For steam requirements above 30 $g.min^{-1}$ the electric boiler was instead activated and steam flow rate set accordingly. Temperatures inside the reactor were again allowed to reach equilibrium once the steam-air mixture was introduced.

Once equilibrium reactor temperature was reached, air flow was replaced with nitrogen to create an inert atmosphere. Nitrogen flow was set at the same flow rate as the desired airflow rate for the experiment to preserve the superficial velocity. Approximately 2 minutes was sufficient to render the reactor environment inert from combustion. Once inert, the screw feeder was turned on to the desired coal feed rate. Coal was fed until 40 g of char was present in the reactor before being temporarily halted. This weight ensured that the entire conical section of the vessel was filled with char, providing an initial bed to begin gasification. Once the pressure drop and thermocouple readings were stabilised for the initial char bed, the nitrogen was again replaced with air, and the gasification process was commenced.

3.3.2 During Operation

Close monitoring was required of several operational aspects of the reactor during gasification experiments. Coal level in the primary hopper was monitored through the Perspex window on its side. The feed supply was replenished whenever the level dropped below approximately one-third of its capacity.

Condensate was manually discharged from the condenser section at regular intervals. Build-up of condensate in the solids canister at the base of the reactor vessel was avoided using the condensate tap. This was only a significant issue during the early stages of experiments when using the boiler for steam generation. Pressure lines were also regularly purged with nitrogen backflow to remove possible condensate build-up in the lines. This again was only a major problem when the steam boiler was used.

Operation of the bed was monitored using temperature and pressure drop trends on the PC. Fluidisation and coal feed operation could also be observed through the view port at the top of the vessel, although this was only useful for approximately 10 to 40 minutes operating time depending on process parameters used for the experiment. After this time, deposition of fine material on the underside of the glass reduced visibility of the bed until it was completely covered. Once the desired run length had been achieved for the experiment, shutdown of the reactor was commenced.

3.3.3 Shutdown

At the conclusion of each experiment, all heating sources were disabled, steam was turned off, and air was replaced with nitrogen to cool the bed under inert conditions. Nitrogen flow rate was set at a velocity sufficiently high to ensure that fluidisation of the bed was maintained during cooling. Once the bed temperature had been reduced to below approximately 200°C maximum temperature, the conical distributor of the reactor was removed, and the bed material allowed to drain into the bottom solids canister. Switching back to air completed cooling of the reactor.

Once the reactor had been cooled completely and air flow turned off, the bed material and any agglomerates from the ash can were placed in a sealed sample container to prevent contamination by foreign material and moisture. Any remaining agglomerates in the reactor vessel were also manually removed with as little breakage as possible, and added to

the bed sample. Material from the cyclone was collected and similarly placed in a sealed container. Deposits forming on the surface of the removable conical distributor were also scraped off and collected in sealed containers. Each sample was weighed before further analysis.

3.3.4 Maintenance

To ensure that repeatable conditions were met for each experiment, the reactor was thoroughly cleaned on the inside to remove any deposits or other such material that may affect future experiments. These include deposits of fine char forming on the wall in the freeboard of the bed, which may grow with further experimental runs and restrict flow of gas, and on thermocouples, which may reduce the effectiveness of temperature measurements. Any blockages forming in pressure lines were also removed to ensure reliable pressure drop measurements. The condenser was cleaned to remove any carry-over fines that may have become trapped in the condensing steam, ensuring that no blockages impacted on subsequent experiments.

3.4 Experimental

3.4.1 Feed Coal Preparation

Care was taken to ensure the coal feed was as uniform as possible between experiments. All coal was obtained from the same storage bag for the duration of experiments, with good mixing ensured during preparation. Analyses were conducted at various times on the coal, which demonstrated negligible variation in composition between experiments.

A sufficient quantity of coal was prepared before each experiment by drying under ambient conditions. Coal was laid out on drying trays in 10 mm thick layers, as in Figure 3.8a, and allowed to sit until equilibrium with the laboratory atmosphere was achieved. The coal was placed in a dry part of the lab away from direct sunlight and draughts, and stirred periodically in accordance with Australian Standard method AS 1038.1–1992, Section 2. Dried samples were typically obtained after two to three days drying time. Cracking of the coal layers is the indication that equilibrium moisture content has been reached, as shown in Figure 3.8b.

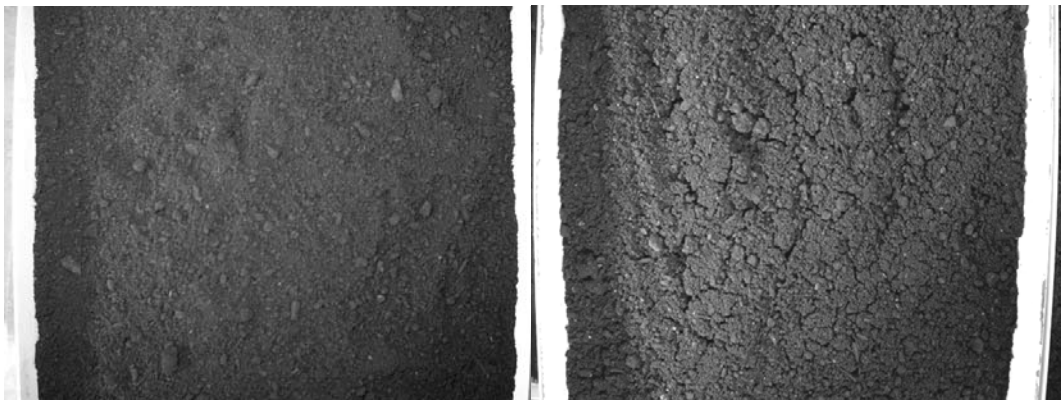

(a) (b)

Figure 3.8. Pre-sieving Lochiel coal on drying tray. (a) As-mined coal, (b) Air dried coal.

Coal that has reached equilibrium moisture content was sieved to a size fraction of between 1.00 and 3.35 mm diameter using a Sieve Shaker. A period of 10 minutes shaking time was sufficient to separate the particles outside the desired size range. The coal was removed from the sieves and placed in sealed buckets in a cool, dry place until ready for use.

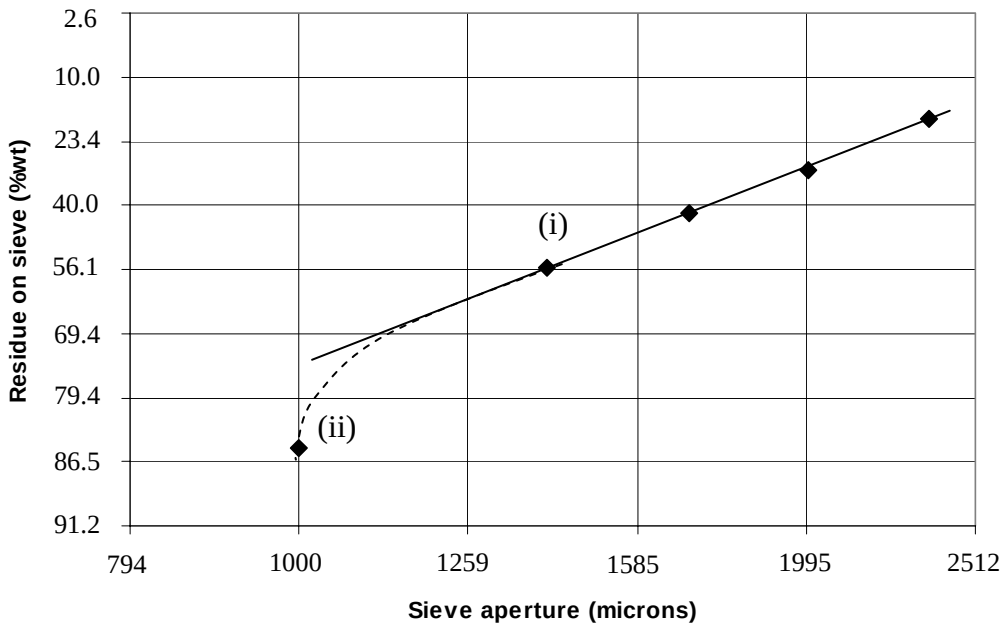

Figure 3.9. Particle size distribution of sieved, air-dried Lochiel coal, 1.00 to 3.35 mm diameter particle size range. (i) Ideal curve for Rosin-Rammler distribution, (ii) Curvature of distribution at 1.00 mm particle diameter.

Particle size distribution of the sieved coal is presented in Figure 3.9 using the method devised by Rosin and Rammler (1933). Note that curvature exists at the fine particle end of the distribution, while a natural body of particles ideally produces a straight line through a

Rosin-Rammler distribution. The curvature is due to the removal of particles smaller than 1.00 mm in diameter, and thus the coal feed is not a natural body of particles as such. This does not impact on experiments however, as finer particles are elutriated quickly from the bed in any case.

3.4.2 Calibration of Instrumentation

Flow meter

Each variable-area flow meter used for gas flow measurement was calibrated using a volumetric flow meter, which was attached to the gas outlet of the spouted bed gasifier. Compressed air at ambient temperature was used as the calibrating gas. The total volume of air passing through the reactor was measured for 1 minute at each graduation on the rotameter tube, and flow rate was calculated. This method was repeated for each graduation, spanning the entire range of the rotameter. The calibration curves for the flow meters are shown in Figure 3.10 and Figure 3.11.

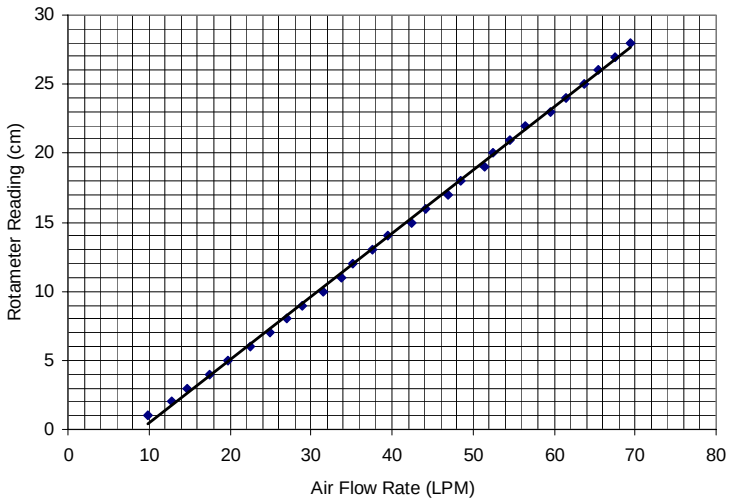

Figure 3.10. Rotameter calibration curve for Metric Size 18E flow meter.

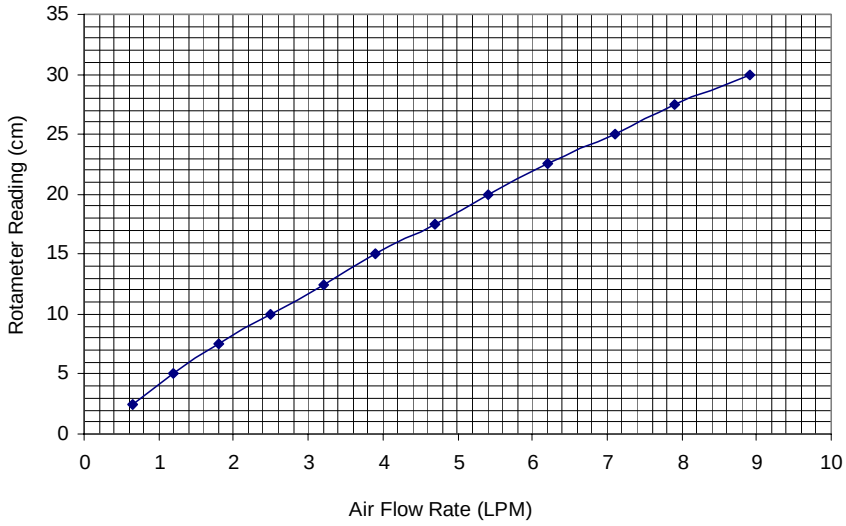

Figure 3.11. Rotameter calibration curve for Metric Size 7 flow meter.

Coal feeder

The coal feeder was calibrated with the feed coal used in experiments, namely air-dried Lochiel coal with size range 1.00 to 3.35 mm. Coal was fed through a cold reactor for 1 minute at each feeder motor speed, and collected at the base of the reactor. The collected coal was weighed, and a feed rate for each speed setting was calculated. Figure 3.12 shows the calibration curve for air-dried Lochiel coal feed rate.

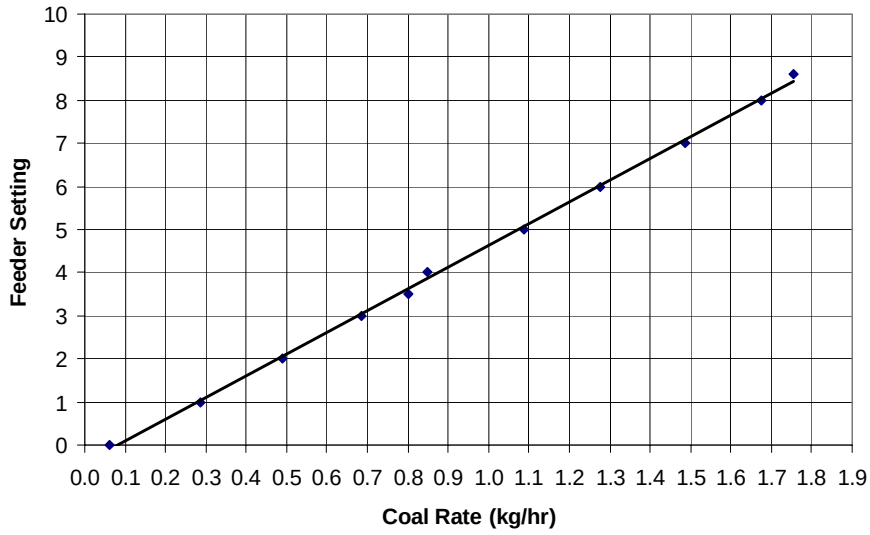

Figure 3.12. Calibration curve for coal screw feeder using air-dried Lochiel coal.

Steam flow rate

The two different steam options necessitated different calibration methods to be performed for each option.

For low steam flow rates using the peristaltic pump, a measuring cylinder was filled with deionised water from the feed tank and the feed tubes were placed into the vessel. The volume of water pumped out of the measuring cylinder over 1 minute was measured, and a mass flow rate of water was calculated for each pump speed setting. The calibration curve for steam flow rate using the peristaltic pump is shown in Figure 3.13.

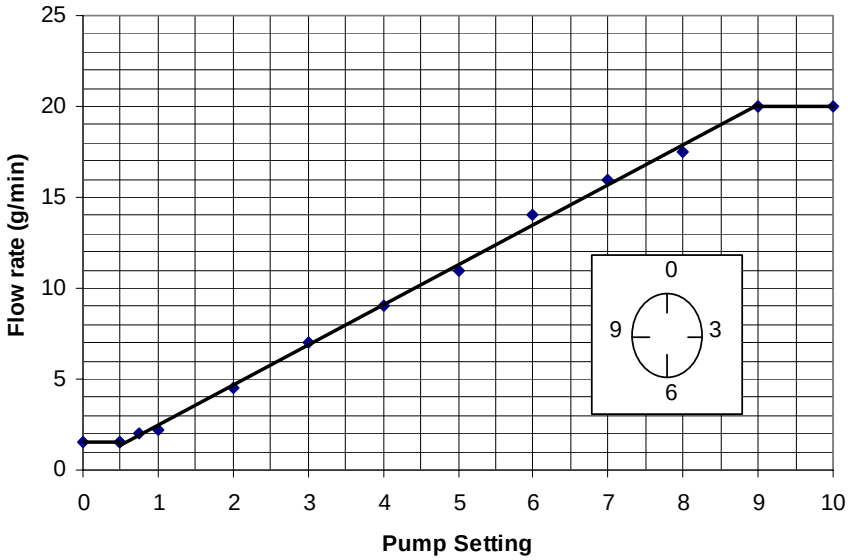

Figure 3.13. Feed water peristaltic pump calibration curve for steam generation.

Measurement of steam flow rate from the boiler was complicated by the fact that water was topped up periodically in the boiler rather than continuously, and thus water mass flow rate could not be measured directly. Instead, a trial-and-error method of determining approximate steam flow rate was used. To commence calibration, the steam line valve was opened one full turn, and steam produced from the boiler was passed through the condenser. The condensate produced over 1 minute was collected and weighed to give an approximate steam flow rate. Several measurements of condensate were obtained at the valve position to ensure that a constant flow rate was attained. The approximate flow rate obtained was measured against the required flow rate to achieve the desired experimental conditions, and the steam line valve position adjusted accordingly to provide either more or less steam if required, and the process repeated. This method assumes that most of the steam was condensed in the condenser, and as such represents the minimum possible steam flow rate for each valve setting. This ensures that spouting velocity is greater than the

minimum, such that defluidisation would not be specifically due to too low a superficial velocity.

3.4.3 Calculation and Measurement of Operating Parameters

Operating parameters used in gasification experiments were selected in order to ensure that superficial gas velocity remained above the "normal" minimum spouting velocity of the bed (i.e. in the absence of significant ash sintering), and that gasification was achieved. The control variables important to achieve these requirements include superficial velocity, air/fuel ratio, steam/fuel ratio, and bed temperature. Only bed temperature and air flow rate (ambient temperature) was directly measurable from experiments, with calculations required for the remaining parameters. The following sections identify how the appropriate parameters were calculated and measured.

Maximum Bed Temperature

Bed temperature was used as the basis for calculating superficial gas velocity. This was characterised by the maximum (measured) average temperature in the bed. Average temperature was calculated at each thermocouple location, with the maximum value selected from these values. The location of this temperature varied from experiment to experiment, but was typically measured at either TC 3 (65 mm above the fluidising gas inlet) or TC 4 (approximately 100 mm above the inlet). Where stable operation for the entire run was achieved, the average temperature was calculated for the total length of the run. Where agglomeration and defluidisation occurred, temperature was only averaged for operation up to the point of defluidisation.

Prior to each run, the maximum bed temperature was unknown. In order to calculate the amount of ambient air required to achieve the desired superficial velocity for each run, an approximate bed temperature was initially assumed. This temperature was determined using the set-point temperature of the external furnace as a guide. It was assumed, based on reactor commissioning experience, that bed temperatures were approximately 100°C higher in the bed than in the furnace. This allowed a superficial velocity that was higher than the minimum to be approximated, which could be corrected for actual temperature at the completion of the run. Furnace temperature was chosen based on the bed temperature desired for the experiment, giving limited control over the final bed temperature.

Minimum Spouting Velocity

Minimum spouting velocity was determined by conducting cold tests in the spouted bed with pre-prepared Lochiel char. The volumetric flow meter used for calibration of the variable-area flow meters was used to measure air flow rate through the reactor. This is because the high air flow rates required under ambient conditions to emulate flow rates at experiment temperatures extend beyond the measurement range of the variable-area flow meters.

The static bed height was identified as a variable for minimum spouting velocity determination (refer to Eq. 2.1). Therefore, minimum spouting velocity was determined based on a variety of different weights of bed char, namely 40, 60, 80, 100 and 200 g. For each weight, the reactor was charged with char through the view port on top of the main reactor column. Compressed air flow through the reactor was increased until vigorous spouting was achieved, as indicated by visual observations of the bed. Air flow rate and pressure drop across the bed and distributor was recorded, and flow rate was incrementally decreased with subsequent measurements recorded. The procedure was repeated for all bed weights, and the plots shown in Figure 3.14 were achieved.

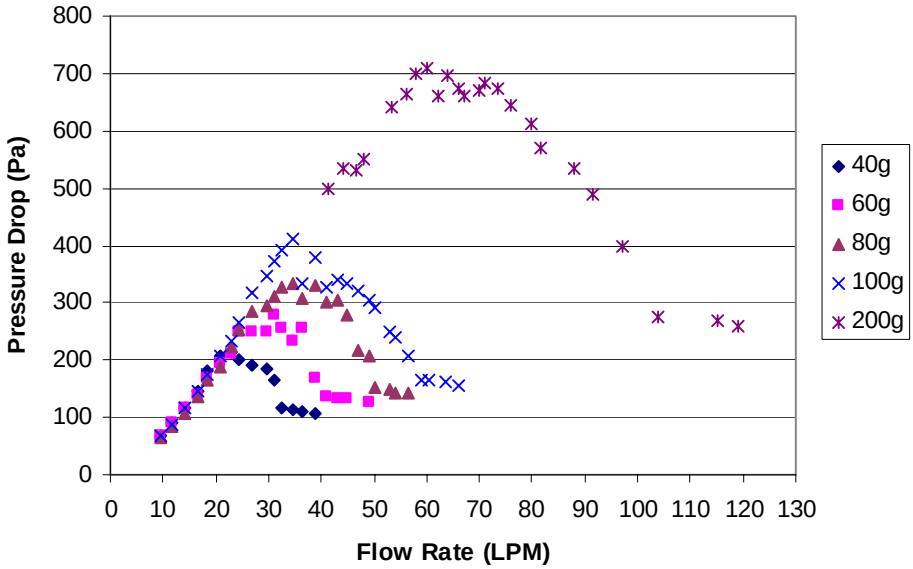

Figure 3.14. Pressure drop versus air flow rate for different bed weights of Lochiel coal char.

Flow rates were converted to superficial velocity by dividing by the area of the cylindrical section of the reactor. Minimum spouting velocity for each bed weight was identified as the point at which pressure drop levelled out after the initial increase and subsequent

decrease. This resulted in an approximately linear increase in minimum spouting velocity with bed weight, as shown in Figure 3.15.

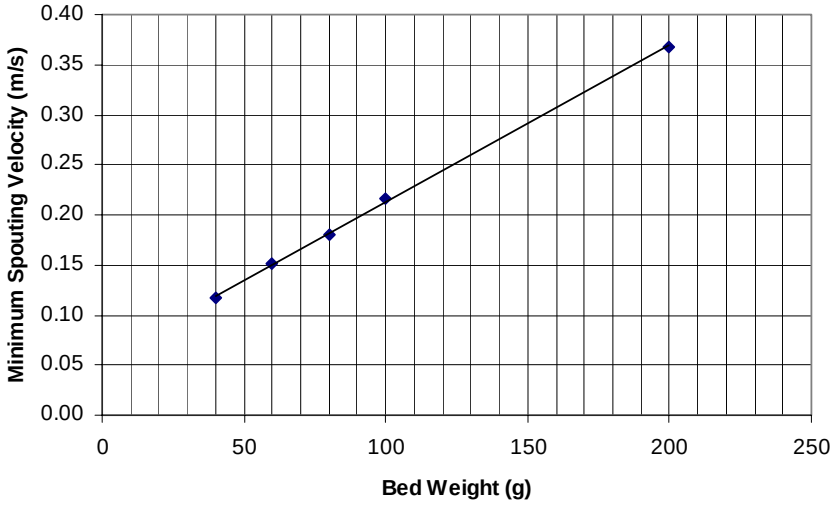

Figure 3.15. Variation of minimum spouting velocity with bed weight.

A nominal minimum spouting velocity was chosen in order to ensure operation above minimum spouting conditions in all experiments. A safety factor of 4 times the initial bed weight was allowed for in determining the minimum spouting velocity. Given that 40 g of char was initially present in the bed of each run, a maximum final bed weight of approximately 160 g was assumed, or approximately 0.30 m/s minimum spouting velocity. Experimental operating parameters were thus set based on superficial velocities exceeding this minimum value.

Air/Fuel and Steam/Fuel Ratios

Air/Fuel (A/F) and Steam/Fuel (S/F) weight ratios were calculated based on two parameters, which include:

- Superficial velocity of the bed; and
- Steam concentration of the fluidising (inlet) gas.

As discussed in the preceding sections, superficial velocity of gas through the bed was dependent on the bed temperature. Steam concentration of the fluidising gas allowed determination of the flow rate of water/steam and air required for achieving the desired gas velocity.

For the majority of experiments, the superficial velocity was set at twice the nominal minimum spouting velocity, or approximately 0.60 m/s, to provide an additional safety factor for maintaining operation above the minimum velocity. In a number of cases, velocity was set lower or higher than this value, but always greater than the minimum. Steam concentration was subsequently selected via a steam/air ratio (S/A), and temperature of the gas was estimated based on the furnace temperature. This allowed calculation of the mass flow rates of both steam and air to provide a steam air mixture at the desired flow rate, with correction for temperature to ambient conditions enabling flow rates of the variable-area flow meter and peristaltic pump (or boiler) to be set. The user also defined the A/F, allowing determination of the required coal feed rate. Note that at the completion of the experiments, the variables of A/F, S/F and superficial velocity were corrected for the actual bed temperature achieved.

3.5 Analytical

3.5.1 Standard Coal Analysis

Several standard techniques and confidential methods are employed for characterising the feed coal for experiments, results shown in Table 3.1. Moisture and ash yield are determined according to HRL method 1.6, an in-house confidential method used by HRL Pty. Ltd. Fixed carbon and volatile matter are determined according to Australian Standard method AS 2434.2. Sulphur and chlorine content are carried out according to AS 2434.6 and AS 1038.8, respectively. Ash composition analysis was determined using borate fusion of the sample and analysed with Inductively Coupled Plasma-Atomic Emission Spectrometry (ICP-AES) according to AS 1038.14. Both acid extractable (AS 2434.9) and water extractable (modified AS 2434.9 method, excluding the ash matrix) elemental analyses are carried out to indicate the relative combinations of the elements in the coal structure, while a confidential HRL calculation method was used to determine the coal mineral content.

Table 3.1. Lochiel Coal Properties

Coal Analysis:	**Composition**
Proximate analysis	wt%
Moisture[a] (ROM, wb)	60.3
Moisture[a] (air-dried, wb)	12.7
Ash yield (db)[a]	15.7
Fixed carbon (db)[b]	38.1
Volatile matter(db)[b]	46.2
Additional assays (db)	
Sulphur[c]	3.5
Chlorine[d]	0.5
Ash composition[e]	
SiO_2	31.4
Al_2O_3	8.30
Fe_2O_3	4.05
MgO	8.58
CaO	9.97
Na_2O	8.68
K_2O	0.30
TiO_2	0.48
SO_3	27.5
Coal Minerals (db)[f]	
SiO_2	4.31
Al_2O_3 (clay form)	0.60
K_2O	0.02
TiO_2	0.12
FeS_2	0.20
Acid-soluble elements (db)[g]	
Al (non-clay form)	0.31
Fe (non-pyritic)	0.49
Ca	1.55
Mg	0.86
Na	0.89
Water-soluble elements (db)[h]	
Al	<0.01
Fe	0.13
Ca	0.18
Mg	0.22
Na	0.69
S	0.71

ROM – Run-of-mine coal; db – dry basis; wb – wet basis.
Analysis methods: (a) HRL method 1.6, (b) AS 2434.2, (c) AS 2434.6, (d) AS 1038.8, (e) AS 1038.14, (f) HRL calculation method, (g) AS 2434.9 (h) Modified AS 2434.9 (excluding acid matrix).

Lochiel coal is high in moisture content at approximately 60% (wt) of the total coal, with ash content of almost 16% (wt, dry basis). The ash is high in silica (31.4%) and sulphur (27.5%), with lesser amounts of aluminium (8.3%), magnesium (8.6%), calcium (10.0%), and sodium (8.7%). Water-soluble elemental analysis indicates those elements that are present in the inherent moisture of the coal, while acid-soluble elements represent those that are exchangeable or extractable by hydrochloric acid, including organically-bound inorganics. Coal minerals are insoluble, and are calculated by difference.

The analyses in Table 3.1 show that SiO_2, Al_2O_3 (clay form), K_2O, and TiO_2 are predominantly in crystalline mineral form, while iron is present as disulphide. Calcium and magnesium are predominantly bound to the coal structure, with smaller amounts of each dissolved in the moisture. Some of the aluminium and iron in the coal are also organically-bound, with only minor amounts dissolved in the moisture. Sodium is split relatively equally between organically-bound and dissolved forms in significant amounts. Chlorine is also present in the coal at 0.5% (wt, db), which is most likely dissolved in the inherent moisture (Hodges et al., 1983). With chlorine present wholly in the moisture, it can be inferred that most of the dissolved sodium is associated with chlorine, indicating that other dissolved species such as calcium and magnesium are likely to be combined with sulphur, most likely as sulphates (Readett and Quast, 1987).

3.5.2 X-Ray Diffraction

X-Ray Diffraction (XRD) analysis provides mineralogical information, giving the crystalline structures existing in the ash. Analysis was carried out commercially by the CSIRO Division of Land and Water. Samples for analysis were oven dried to 60°C then ground with mortar and pestle before being lightly pressed into aluminium sample holders. The XRD patterns were recorded with a Philips PW1800 microprocessor-controlled diffractometer using Co Kα radiation, variable divergence slit, and graphite monochromator. The diffraction patterns were recorded in steps of 0.05° 2θ with a 3.0 second counting time per step, and logged to data files for analysis. CSIRO technicians interpreted the diffraction patterns.

3.5.3 X-Ray Fluorescence

X-Ray Fluorescence (XRF) analysis was carried out to determine the elemental composition of each sample as a percentage of the total weight of the original sample.

Analysis was carried out by the CSIRO Division of Land and Water. The sample for analysis was oven-dried at 105°C, and approximately 1-2 g of each sample was accurately weighed with 4 g of 12-22 lithium borate flux directly into Pt/Au crucibles. The mixture was then heated slowly to 700°C to oxidise the organic matter, and then further heated to 1050°C for 12 minutes. The resulting melt was poured into a 32 mm Pt/Au mould heated to a similar temperature. The melt was cooled quickly over a compressed air stream and the resulting glass disks were analysed on a Philips PW1480 wavelength dispersive XRF system using a dual anode Sc/Mo tube and algorithms developed at CSIRO Land and Water.

3.5.4 Scanning Electron Microscopy-Energy Dispersive Spectrometry

Scanning Electron Microscope with Energy Dispersive Spectrometry (SEM-EDS) was employed to determine qualitative information regarding the arrangement of various elements within the agglomerate structure. Agglomerates were mounted in resin and placed in a vacuum oven to ensure that the resin reached all open pores. Finished samples were cut using a diamond saw to obtain cross-sections for mounting on stubs. Samples were carbon coated to reduce charging of the sample. The samples were then inserted into a Philips XL30 Field Emission Gun Scanning Electron Microscope, operating in backscattered electron (BSE) mode using an accelerating voltage of 20 kV and a beam spot size of 5. Point analysis could then be carried out using Energy Dispersive Spectrometry so that specific mineral structures could be identified. Further to this, an X-Ray Mapping (XRM) function in the Scanning Electron Microscope software was used to gain overall elemental distribution data for each selected area.

3.5.5 Particle Size Distribution and Extent of Agglomeration

The particle size distribution for each sample of bed material collected was quantified using the Rosin-Rammler particle size distribution method (Rosin and Rammler, 1933), as shown in Fig. 3.8 for the feed coal. This method enables a straight curve to be drawn through the distribution of any natural body of particles. Note that distribution curves will have slight curvature at the extremes of the line, which is a result of particles neither tending towards infinitely large nor infinitely small sizes (Rosin and Rammler, 1933). The axes on a Rosin-Rammler distribution plot are determined using the calculation method as in Equation 3.1.

$$x = \log(\text{Sieve aperture}, \mu\text{m})$$
$$y = \log\left[\log\left(\frac{100}{\text{Residual particle mass on sieve}, \%}\right)\right] \quad (3.1)$$

Of particular interest from the Rosin-Rammler plots are the gradients and y-intercepts of the curves produced, as these allow comparisons between experiments regarding the coarseness and distribution of larger particles within the beds. For instance, an increase in the particle mass of larger size fractions (and hence a decrease in finer particle mass) brought about by agglomeration would be indicated by a decrease in the gradient of the distribution curve. While the Rosin-Rammler technique is useful for particle size distribution analysis, no evidence has been collected regarding the use of the Rosin-Rammler method for characterisation of effect of agglomeration and defluidisation on bed material from a fluidised bed.

The extent of agglomeration is determined using a sieving technique. The mass percentage of each bed that exists above the top size of coal, namely 3.35 mm diameter, which gives an indication as to the approximate amount of agglomerates forming in the bed for each run. This method can also be used in conjunction with results obtained from the Rosin-Rammler technique to give an overall view of any particle growth taking place in beds, and hence the extent of agglomeration.

3.5.6 Micro Gas Chromatograph

Gas analysis was performed in order to verify that gasification conditions were being achieved with the defined experimental settings. An Agilent Technologies Micro GC 3000A was used to perform online analysis of gas during selected experiments. The Micro GC is a 2-channel instrument, with specifications for each column summarised in Table 3.2. For the experiments in which gas analysis was performed, a small portion of gas from the condenser outlet was extracted and passed through the Micro GC, with measurements collected every 1.5 minutes.

Table 3.2. Agilent 3000A Micro GC column and operating specifications

Specification	Units	Channel A	Channel B
Type of column	-	PLOT Q	Molecular Sieve
Sample inlet temperature	°C	90	90
Injector temperature	°C	100	100
Column head pressure	psi	43.0	44.0
Column temperature	°C	108.0	114.0

CHAPTER 4

PHYSICAL MECHANISM OF AGGLOMERATION AND DEFLUIDISATION FOR SPOUTED BED GASIFICATION OF A HIGH-SODIUM, HIGH-SULPHUR CONTENT LIGNITE

4.1 Introduction

This chapter presents an investigation into the mechanism of agglomeration and defluidisation of South Australian lignite under spouted bed gasification conditions. The investigation was designed to address the following areas:

- To account for bed behaviour via visual observations and process monitoring;
- To assess particle growth occurring during gasification; and
- To identify the impact of gasifier operating parameters on agglomeration and defluidisation, including bed temperature, superficial velocity, air-to-fuel ratio (A/F), steam-to-fuel ratio (S/F), steam concentration in the fluidising gas, and inorganic content of the bed matter.

Combining analyses from these areas will provide a basis for identifying the physical mechanisms of agglomeration and defluidisation, and to quantify their occurrence.

4.1.1 Experimental Program

As indicated in Chapter 3, experiments were performed in a 77-mm diameter, atmospheric pressure, spouted bed gasifier. Three separate experimental sets were designed to investigate agglomeration and defluidisation during gasification of lignite containing high

sodium and sulphur compositions. The preliminary set of experiments ('Set B') was designed to gain an overview of gasifier bed behaviour over a wide range of operating settings. The second set of experiments ('Set A') was designed to target the operating conditions that were shown to be conducive to agglomeration and defluidisation in the preliminary experimental set. The final experimental set ('Set C') was constructed to investigate the impact of high steam content in the fluidising gas on spouted bed behaviour. Each experimental set is described in greater detail in the following sections. The general method followed for calculating operating parameters in each experimental set is detailed in Appendix A.

Experimental Set: Overview of Gasification Behaviour

The operating conditions for the preliminary experiments were chosen to correspond with gasifier operating parameter values from the literature, shown in Table 2.4, Chapter 2. The experimental settings for 'Set B' experiments are shown in Table 4.1. Each experiment was conducted over a period of 4 hours run time regardless of whether agglomeration and defluidisation were detected. Only one run was operated for less than 4 hours; Run B05 was stopped after 3.7 hours due to equipment safety concerns as the bed temperature increased above 1000°C. The maximum coal feed rate was limited to approximately 1 kg/hr (dry basis) in order to avoid unsteady state increase of the bed height, given that no bed material removal during experiments is undertaken.

Table 4.1. Experimental operating conditions for evaluating agglomeration and defluidisation behaviour during spouted bed gasification of Lochiel coal

Run	Run Time (hr)	Coal rate (db) (kg/hr)	Air rate (LPM)	Steam (g/min)	U_s (m/s)	Air/ Fuel (wt/wt)	Steam/ Fuel (wt/wt)	Steam conc (wt%)	$T_{furnace}$ (°C)	$T_{bed\ max}$ (°C)
B01	4.0	1.09	33.5	7.1	0.59	2.2	0.4	15.1	775	831
B02[ab]	4.0	0.75	30.0	6.4	0.57	2.8	0.5	15.2	825	914
B03	4.0	0.88	31.2	7.4	0.57	2.5	0.5	16.7	775	844
B05[ab]	3.7	0.75	27.0	6.5	0.50	2.5	0.5	16.7	775	861
B06	4.0	0.83	29.5	7.1	0.51	2.5	0.5	16.7	675	789
B07	4.0	1.09	32.5	6.9	0.57	2.1	0.4	15.3	775	823
B08[ab]	4.0	0.88	34.4	6.7	0.62	2.8	0.5	14.2	775	887
B09	4.0	1.27	34.0	8.2	0.60	2.0	0.4	16.3	750	799
B10	4.0	1.05	32.0	6.8	0.58	2.2	0.4	15.1	825	872
B11	4.0	0.92	36.5	7.7	0.64	2.8	0.5	15.2	675	826
B12	4.0	0.88	31.4	7.4	0.61	2.5	0.5	16.7	825	910

(a) Defluidisation detected.
(b) Agglomerates detected.

Bed temperature was the main variable of interest in the preliminary experiments. Bed temperature was indirectly controlled by adjusting both the A/F ratio and external furnace temperature. Each of coal feed rate, air flow rate and steam flow rate were varied in order to alter A/F values between experiments. Air flow and steam flow rates were constrained by both superficial velocity and steam concentration of the fluidising gas, while coal rate was constrained by the lack of bed material removal during experiments.

The desired velocity for most of the experiments was 0.60 m/s (i.e. double the nominal minimum spouting velocity), with 0.50 m/s set for runs B05 and B06. The flow rates for steam and air required to achieve the desired superficial velocities were calculated using estimated bed temperatures prior to experiments, which were subsequently corrected for temperature following each experiment.

Experimental Set: Investigation of Agglomeration and Defluidisation Operating Conditions

Operating conditions identified as being conducive to agglomeration and defluidisation in preliminary experiments were used as a basis for the following set of experiments. These secondary experiments were designed to investigate, in greater detail, the operating conditions that were shown to contribute to agglomeration and defluidisation, namely high bed temperatures. Operating parameters used for these secondary experiments are shown in Table 4.2. Steam concentration and coal feed rate were the constraining variables to which the remaining operating parameters were set, with superficial velocity allowed to vary accordingly.

Table 4.2. Experimental settings for investigation of agglomeration region as identified in preliminary experiments

Run	Run Time (hr)	Coal rate (db) (kg/hr)	Air rate (LPM)	Steam (g/min)	U_s (m/s)	Air/ Fuel (wt/wt)	Steam/ Fuel (wt/wt)	Steam conc (wt%)	$T_{furnace}$ (°C)	$T_{bed\ max}$ (°C)
A01	4.0	0.92	35.3	6.2	0.65	2.7	0.4	13.1	825	926
A02[a]	4.0	0.77	32.9	5.0	0.59	3.0	0.4	11.5	825	920
A03[ab]	4.0	0.77	38.2	5.2	0.68	3.5	0.4	10.3	825	939
A04[ab]	4.0	0.77	35.0	5.2	0.65	3.2	0.4	11.1	825	967
A05[ab]	4.0	0.77	35.0	5.2	0.62	3.2	0.4	11.1	775	915
A06[ab]	4.0	0.77	35.0	5.2	0.61	3.2	0.4	11.1	725	909

(a) Defluidisation detected.
(b) Agglomerates detected.

Experimental Set: Effect of Steam on Agglomeration and Defluidisation

One of the major findings from Kosminski (2001), as identified in Chapter 2, is that steam enhances the agglomeration potential of high sodium lignite in a gasification atmosphere. His work has yet to be validated in a fluidised bed environment, and as such the impact of steam on agglomeration and defluidisation of lignite with high sodium content is the focus of further experiments.

Operating parameter settings for 'high steam' experiments are shown in Table 4.3. All experiments were conducted over 4 hours. Steam concentration of the fluidising gas was controlled at a constant level (approximately 91 wt% steam in air), with bed temperature varied across the experiments. The external furnace set point temperature was primarily used to control bed temperature.

Table 4.3. Experimental operating conditions to elucidate the effect of steam on agglomeration and defluidisation during gasification

Run	Run Time (hr)	Coal rate (db) (kg/hr)	Air rate (LPM)	Steam (g/min)	U_s (m/s)	Air/ Fuel (wt/wt)	Steam/ Fuel (wt/wt)	Steam conc (wt%)	$T_{furnace}$ (°C)	$T_{bed\ max}$ (°C)
C01[a]	4.0	0.31	2.50	30.8	0.59	0.6	6.1	91.3	1000	811
C02[a]	4.0	0.25	2.54	31.3	0.59	0.7	7.5	91.2	1000	791
C03[a]	4.0	0.52	2.54	31.3	0.63	0.4	3.6	91.1	1050	861
C04	4.0	0.20	2.81	34.7	0.64	1.0	10.5	91.3	950	759
C05[a]	4.0	0.55	2.50	30.5	0.63	0.3	3.3	91.2	1075	891

(a) Agglomerates detected.

Experimental Summary

The experimental program described in Section 4.1.1 enables an assessment to be conducted regarding the impact of the following criteria on agglomeration and defluidisation:

- Bed temperature;
- Superficial velocity;
- A/F ratio and S/F ratio; and
- Steam concentration of the fluidising gas.

In particular, the experiments were designed to emphasise the effect of steam on agglomeration and defluidisation. Experiments from Set A and Set B were operated with S/F ratios that are within the range of values used in a 'typical' gasification reactor. Experiments from Set C were operated with high S/F ratios that would not be practical to

use in a typical gasification process. While these extreme S/F ratios in the Set C experiments do not represent realistic gasification conditions, they provide a basis for identifying the impact of steam on agglomeration and defluidisation behaviour. The results from the spouted bed gasification experiments allow the conclusions reported by Kosminski (2001), regarding the effect of steam on gasification of high sodium lignite, to be tested in an actual fluidised bed environment.

4.2 Physical Assessment of Bed Behaviour

4.2.1 Bed Operation Monitoring

Output gas analysis was performed in order to assess whether gasification was achieved in the bed with the operating parameters shown in Table 4.1 to Table 4.3. The flue gas off-take was located downstream of the condenser. Gasification was confirmed under each set of conditions, with key gasification species H_2 and CO detected in each case. Oxygen was not detected in the flue gas from any of the tests, indicating that all of the oxygen from the fluidising gas had reacted within the bed. Table 4.4 shows the composition ranges of gas species in the flue gas from the gasifier.

Table 4.4. Flue gas compositions for extremes in fluidising gas steam content i.e. 'Typical' steam gasification conditions (<20 wt% steam in the fluidising gas), and 'high' steam gasification conditions (~90 wt% steam in the fluidising gas).

Gas Component	Units	Typical steam gasification	High steam gasification
CO	mol% (d.b.)	8.5-9.5	6.2
CO_2	mol% (d.b.)	13.0-14.0	11.5
H_2	mol% (d.b.)	9.0-10.0	33.1
CH_4	mol% (d.b.)	0.5-0.7	0.7
H_2S	mol% (d.b.)	0.02-0.03	N/D

N/D – Not detected.

Hydrogen in the output gas varied significantly with the steam content of the fluidising gas. The hydrogen composition of the flue gas from high steam gasification conditions (i.e. approximately 90 wt% steam in the inlet fluidising gas) is over three times the composition in the flue gas formed under 'typical' steam gasification conditions (i.e. less than 20 wt% steam in the fluidising gas). Also, no H_2S was detected in the flue gas from high steam conditions, while H_2S formed 0.02 to 0.03 wt% of the flue gas composition under typical

steam gasification conditions. The lack of H_2S in the gas is a possible effect of the high moisture content of the gas exiting the bed in these cases. This moisture was removed as condensate from the condenser, and may have stripped the outlet gas of sulphur compounds. The high concentration of H_2 was most likely due to the large influence of the water-gas reaction (i.e. reaction of solid carbon with steam to form CO and H_2) and the shift reaction on output gas composition in the moist fluidising gas.

Steady-state gas composition was achieved after approximately 5 to 10 minutes operating time in most typical steam gasification experiments. Significantly longer operating time was required to achieve gas composition equilibrium under high steam conditions, at approximately 50 to 100 minutes of operating time. These differences appear to be related to the behaviour of bed temperature during gasification in each case, as discussed later in this section.

The state of spouting during gasification was primarily monitored using the bed temperature and the pressure drop from below the distributor to the freeboard. Based on findings in the literature, rapid and sustained changes in bed temperature and pressure drop indicate agglomeration and defluidisation (Siegell, 1984; Manzoori, 1990). Operating profiles from all experiments are presented in Appendix B. Each operating profile consists of temperature readings from thermocouple sensors TC 1 to TC 5, measured from commencement of gasification to completion of the experiment. Sensor TC 1 is located below the conical gas distributor to the bed; TC 2 is located 35 mm above the gas inlet to the bed; TC 3 at 65 mm above the inlet; TC 4 at 105 mm above the inlet; and TC 5 at 155 mm above the inlet. Pressure drop across the bed is measured between two pressure tappings located just below the conical distributor and at a height of 185 mm above the conical distributor.

Steam content of the fluidising gas was found to influence the bed temperature and pressure drop profiles during operation. A typical operating profile from a stable spouting run operated with typical steam content in the fluidising gas is shown in Figure 4.1. This figure shows that from the commencement of gasification, the measured axial temperatures in the bed increased rapidly for an initial period of approximately 15 minutes before achieving relatively constant values for the remainder of the run. Pressure drop across the bed and distributor also increased initially before reaching a relatively steady value. A

comparatively longer time of operation was required in attaining a steady pressure drop, achieved after approximately 100 minutes of operation. The operating time required to achieve temperature equilibrium under each set of conditions corresponds to the time taken for gas compositions to equilibrate in each case. This behaviour demonstrates the effect of bed temperature on gas composition in the spouted bed.

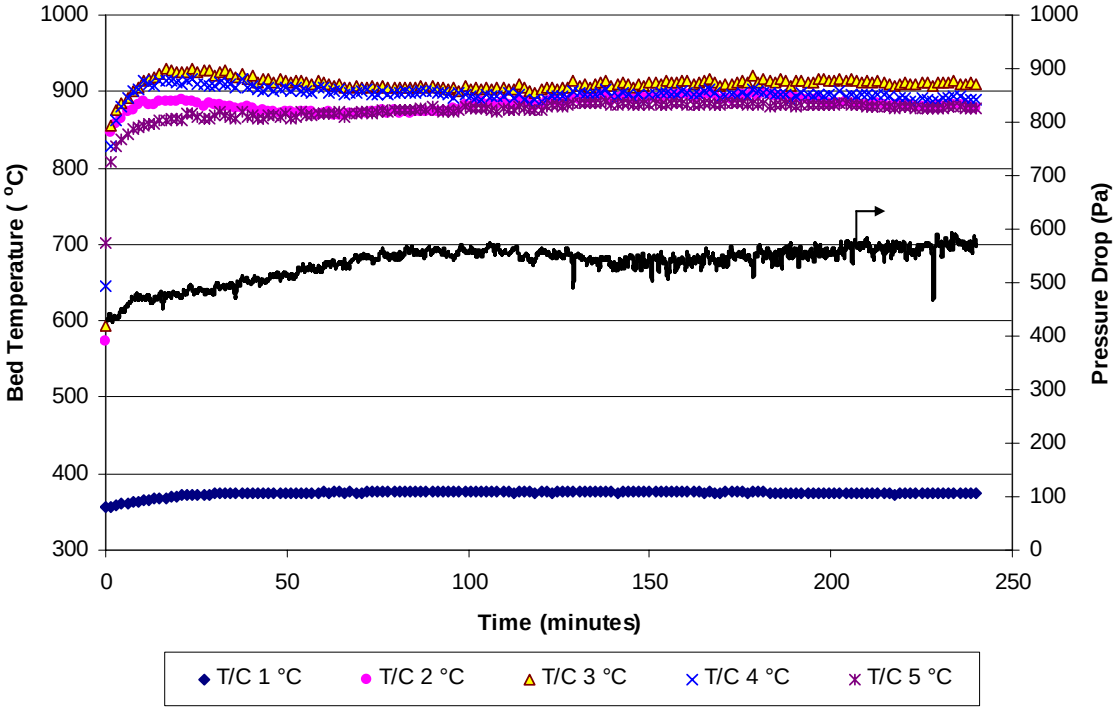

Figure 4.1. Bed temperature and pressure drop profiles for a stable-spouting experiment (Run B12).

An example of bed temperature and pressure drop profiles for high steam conditions is shown in Figure 4.2. While pressure drop behaved similarly to that of typical steam gasification experiments, bed temperatures showed a marked difference in behaviour. Temperatures measured at the top of the bed, namely at sensors TC 4 and TC 5, are shown to decrease rather than increase from the commencement of gasification. In particular, temperature measured at TC 5 decreased from approximately 840°C at time zero to a steady-state temperature of approximately 750°C after 70 minutes. The time taken for temperature to reach steady state corresponded to the time taken for pressure drop to stabilise.

The reason for the drop of temperatures measured at TC 4 and TC 5 appears to be related to the increase in bed height during the initial stages of each high steam run (i.e. 90 wt%

steam in the inlet fluidising gas). At the commencement of gasification, the initial charge of 40 g of char in the bed is sufficient to immerse only temperature probes TC 2 and 3 (i.e. initial bed height between 65 and 105 mm above the gas inlet), leaving TC 4 and 5 measuring only the temperature in the freeboard. The furnace temperatures used under high steam conditions are up to 400°C greater than those used under typical steam gasification conditions (refer to Table 4.1, Table 4.2, and Table 4.3), indicating that radiation heat transfer from the reactor walls is significantly greater under the high steam conditions. Thus, as the bed increases in height during the run, the char eventually shields thermocouples TC 4 and 5 from radiation from the walls, thereby resulting in a decrease of measured temperatures at these locations in the bed. In the case shown in Figure 4.2, the temperature measured at TC 4 enters a similar pattern of behaviour to TC 2 and 3 after approximately 40 minutes operating time, indicating that the top of the bed reached thermocouple TC 4 at this time. Similarly, the temperature measured at TC 5 conforms to the trends of the other temperature profiles after approximately 70 minutes of operation, indicating that the bed height had reached TC 5 at this time.

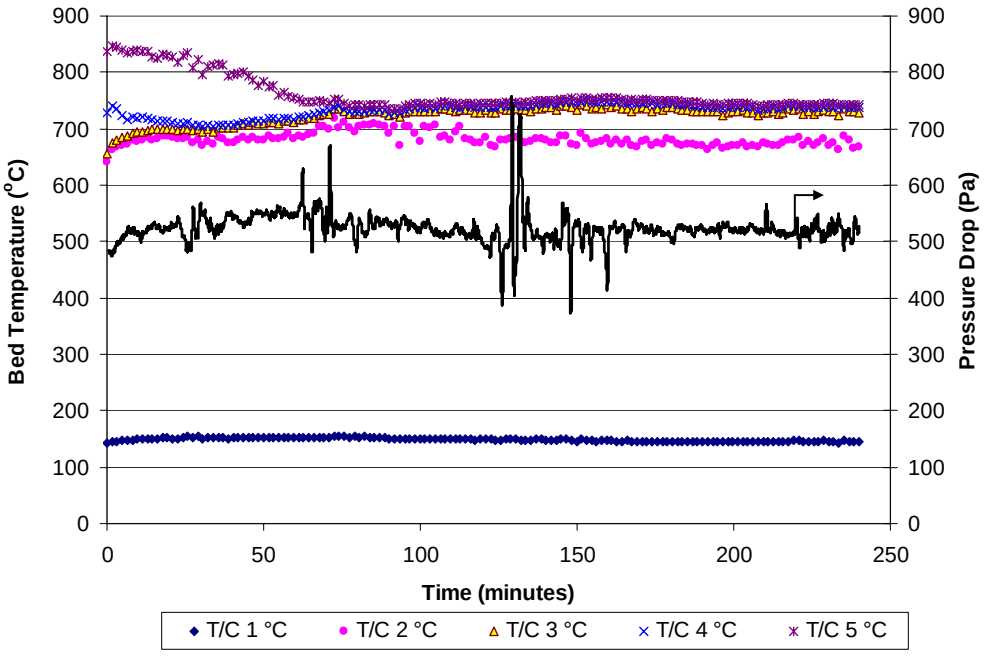

Figure 4.2. Bed temperature and pressure drop profiles for high steam gasification conditions (Run C04).

Typical bed temperature distributions for gasification experiments conducted using typical steam gasification conditions, and using high steam conditions, are shown in Figure 4.3a

and Figure 4.3b, respectively. Axial temperature distributions for spouted bed gasification, similar to Figure 4.3a, have been observed elsewhere (Watkinson et al., 1983). The maximum temperature shown in Figure 4.3a represents the location of the 'combustion zone' (Manzoori, 1990), which is submerged below the upper surface of the bed. Bed temperature distribution along the centreline of the bed of a high steam experiment is shown in Figure 4.3b. Maximum bed temperature in this case is located at the top of the bed, implying that heat from the walls causes the gas temperature to rise as it passes through the bed from the inlet. These observations indicate that maximum bed temperature is controlled via two main mechanisms, depending on the steam-air composition of the fluidising gas. These controlling mechanisms include:

- by combustion where steam is approximately less than 20 wt% in the fluidising gas; and
- by the combined influence of gas and wall temperature under 90 wt% steam conditions.

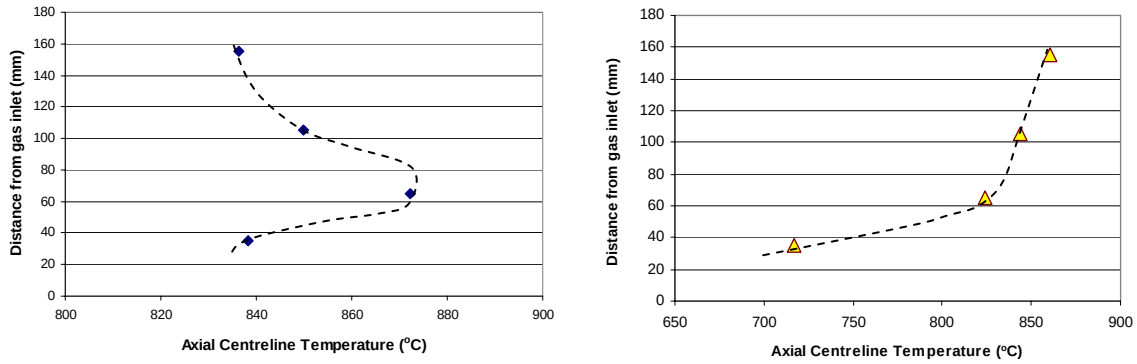

(a) (b)

Figure 4.3. Axial temperature distribution measured along centre axis of spouted bed vessel. (a) 15.1 wt% steam in the fluidising gas (Run B10); (b) 91.1 wt% steam in the fluidising gas (Run C03).

In the high steam runs, set point furnace temperatures were up to approximately 200°C greater than the defined maximum axial bed temperatures. However, temperature measurements of the furnace-side wall of the reactor vessel indicates that the shielding employed to avoid hotspots on the reactor wall was effective in reducing the radiation heat transfer from the elements to the thermocouple. Outer wall temperatures of the cylindrical section of the gasifier were found to be typically 150° to 200°C below the set-point furnace temperature, close to the nominal maximum bed temperatures assigned for each high steam run. These differences in measured temperatures suggests that the set-point temperatures

within the external furnace were higher than the actual temperatures acting on the spouted bed vessel due to radiation heat transfer.

4.2.2 Identification of Defluidisation

The occurrence of defluidisation, where applicable, was identified based on four main factors, which include:

- Significant increase in bed temperature following an initial period of steady temperatures;
- Significant decrease in pressure drop (from below the inlet to the freeboard) following an initial period of steady pressure drop;
- Ash agglomerates identified in the bed char extracted from the gasifier at the completion of the run; and
- Visual observations of loss of vigorous spouting motion in the bed (where possible).

The point of onset of defluidisation is subsequently identified based primarily on temperature and pressure drop monitoring data, and was found to vary widely after operating periods of between 30 minutes to almost 4 hours (i.e. total duration of the experiments).

In experiments operated with typical steam contents in the fluidising gas, defluidisation was clearly identifiable based on a rapid increasing temperature and decreasing pressure drop. All but one experiment operated with this level of steam in the fluidising gas showed agglomerate formation in the bed char at the completion of the experiment. Under high steam conditions however (i.e. 90 wt% steam), identification of the onset of defluidisation was complicated given that:

- No rapid rise of bed temperature was encountered; and
- pressure difference readings were affected by condensation of steam in the pressure lines.

However, the presence of agglomerates in each of the beds suggested that defluidisation did occur during operation under these high steam conditions.

Figure 4.4 shows an operating profile of a run displaying typical defluidisation behaviour. After approximately 100 minutes of operation, temperatures in the upper part of the bed (TC 3-5) increase rapidly, reaching approximately 1000°C. At the same time, pressure

drop across the bed decreased from approximately 800 Pa to 700 Pa over a period of approximately 40 minutes, indicating that defluidisation occurred gradually over time rather than in an instantaneous manner. This temperature and pressure drop behaviour corresponds to observations recorded by other authors on the occurrence of defluidisation (Gluckman et al., 1975; Siegell, 1984; Manzoori, 1990).

Following the initial bed temperature increase at the onset of defluidisation, certain temperature readings began to fall away. The temperature measured at the bottom of the bed (TC 2) dropped from 1000 to 700°C, while the temperature at the top of the conical section of the vessel (TC 3) fell to 850°C over a period of 100 minutes after the onset. The sensors at the two upper locations in the bed (i.e. TC 4 and TC 5) showed no sign of falling temperatures during the 4-hour period of operation. Observations of probes TC 2 and 3 following the experiments suggested that fouling of the probes caused the fall in measured temperatures at these locations. Figure 4.5 shows a photograph of the tip of TC 2, covered with a deposited layer of ash. Such coatings were found on both TC 2 and TC 3 probes, yet little was found on the temperature probes further up in the bed.

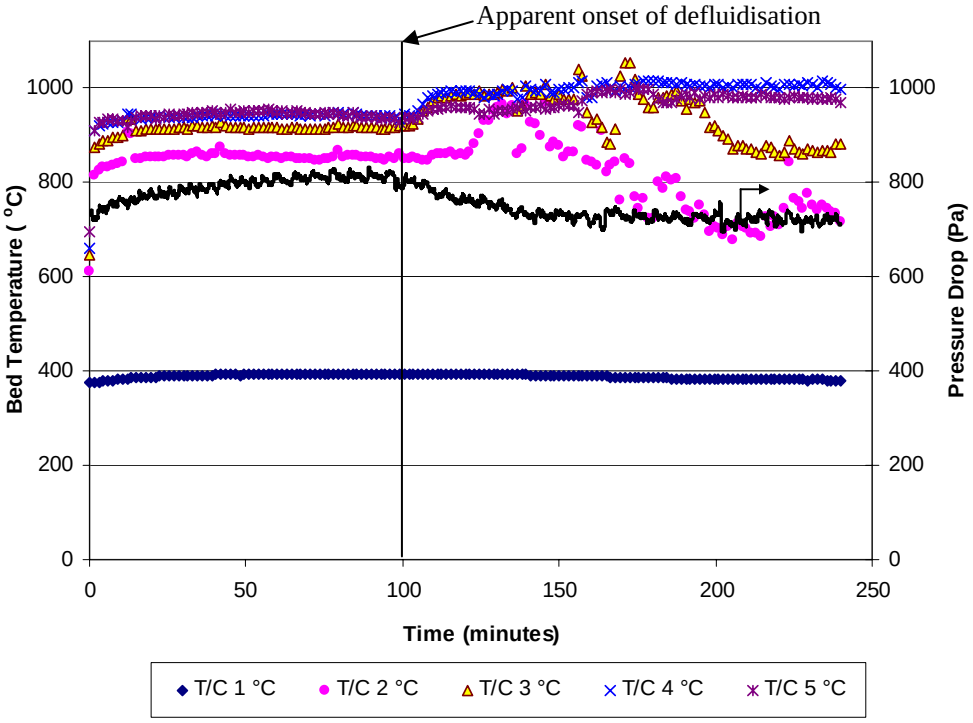

Figure 4.4. Bed temperature and pressure drop profiles for a run exhibiting defluidisation (Run A03).

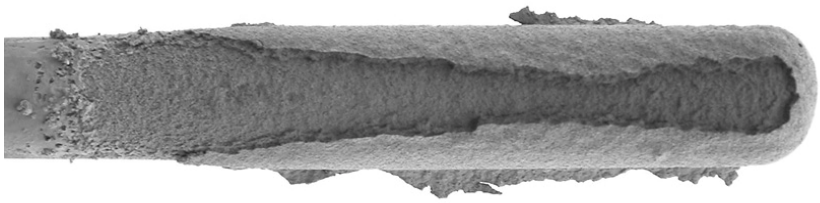

Figure 4.5. Thermocouple probe TC2 coated in deposited ash (completion of Run A03).

Only limited evidence of defluidisation was apparent from operating profiles of high steam experiments. None of the runs showed a rapid increase in temperature to signify defluidisation, suggesting the creation of 'hot spots' under typical steam gasification conditions is related to combustion reactions. Pressure drop measurement under high steam conditions was also affected by condensation in the pressure lines, which required manual purging with nitrogen to remove condensate. Due to this experience, difficulty was encountered in identifying specific evidence of decrease in pressure drop to signify defluidisation.

The highest temperature run in the high steam experimental set (Run C05, maximum bed temperature of 891°C), was the only experiment exhibiting defluidisation-like behaviour. Figure 4.6 shows a clear decrease in temperatures measured at TC 2 and 3, with a corresponding decrease in pressure drop across the bed, after approximately 50 minutes of operation. Pressure drop readings were particularly erratic in this run, reducing the ability for defluidisation behaviour to be accurately identified. Nevertheless, pressure drop decreased from approximately 600 Pa to 450 Pa over the remainder of the run following the decrease in temperature readings.

Agglomerates were found in all but one of the experiments in which defluidisation was identified, as indicated in Table 4.1. Run A02 (A/F = 3.0, S/F = 0.4, maximum bed temperature of 920°C) yielded no evidence of agglomerates in the char bed at the completion of the experiment, yet demonstrated possible defluidisation behaviour. The operating profile shown in Figure 4.7 shows increasing bed temperatures with decreasing pressure drop observed after approximately 220 minutes of operation. Runs B06 and B07 also showed a decrease in pressure drop towards the end of the run with no agglomerates yielded in the bed (refer to Appendix B). However, in these runs a partial blockage occurred in the gas outlet (after the condenser) as indicated by rising pressure within the

vessel, which appeared to directly affect pressure drop measurements. No such behaviour was observed in Run A02 however, suggesting that the rise in temperatures and fall in pressure drop was a result of defluidisation.

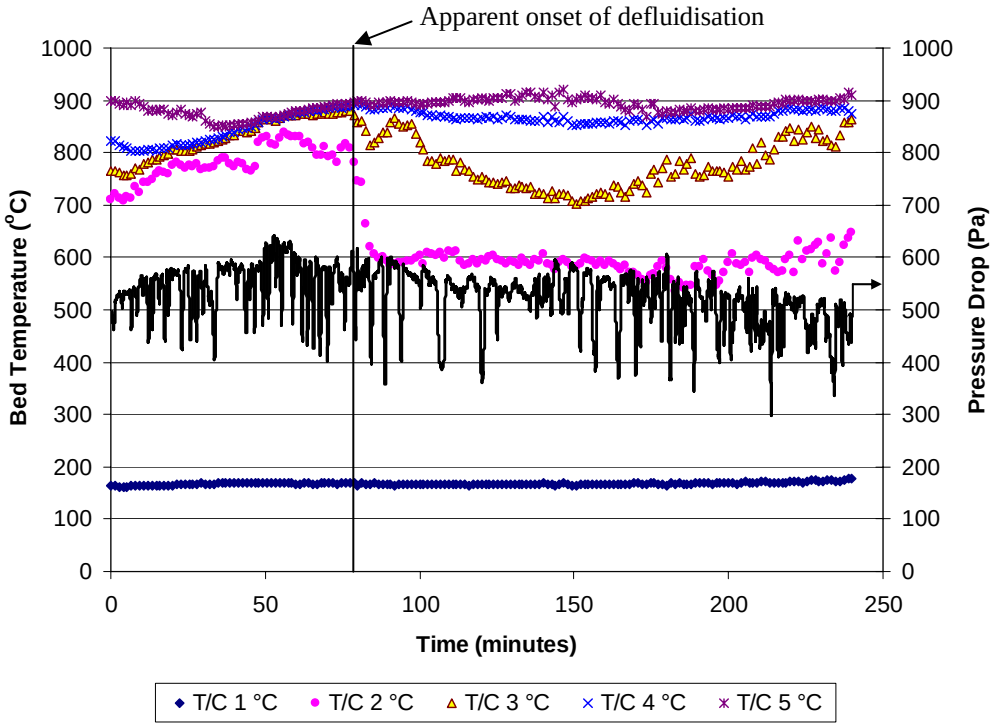

Figure 4.6. Defluidisation behaviour under high steam gasification conditions (Run C05).

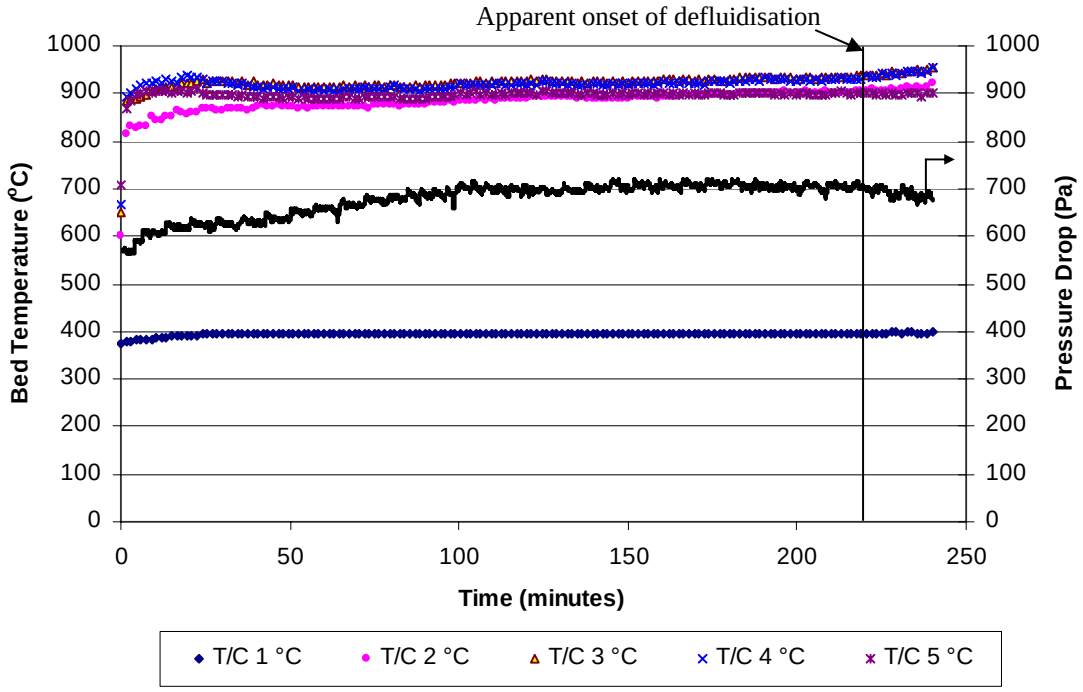

Figure 4.7. Bed temperature and pressure drop profiles for run exhibiting apparent defluidisation behaviour with no significant agglomeration encountered (Run A02).

The identified operating times at which defluidisation commenced for each run are shown in Table 4.5. Note that times for onset of defluidisation could not be accurately identified for the high steam runs. The percentage of bed mass exceeding the top size of the feed coal at the completion of each experiment is also included. The percentage was calculated by passing the bed material through a 3.35 mm aperture sieve and measuring the mass of particles retained on the sieve. By inspection, the retained particles consisted mostly of agglomerated ash, while little agglomerated ash was evident in the remaining char. The length of time before defluidisation onset is also given as a percentage of total operating time, accounting for Run B05, which was prematurely shut down before the full 4-hour run period used in other tests had been reached.

Table 4.5. Operating times before and after onset of defluidisation, and mass of particles exceeding 3.35 mm in diameter as a percentage of the total bed mass, for each experiment in which defluidisation and/or agglomeration was detected.

Defluidisation experiment	Operating time before onset of defluidisation (minutes)	Operating time after onset of defluidisation (minutes)	Mass of particles >3.35 mm as percent of bed mass (%wt)
A02	220	20	0.3
A03	100	140	26.3
A04	50	190	37.7
A05	195	45	4.6
A06	170	70	18.0
B02	120	120	40.0
B05	180	42	15.8
B08	170	70	27.2
C01	210?[a]	30?[a]	1.9
C02	?[a]	?[a]	1.1
C03	?[a]	?[a]	4.7
C05	50?[a]	190?[a]	8.6

[a] Onset of defluidisation times uncertain in high steam runs due to condensation in the pressure tapping lines.

The extent of agglomeration in each bed appeared to vary inversely with length of operation prior to defluidisation. Figure 4.8 indicates that as the period of stable spouting decreases, the proportion of bed mass present as agglomerates increases. Separate trends based on the steam concentration of the fluidising gas are also indicated. In typical steam gasification experiments (i.e. <20 wt% steam in the fluidising gas), the proportion of oversize agglomerated particles (i.e. >3.35 mm diameter) increases from negligible amounts where defluidisation occurred at the end of the 4-hour operating period, up to approximately 40% of the bed mass where defluidisation occurred within an hour of

commencing gasification. The estimated trend line (a) shown in Figure 4.8 indicates that the proportion of oversize agglomerates forming within a bed of pure char does not exceed 40% of the total bed mass in any case. This is likely due to the fact that smaller char particles continue to be charged to the spouted bed following the onset of defluidisation, while breakage of ash agglomerates may also occur during removal, which forms agglomerate fragments smaller than 3.35 mm.

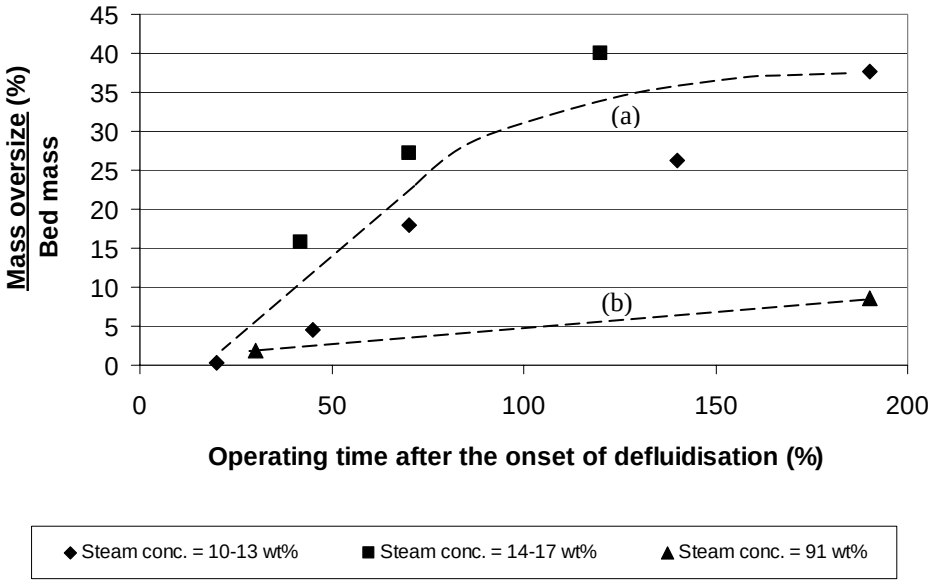

Figure 4.8. Percentage of agglomerates exceeding 3.35 mm diameter in each defluidised bed versus the time of operation before onset of defluidisation. (a) Approximate trend for typical steam gasification runs (Sets A and B); and (b) Approximate trend for high steam gasification runs (Set C).

Only two data points were available for high steam gasification experiments (i.e. Runs C01 and C05), and are approximate values only given the difficulty in identifying defluidisation under high steam conditions. However, these data points indicate agglomeration extent, as indicated by trend line (b) in Figure 4.8, is significantly reduced in comparison to typical steam gasification experiments for a given onset of defluidisation.

The reason for the difference in agglomeration extent between the different steam conditions may be directly related to the behaviour of the bed following defluidisation. In each experiment operated with typical steam gasification conditions, defluidisation resulted in an increase in bed temperature due to poor fluidisation. The higher rate of agglomeration in the bed that this would promote would result in a rapid upset of bed hydrodynamics. However, no such bed temperature increase was found in high steam runs that yielded

agglomerates. With increased viscosity of the melt phase in the ash under lower temperature conditions, this would likely result in a slower impact on spout hydrodynamics, and hence a more gradual loss of fluidisation.

Beyond the onset of defluidisation, bed temperatures reached in the bed often far exceeded the maximum bed temperatures achieved during stable spouting. Table 4.6 shows the maximum temperature of operation for each defluidisation experiment conducted with <20 wt% steam in the fluidising gas, and the corresponding maximum temperature achieved after the onset of defluidisation. Bed temperature after defluidisation is shown to be from 30 to 140°C greater than normal operating temperature under typical steam conditions, compared to negligible or negative temperature changes in high steam experiments. Thus, agglomeration extent has the potential to be much greater as steam content of the fluidising gas is decreased.

Table 4.6. Maximum bed temperatures before and after defluidisation for each defluidisation experiment operated with <20 wt% steam in the fluidising gas

Run	A/F ratio (wt/wt)	S/F ratio (wt/wt)	T_{max} before onset defluidisation (°C)	T_{max} after onset defluidisation (°C)
A02	3.0	0.4	920	954
A03	3.5	0.4	939	1055
A04	3.2	0.4	967	1036
A05	3.2	0.4	915	1042
A06	3.2	0.4	909	1034
B02	2.8	0.5	914	963
B05	2.5	0.5	861	954
B08	2.8	0.5	887	1023

4.2.3 Particle Growth

In the mechanism of agglomeration and defluidisation developed for fluidised bed combustion conditions, particle growth via agglomeration of 'inert' bed material was the main contributing factor to destabilisation of the bed, ultimately leading to defluidisation (Manzoori, 1990; Bhattacharya et al., 1999). However it is not clear whether the same mechanism also contributes to agglomeration and defluidisation during fluidised bed gasification of pure char beds.

The particle size distribution of each char bed was calculated and characterised using the method developed by Rosin and Rammler (1933). This gives an approximately straight-line distribution for any natural body of particles, allowing comparison of particle size

distribution in beds from different runs. Size distributions of bed char from typical gasification conditions are shown in Figure 4.9 and Figure 4.10, with distinction made between runs that defluidised (Figure 4.9), and those that demonstrated stable operation for the entire 4-hour period (Figure 4.10). Size distributions of char beds from high steam conditions are shown separately in Figure 4.11. The average feed coal size distribution is also shown on each plot to provide an indication of the change in size distribution during each run.

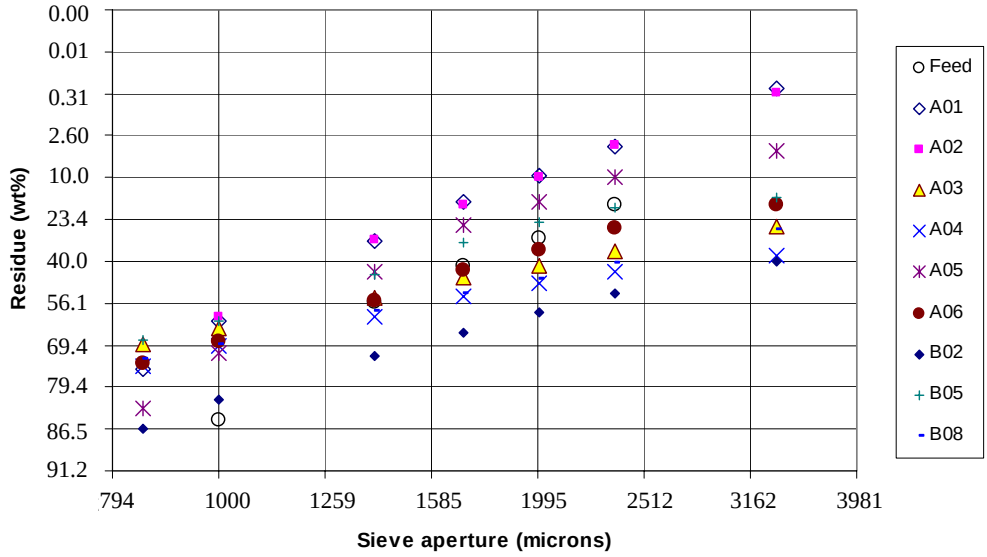

Figure 4.9. Rosin-Rammler particle size distributions for defluidisation experiments. Includes particle size distributions for feed coal and a non-defluidisation run (Run A01) for comparison purposes.

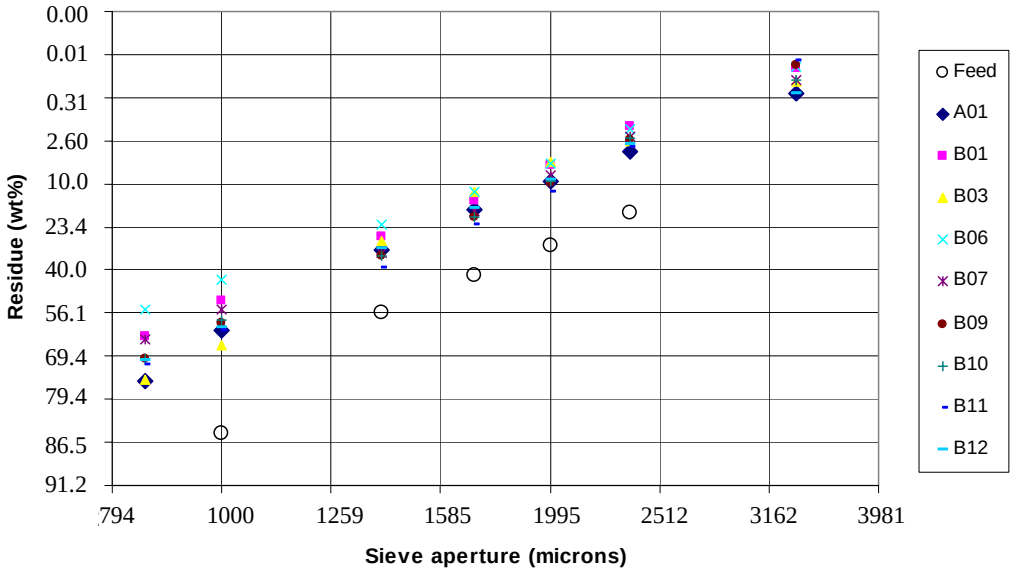

Figure 4.10. Rosin-Rammler particle size distributions for non-defluidisation experiments. Includes particle size distribution for feed coal.

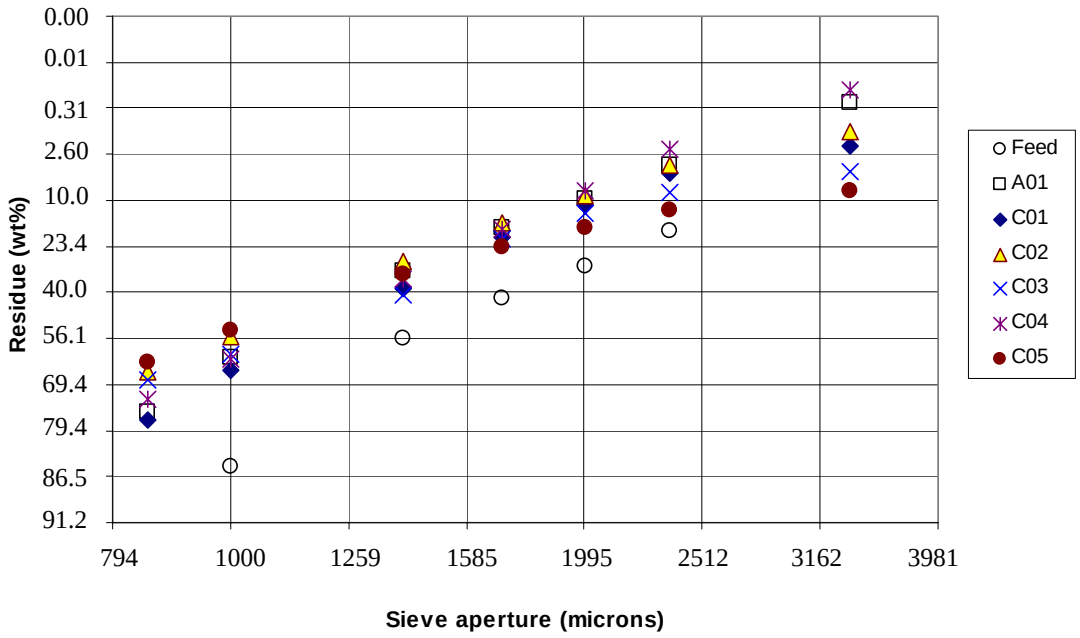

Figure 4.11. Rosin-Rammler particle size distributions for 90 wt% steam experiments. Includes size distribution of feed and Run A01 (13.1 wt% steam) for comparison purposes.

Size distributions of bed material from stable spouting experiments (Figure 4.10) appear to be relatively consistent regardless of experimental conditions, with only small variation in distribution apparent between each run. The distributions also appear to be relatively linear, with little evidence of curvature at the extremities of each distribution. The distribution of the coal feed is also shown on the plot, and exhibits significant curvature at the fine end of the body of particles. This curvature is due to the removal of fine particles from the feed, lowering the proportion of the bed weight in the finer size fractions. All of the bed char distributions lie to the left of the feed coal distribution in the plot area, indicating that the feed coal is coarser than the bed char. This is expected given that gasification involves the conversion of solid to gas, while fluidised bed motion results in particle size reduction due to particle fragmentation.

Defluidisation runs (Figure 4.9) show a significantly more diverse range of particle size distributions than non-defluidisation runs, with distribution lines varying widely in position on the Rosin-Rammler plot. Curvature is also apparent at the coarse size fraction end (greater than 3.35 mm size fraction) of each distribution, a result of agglomerate formation within the beds of these experiments. Some of the beds are significantly coarser than the feed coal, with distributions lying to the right of the feed coal distribution in the plot area. In high steam experiments (Figure 4.11), the distributions also show a pronounced

curvature at the coarse size fraction end for the runs that showed defluidisation behaviour. However, the positioning of the distributions on the plot area does not vary to the extent of the typical steam gasification experiments, possibly due to the lower percentage of agglomerates in the beds of the high steam runs.

In order to quantitatively assess the variation of size distribution with operating parameters, a trend line was determined for each body of particles. Particle size distribution lines were based on particle sizes at and below 2.36 mm only, neglecting any curvature existing at the coarse, 3.35 mm size fraction end of the trend line. This was to avoid skewing the plot lines of defluidisation runs as a result of the significant curvature at coarse fractions due to agglomeration. Table 4.7 shows the characteristics of particle size distribution curves for each char bed, namely the gradient and y-intercept.

Table 4.7. Gradient and y-intercept of Rosin-Rammler particle size distribution line for each bed material, including coal feed.

Rosin-Rammler curve parameters		
Run No.	Gradient	y-intercept
Feed coal	2.03	-6.99
Non-defluidisation		
C04	2.45	-8.05
B11	2.44	-8.06
B10	2.42	-7.96
B07	2.37	-7.80
B09	2.36	-7.77
B01	2.26	-7.36
B12	2.11	-6.93
B03	2.07	-6.76
A01	1.99	-6.57
B06	1.96	-6.37
Defluidisation		
C01	2.40	-7.94
C03	2.10	-6.99
C02	2.05	-6.72
A02	1.96	-6.46
A05	1.96	-6.58
A06	1.53	-5.41
C05	1.49	-5.03
B05	1.39	-4.82
B02	1.34	-5.06
B08	1.00	-3.80
A03	0.97	-3.62
A04	0.93	-3.59

Significant variation was observed in the size distributions of beds from defluidisation experiments. This variation also appeared to be affected by the content of steam in the fluidising gas. The average gradient of distribution lines for runs that defluidised under typical steam gasification conditions is 1.39, with a standard deviation of 0.42, giving a percentage variation of 30%. Defluidisation experiments conducted with high steam in the fluidising gas possessed an average gradient of 2.01, but with a standard deviation of 0.38, giving a comparatively smaller percentage variation of 18.9%. In comparison, all runs from stable spouting experiments yielded an average gradient of 2.24 and standard deviation of 0.19, or 8.6% variation, showing the relative consistency of these distribution trend lines between experiments. The similarity of trend line gradients from defluidisation runs under high steam experiments to those of stable runs reflects the relatively low quantity of agglomerates forming within these experiments.

The differences in positioning of the size distribution trend lines from defluidisation runs can be attributed to a number of possible factors, including time before defluidisation occurred, the temperature of operation, and relative velocity of the fluidising gas. Figure 4.12 shows the gradient of the Rosin-Rammler distribution from each defluidisation run plotted against the time at which defluidisation occurred. Runs from typical steam gasification conditions show a clear trend in size distribution, with gradient increasing for increasing operating time before defluidisation occurred. Although only two defluidisation points could be identified for high steam gasification runs, these also tend to show an increase in gradient for increasing operating time prior to defluidisation. These trends indicate that the particle size distribution becomes coarser (i.e. lower gradient) as the period of stable spouting achieved before defluidisation occurs becomes shorter. This trend can primarily be related to the amount of time the ash remains in the bed to coalesce and grow in size.

Plotting gradient against y-intercept for each trend line (Figure 4.13) shows that as gradient increases, the y-intercept of the trend line decreases linearly. Data points for stable spouting gasification runs are mostly collected in the lower right hand corner of the plot area, while data points for defluidisation runs are distributed towards the upper left hand corner. Thus, it is inferred that as particle size increases, the slope of the curve decreases. There also exists a ‘mixed’ region in the plot area where stable and defluidisation runs overlap, as indicated by the enclosed area in Figure 4.13.

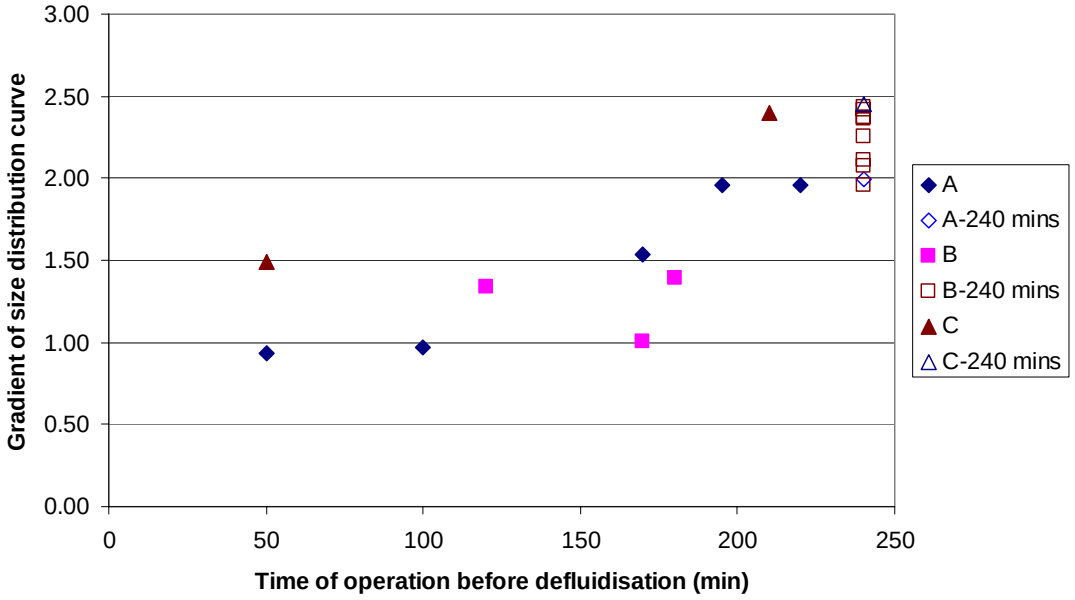

Figure 4.12. Gradients of each Rosin-Rammler particle size distribution versus time of operation prior to defluidisation. Runs which did not defluidise are indicated by hollow points at 240 minutes runs (i.e. maximum time of gasifier operation).

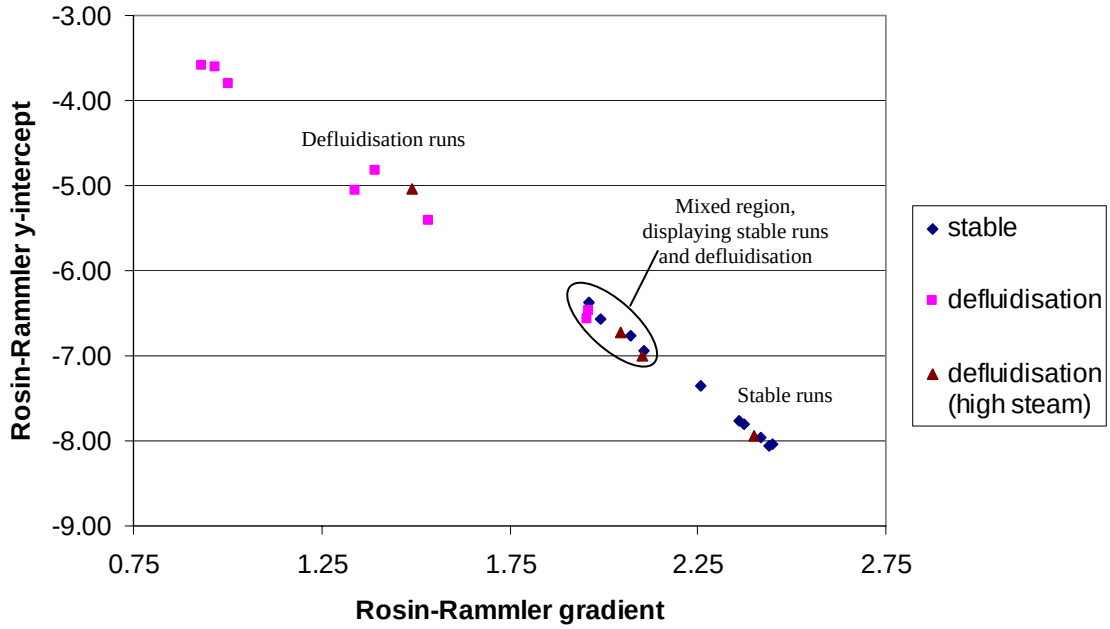

Figure 4.13. Rosin-Rammler size distribution curve parameters, y-intercept versus gradient. Stable and defluidisation runs indicated, including mixed region in which both stable and defluidisation runs are present.

Each of the stable runs in the enclosed stable-defluidisation 'mixed' region in Figure 4.13 show characteristics conducive to agglomeration and defluidisation, as identified in the literature. These include:

- Relatively low superficial velocity (i.e. B06 – gradient = 2.0, y-intercept = -6.4, at 0.51 m/s; and B03 – gradient = 2.1, y-intercept = -6.8, at 0.57 m/s); and
- High maximum bed temperature, exceeding 900°C (i.e. A01 – gradient = 2.0, y-intercept = -6.6, at 926°C; and B12 – gradient = 2.1, y-intercept = -6.9, at 910°C).

In addition to these characteristics, both of the defluidisation runs in the overlap region exhibited defluidisation at the latter stages of the runs, at approximately 195 minutes (out of 240 minutes) for Run A05 (gradient = 2.0, y-intercept = -6.6), and 220 minutes for Run A02 (gradient = 2.0, y-intercept = -6.5). These defluidisation times were greater than any of the other defluidisation runs from typical steam conditions, indicating that severe agglomeration was not able to proceed as extensively in these cases as in the other defluidisation runs. These findings provide evidence that during spouted bed operation there exists a critical particle size limit, whereby exceeding this limit results in defluidisation and rapid continued growth of agglomerates within the bed. This infers that defluidisation can be avoided if particle growth can be kept in check, by physical methods such as particle removal, and/or by limiting operating parameters such as bed temperature and superficial velocity to values which may reduce the rate of particle growth.

4.2.4 Visual Observations of Agglomeration and Defluidisation

The spouting action of beds in all experiments could be visually observed through the view port at the top of the reactor. Visibility through the sight glass was limited in the later stages of runs owing to deposition of elutriated fines from the bed on the underside of the sight glass. Complete coverage of the sight glass generally occurred after 30-60 minutes of operation. Stable spouting was confirmed in each experiment (prior to defluidisation, where applicable), with vigorous spouting of the bed observed. Stable spouting was characterised by a relatively even motion of particles from the centre of the bed towards the vessel wall (when viewed from the top of the bed).

In a limited number of cases, visibility through the sight glass was sufficient to allow a visual account of defluidisation. The onset of defluidisation was observed to commence with a noticeable destabilisation of the spout. This was characterised by irregular bursts of particle movement from the centre of the bed, with noticeable reduction of movement in

the annulus. Starting at the wall, this sluggishness spread towards the centre of the bed to complete the defluidisation process.

Sluggish particle movement at the walls appeared to create conditions favourable for agglomerate formation in the annulus of the bed. At the completion of experiments that displayed defluidisation behaviour, char with small agglomerates could be removed from the reactor via gravity, while larger agglomerates typically remained inside the spouted bed vessel. Inspection of the inside of the reactor showed a torus-shaped agglomerated mass collected around the wall in the most severe cases, as in Figure 4.14. This high-ash material could only be removed from the reactor vessel by manual breakage. This observation indicates that, as expected, agglomeration occurs primarily in the close-packed section of the bed.

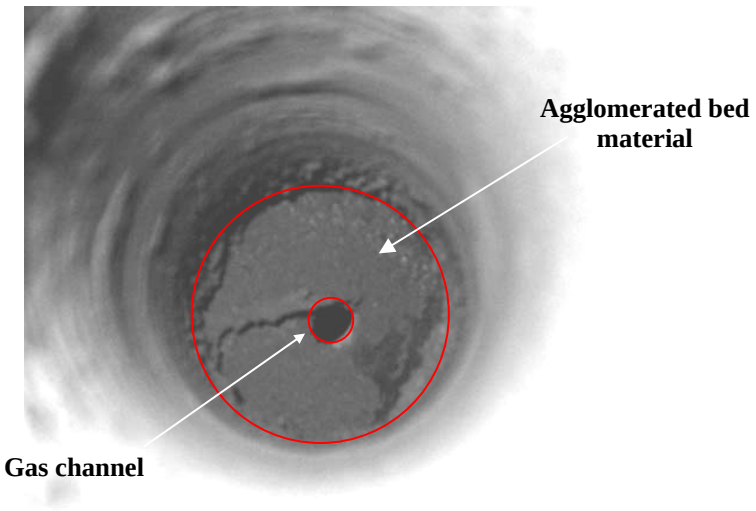

Figure 4.14. Top view of defluidised bed (Run A03) at completion of experiment.

Glowing char particles were visually observed to exit from the spout in all experiments operated under typical steam gasification conditions, regardless of whether defluidisation occurred. Glow of the bed increased in intensity following the onset of defluidisation, suggesting an increase in bed temperature. In contrast, no observation of glowing particles was made under high steam gasification conditions, with char particles retaining a dark colour throughout the bed. This observation suggests that the difference between particle temperature and bulk bed temperature is greater under typical steam gasification conditions in comparison to those of high steam experiments.

At the completion of most runs under typical gasification conditions, small ash particles of various sizes were observed in the char bed material, regardless of whether defluidisation affected operation. Typical examples of such particles are displayed in Figure 4.15 (other photographs of ash particles from the experiments can be found in Appendix C). The displayed particles exceed the top size of the feed coal (i.e. 3.35 mm diameter), indicating that they formed during gasification rather than entering the bed with the coal. These particles were observed to fall from the reactor first when the bed char was removed at the conclusion of each experiment, indicating that they had collected at the bottom of the bed during gasification. However, no such particles were observed in the beds from high steam gasification experiments.

Figure 4.15. Coated ash particles collected from bed char of Run A01 at completion of run.

Spherical ash agglomerates have been encountered in a previous study of spouted bed gasification of an Australian bituminous coal (Kikuchi et al., 1985). Closer examination of the particles from the spouted bed experiments reveal that they were not multi-particle agglomerates, but rather were single mineral particles coated in a light grey ash. Scanning electron microscopy (SEM), operated in backscattered electron (BSE) mode, was performed on cross-sections of the spherical ash particles. Preliminary phase identification in the images showed that the particles were composed of mineral grains coated in a silicate ash.

Electron micrographs of agglomerates collected in the present work suggest a similar structure to that observed by Kikuchi et al. (1985). Two different coated mineral particles are shown in Figure 4.16a and Figure 4.16b. Figure 4.16a shows a micrograph of a grain of

quartz surrounded by a coating comprised of a mixture of sodium, calcium, magnesium, and aluminium silicates. Figure 4.16b shows a particle of pure calcium sulphide surrounded by a silicate coating of similar composition to that in Figure 4.16a. The former type of particle was the most common coated mineral particle found in experiments; the latter coated particle was primarily found in runs operated at maximum temperatures approaching 800°C.

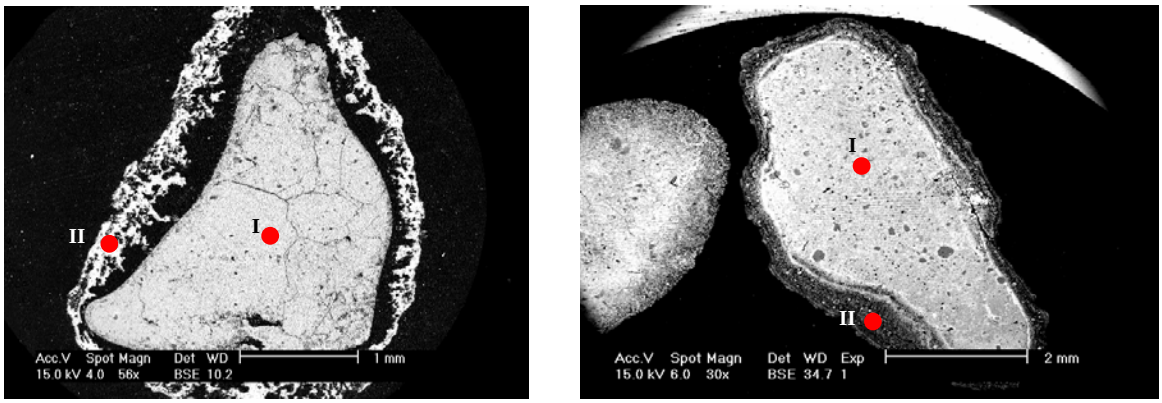

(a) (b)

Figure 4.16. Electron micrographs of a cross section of coated silica grain. Dark areas represent the resin used for sample mounting. (a) Cross section of a coated silica grain, ~3.5 mm diameter, from Run A02 (I – SiO2; II – Na, Ca, Mg, Al and Fe silicate mixture). (b) Cross sections of calcium sulphide grains, ~3 – 4 mm diameter, from Run B07 (I – $CaSO_4$; II – Na, Ca, Mg, Al and Fe silicate mixture).

The fact that average temperature at the bottom of the spouted bed in each experiment was typically 50 to 100°C lower than the maximum of the bed may be the primary reason that the large coated mineral particles shown in Figure 4.15 did not agglomerate, even in runs that showed agglomeration and defluidisation behaviour. Particles such as these were collected from the bottom of the bed at the completion of many typical steam gasification runs. Under the lower temperature conditions in this location of the bed, the ash may have been below its sintering point, resulting in the particles unable to sinter at a rate conducive to multi-particle agglomeration.

Despite coated mineral particles collecting at the bottom of the bed, the smooth nature of the coatings suggests that coating on mineral particles occurred as the particles were circulated in the bed via spouting. It may be that the mineral particles, which existed below the top size of the feed coal, were spouted freely initially, but progressively became coated as they circulated through the bed. Associated particle growth, and hence increase in weight, may have eventually prevented further circulation of the particles, and caused them

to rest at the bottom of the bed. Smaller mineral particles would continue to circulate as coating proceeds however, indicating that an ash deposition mechanism on such particles may be the cause of agglomeration and defluidisation in a spouted bed gasification environment.

Coated mineral particles appear to be the 'building blocks' of multi-particle agglomerates collected from runs that showed defluidisation behaviour. Agglomerates of various stages of sintering are shown in Figure 4.17a to Figure 4.17d.

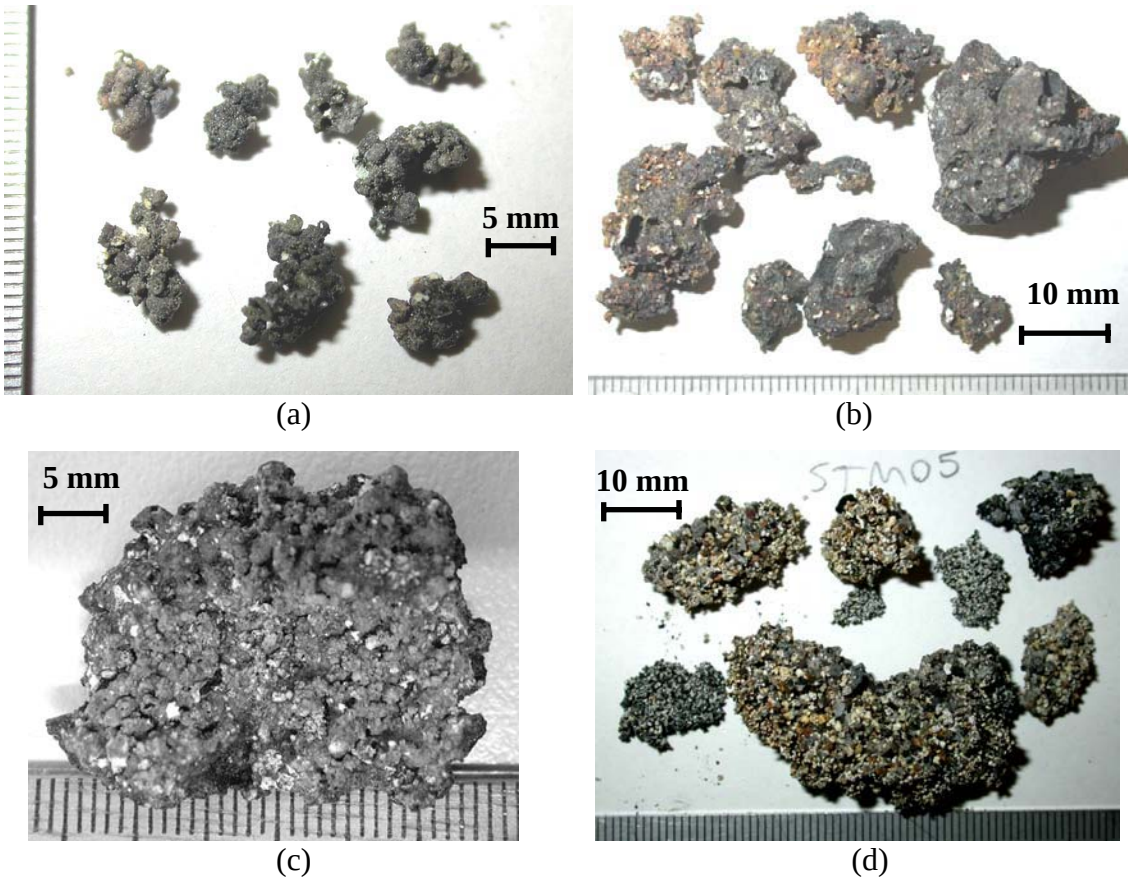

(a) (b)

(c) (d)

Figure 4.17. Typical ash bodies obtained from gasification experiments. (a) Loosely-bound agglomerates (Run A05); (b) Sintered agglomerates, >3.35 mm diameter (Run A04); (c) Surface of a highly-sintered agglomerate (Run B02) (d) Agglomerates from 90 wt% steam conditions (Run C05).

Agglomerates shown in Figure 4.17a were loosely bound structures, clearly showing the rounded shapes of the individual component mineral particles. The rounded lumps are shown to be significantly smaller than the coated particles of Figure 4.15, being less than approximately 1 to 2 mm in diameter in most cases. SEM analysis shown in Figure 4.18 corresponds to the suggestion that coated particles initiated agglomeration, with mineral particles, including silica and clay, shown bonded by a similar silicate coating to the one

covering individual mineral particles. Streaks of iron, which appear to be infused within the silicate coating, are also present, suggesting that iron was acting as a fluxing agent in the ash under the reducing conditions of the gasifier. No inclusions of organic carbon were detected, indicating that agglomerates were composed entirely of inorganic material. The loosely bound nature of these agglomerates indicates that sintering had not progressed to a significant extent before the experiment was concluded.

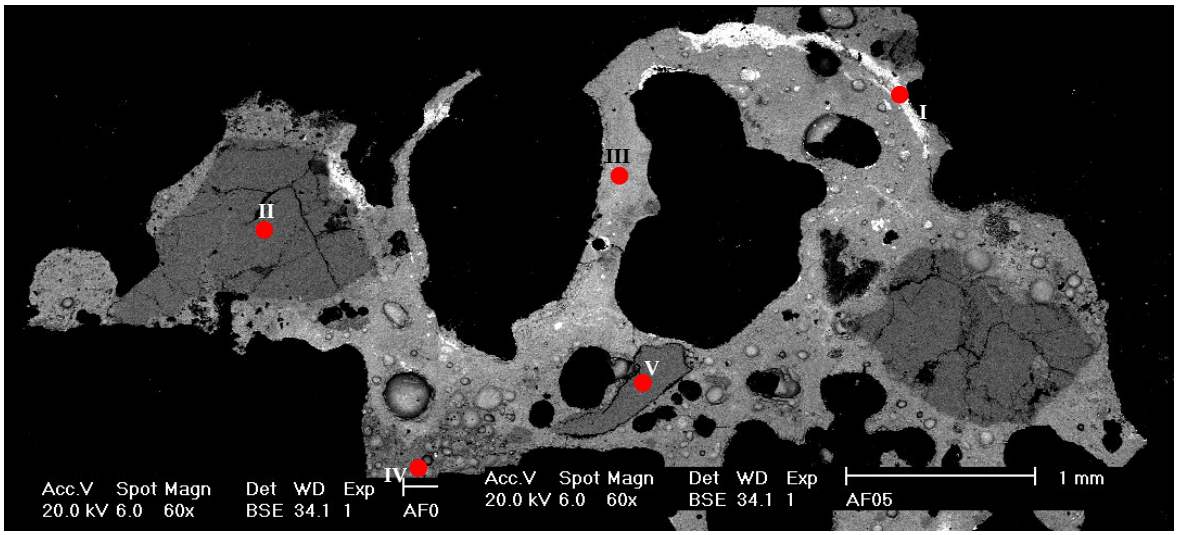

Figure 4.18. Backscattered electron image, cross-section view of loosely bound agglomerate from Run A05. Black areas represent mounting resin. (I – Iron compound; II – SiO2; III – Silicate coating mixture, combined with Na, Ca, Mg, Al and Fe; IV – Sodium aluminosilicate; V – Aluminosilicate).

The agglomerates shown in Figure 4.17b were highly fused structures, and were not as easily broken apart as the loosely bound agglomerates. Such agglomerates were typical of the ash bodies found adhering to the walls inside the reactor after shutdown had completed. A close-up view of the surface of one of the sintered agglomerates is shown in Figure 4.17c. The surface of the agglomerate is composed of small rounded lumps on its surface, much like those in the loosely bound agglomerates (Figure 4.17a).

A backscattered electron image of a highly sintered agglomerate is shown in Figure 4.19. As in Figure 4.18, the agglomerate is found to contain mineral particles surrounded by a silicate matrix. However, the silicate mixture surrounding the embedded mineral particles appears to constitute a much larger percentage of the cross-sectional area than in the loosely bound agglomerates. The ash matrix is also more uniform in appearance than that of the loosely bound agglomerates, which is consistent with the ash being maintained at

high temperatures for a relatively prolonged period, thereby enabling the mixture to coalesce.

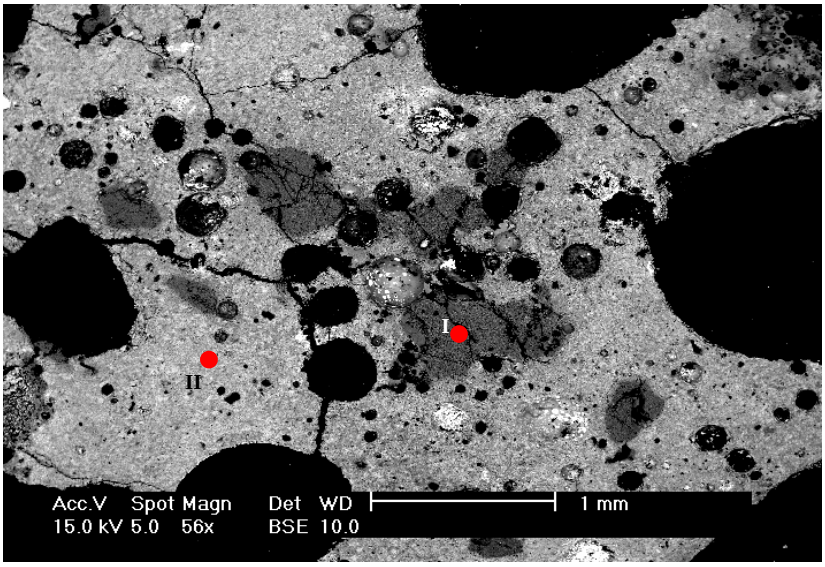

Figure 4.19. Backscattered electron image, cross-section view of highly sintered agglomerate from Run A04. Black area represents mounting resin. (I – SiO2; II – Silicate coating mixture, combined with Na, Ca, Mg, Al and Fe).

Agglomerates formed from high steam experiments showed noticeable differences in appearance to the agglomerates formed under typical steam gasification conditions. Figure 4.17d shows a number of agglomerates collected from the bed of Run C05 (U_s = 0.63 m/s, A/F = 0.3, S/F = 3.3, maximum bed temperature = 891°C). Agglomerates from these runs were still found to be composed of small mineral particles included in the structure. However, these particles did not appear to be evenly coated as for those formed under typical steam gasification conditions. The BSE image in Figure 4.20 corresponds to this observation, showing a highly porous structure as indicated by the black areas (i.e. mounting resin) interspersed throughout the structure. Much of the agglomerate structure consists of silica particles below 0.5mm diameter, which are joined by a thin layer of silicate material. Other mineral inclusions are also observed, such as a clay (aluminosilicate) particle, approximately 1.5 mm in diameter, and interspersed iron-rich phases. Preliminary phase identification suggests that the thin layer of coating is a silicate mixture composed mostly of sodium.

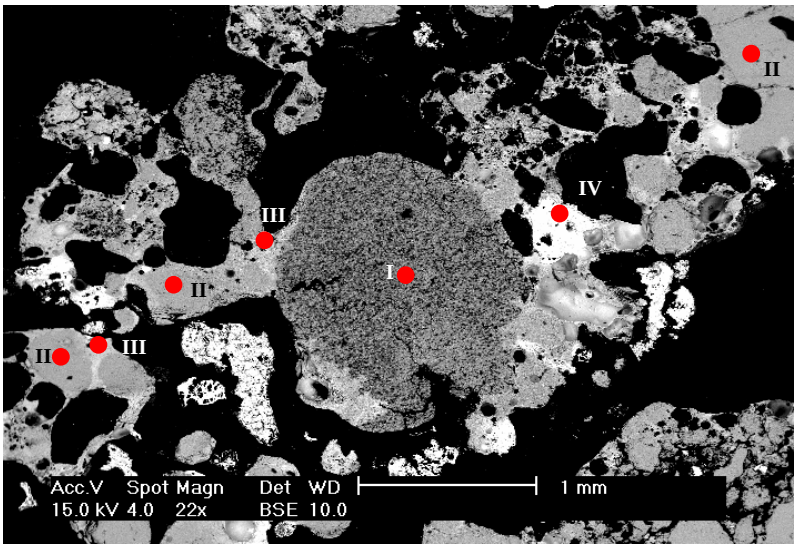

Figure 4.20. Backscattered electron image, cross-section view of agglomerate from Run C03. (I – Clay (aluminosilicate); II – SiO2; III – Sodium silicate; IV – Iron compound).

The preceding observations and preliminary analysis suggests that formation of molten silicate mixture was responsible for agglomeration and defluidisation of high sodium, high sulphur lignite during spouted bed gasification. This differs from the bonding phase associated with spouted bed combustion, where sodium and calcium sulphate eutectic mixtures forming coatings on bed particles. The silicate mixture formed under gasification conditions also appears to change in composition with the steam environment, with noticeably more sodium in the mixture at high steam gasification conditions. This provides preliminary evidence that conclusions arising from the fundamental study by Kosminski (2001), namely that steam promotes the formation of low melting sodium disilicate eutectics, are correct. Further detailed analysis of the chemistry surrounding agglomerate formation is required to assess this further. The results of chemical and mineralogical analyses of agglomerates are presented in Chapter 5.

4.3 Factors affecting agglomeration and defluidisation during spouted bed gasification of high sodium lignite

As identified in Chapter 2, difficulty exists in isolating individual gasifier operating parameters in order to observe the response of agglomeration to alteration of these variables. For instance, a change in air/fuel ratio necessitates either changing the flow rate of air, and/or changing the coal feed rate. This in turn may affect superficial velocity

through the bed, and may also impact upon bed temperature amongst other variables. In addition, certain variables have a direct influence on others, such as A/F ratio on temperature. The effects of important parameters on spouted bed gasifier operation are discussed in the following sections, with specific reference to agglomeration and defluidisation behaviour.

4.3.1 Bed Temperature and Air-to-Fuel Ratio

Bed temperature in the spouted bed gasifier is primarily influenced by two operating parameters: air/fuel ratio (A/F), and external furnace temperature (T_f). A plot of maximum bed temperature as a function of A/F is shown in Figure 4.21, with data points differentiated with respect to T_f. Under typical steam gasification conditions, for a given A/F the bed temperature increases as furnace temperature is increased. Similarly, increasing A/F for any given T_f results in a linear increase in bed temperature. Experiments from high steam conditions are located to the left of the other gasification experiments on the plot. In these experiments, A/F increases while T_f and bed temperature decreases, indicating that furnace temperature has a much more significant impact on bed temperature than A/F under high steam gasification conditions.

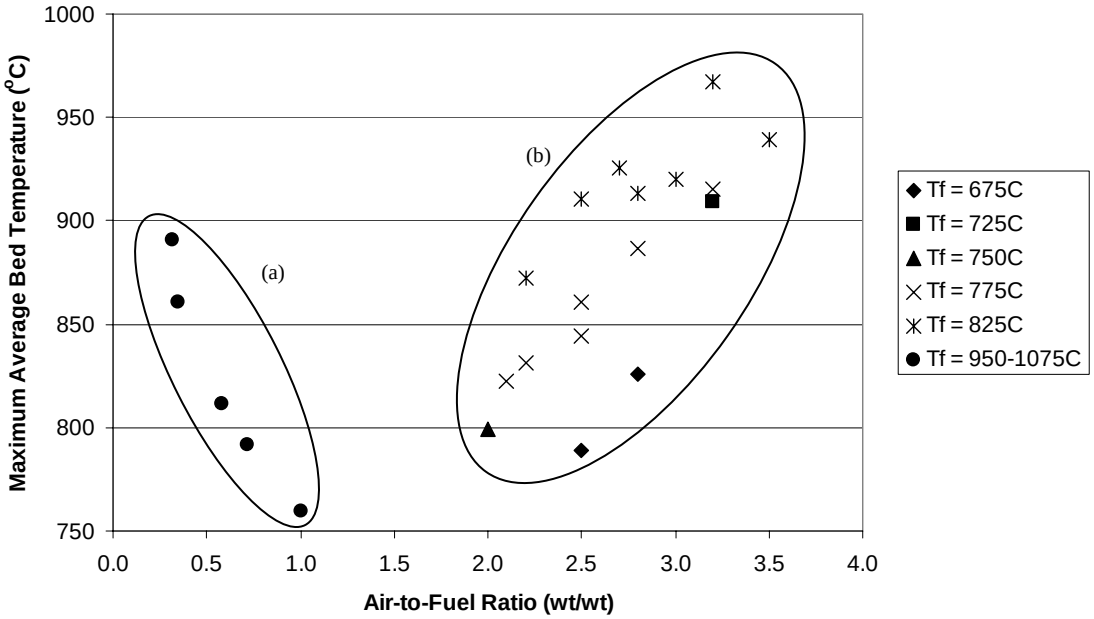

Figure 4.21. Maximum bed temperature as a function of air/fuel ratio for all spouted bed gasification runs, with respect to external furnace temperature. (a) high steam gasification conditions; (b) typical steam gasification conditions.

Each of the aforementioned parameters influences bed temperature by a different mechanism. Increasing T_f increases the wall temperature of the reactor, thereby supplying heat both to particles as they circulate, and to fluidising gas as it passes upwards through the reactor vessel. In contrast, A/F determines the amount of oxygen available to the bed for combustion. Thus, increasing A/F results in more heat released to the bed per unit mass of fuel.

An alternative version of the plot of bed temperature as a function of A/F is shown in Figure 4.22, with each point differentiated with respect to steam concentration of the fluidising gas (i.e. 10-13 wt% steam in the fluidising gas, 14-17 wt% steam, and 90 wt% steam). The enclosed points indicate defluidised runs.

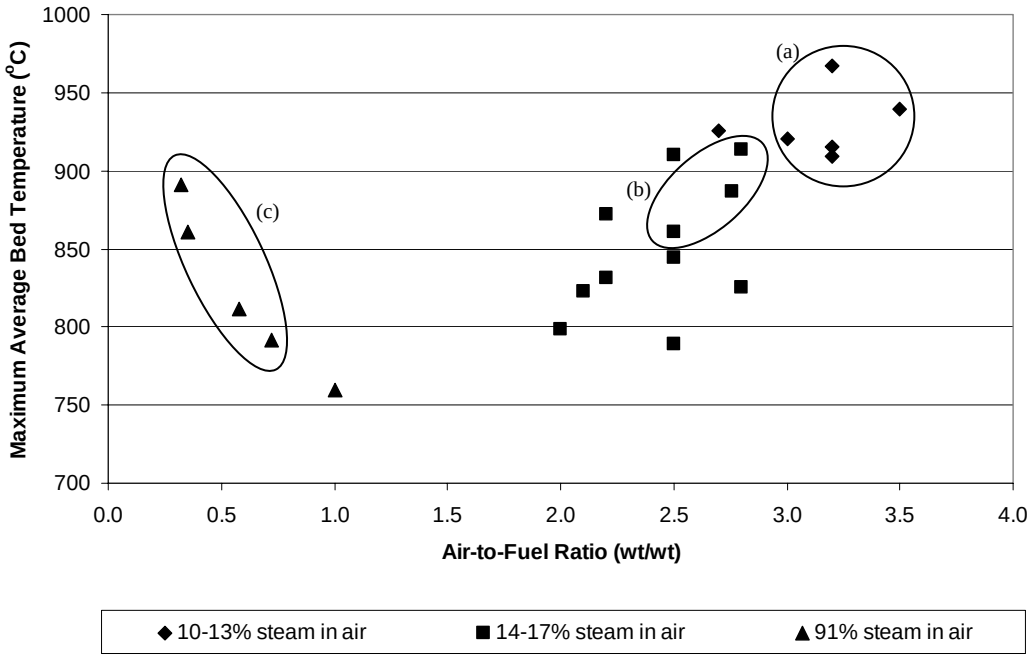

Figure 4.22. Air/fuel ratio versus maximum bed temperature for all spouted bed gasification runs as a function of external furnace temperature. Defluidisation runs indicated by enclosed areas; (a) 10-13 wt% steam gasification; (b) 14-17 wt% steam gasification; (c) 90 wt% steam gasification conditions.

The plot shows that the minimum temperature at which defluidisation initiates decreases from low to high steam concentration. In the set of experiments run under 10-13 wt% steam conditions (refer to Table 4.2 for operating parameters), the minimum temperature of defluidisation is approximately 910°C; under 14-17 wt% steam conditions (Table 4.1), defluidisation occurs as low as approximately 860°C; and under 90 wt% steam gasification conditions (Table 4.3), agglomeration and defluidisation is observed as low as

approximately 790°C. While Figure 4.22 appears to suggest that increasing steam concentration of the fluidising gas decreases the minimum defluidisation temperature, it also indicates that steam is not the only deciding factor in occurrence of agglomeration and defluidisation.

Of the 10-13 wt% steam experiments, Run A01 was operated with T_f of 825°C and an A/F of 2.7, contributing to a maximum bed temperature of 926°C – above the minimum defluidisation temperature for this experimental set – yet showed no sign of agglomeration and defluidisation for the 4-hour run period – although, as mentioned in the preceding section, particle growth was observed within the bed relative to other stable spouting experiments. However, the other runs in the set were operated at or above A/F of 3.0, indicating that the lower A/F in Run A01 may have reduced the agglomeration propensity experienced in the run. The reason for this effect may be due to the rate of char consumption that the A/F promotes. Kosminski (2001) showed that ash forms uniformly throughout char grains when placed in a gasification environment, and suggested that by removing unburnt char from the gasifier, ash could also be removed from the bed, and hence agglomeration potential may be reduced. Hence, increasing A/F – and thus increasing the rate of char consumption via combustion – may be accompanied by a greater level of ash released to the bed, and so agglomeration may proceed more readily.

Two runs from Set B (Runs B10 and B12) were operated above the minimum defluidisation temperature of 860°C, yet showed no sign of defluidisation. Run B10 was operated at 872°C, but at A/F of 2.2, suggesting that the level of char consumption was not sufficient to initiate agglomeration during the 4-hour experiment. Run B12 was operated with T_f of 825°C and A/F of 2.5 to give a maximum bed temperature of approximately 910°C, but did not defluidise – although, as mentioned above, did show relative particle growth within the bed, suggesting that agglomeration and defluidisation may have eventually impacted upon operation. However, Run B05 was also operated at A/F of 2.5, but at lower T_f (775°C) and maximum bed temperature (861°C), and did show defluidisation behaviour. The major difference between Runs B05 and B12 is superficial velocity, at 0.51 and 0.61 $m.s^{-1}$ respectively. The lower superficial velocity of Run B05 would have contributed to a reduced relative particle momentum, and hence a greater propensity to agglomerate, even though bed temperature was lower. Thus, superficial velocity appears to have influenced the time of defluidisation in these cases.

High steam experiments showed a different trend to the typical gasification condition runs, with the only run not to show agglomeration and defluidisation (i.e. C04) operated at the highest A/F (1.0) and the lowest maximum bed temperature (759°C) of all high steam gasification experiments. Note however that, as discussed in the preceding sections, bed temperature in the high steam gasification experiments was controlled primarily by T_f, with A/F showing little obvious effect in terms of combustion zone formation within the bed. As C04 was operated at the lowest furnace temperature of all high steam gasification runs (i.e. 950°C), it appears that T_f was the main contributing factor to agglomeration in these experiments.

The differing impact of A/F on bed temperature from high to low steam gasification experiments may be the reason for differences in agglomerate structure observed between the two conditions. Agglomerates formed under typical steam gasification conditions showed mineral particles embedded in a significant ash matrix, while agglomerates from high steam conditions were composed mostly of mineral particles with significantly less bonding phase between them. At higher A/F, increased char consumption would result in more ash released to the bed, and hence produce a larger proportion of melt phase in the bed. Conversely, the low A/F under high steam gasification conditions is expected to result in a significantly slower release of ash to the bed, with comparatively smaller quantities of molten ash available for bonding. Note however that even though less melt phase appears to have been produced under high steam gasification conditions, agglomeration and defluidisation still occurred at significantly lower maximum bed temperature than for typical steam concentration gasification runs. This suggests that the species forming within the ash is more important than quantity of ash produced.

Figure 4.23 shows the variation of oversized particles (i.e. exceeding 3.35 mm diameter) with bed temperature. The trends provide a clear indication that the relative proportion of agglomerates forming within the bed increases with increasing temperature. These trends also indicate that other operating parameters impact upon the extent of agglomeration. Run A03 (operated at a bed temperature of approximately 940°C, and T_f set at 825°C) contained approximately 26.3 wt% of oversized particles within the bed material removed at the completion of the run, with defluidisation occurring after 100 minutes operating time. Run B08 (bed temperature of approximately 890°C, and T_f of 775°C) showed a

similar amount of oversized particles formed in the bed, yet defluidised after a significantly longer period of operation, namely 170 minutes. Thus, despite Run A03 operating at a higher temperature, and the bed being in a defluidised state for over an hour longer than Run B08, similar agglomeration extents were achieved. Similarly, the agglomeration extents of Run B02 (maximum bed temperature of 914°C, defluidised after 120 minutes of operation), and Run A04 (maximum bed temperature of 967°C, defluidised after 50 minutes) were similar (38-40 wt% oversized particles in the bed) despite the differences in bed temperature and operating time prior to defluidisation.

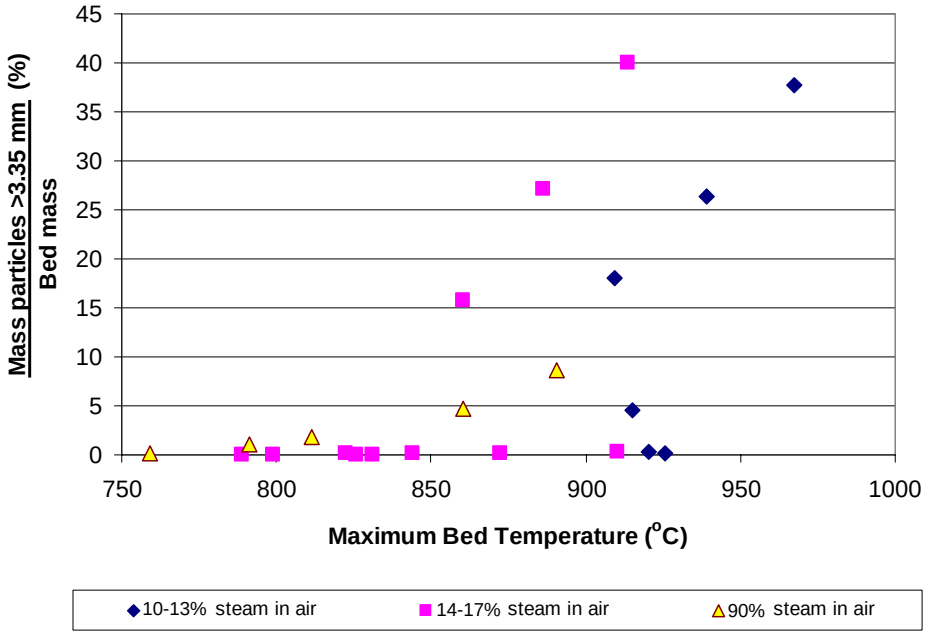

Figure 4.23. Proportion of oversize particles (>3.35 mm diameter) within bed versus maximum bed temperature. Points distinguished by steam concentration in fluidising gas (in wt%).

Superficial velocity and steam content in the fluidising gas were the main differences in operation between the specified runs in the previous paragraph. For Runs A03 and B08, with 26-27 wt% of oversized particles in the bed at the completion of the run, these operating parameter values include:

- Run A03 – superficial velocity of 0.68 m/s, steam concentration of 10.3 wt%; and
- Run B08 – superficial velocity of 0.62 m/s, steam concentration of 14.2 wt%.

Thus, in Run B08 (the lower temperature run), the superficial velocity is reduced by approximately 9.5%, while the steam content is increased by approximately 30%, from the conditions in Run A03.

The corresponding operating parameter values for Runs A04 and B02, with 38-40% of oversized particles in the final bed material, include:

- Run A04 – superficial velocity of 0.65 m/s, and steam content of 11.1 wt%; and
- Run B02 – superficial velocity of 0.57 m/s, steam concentration of 15.2 wt%.

In this case, Run B02 (lower temperature run) was operated with a 14% reduction of superficial velocity, and 27% increase in steam content, compared to Run A04.

Reduced superficial velocities, in the cases highlighted in the previous two paragraphs, would lead to lower relative particle movement in the bed of the lower temperature runs (i.e. Runs B08 and B02, respectively). However, this decreased particle movement is not reflected in the significantly longer onset times of defluidisation in these runs compared to the higher temperature runs (i.e. Runs A03 and A04, respectively). Also, once the bed has slumped, inter-particle movement in the bed is significantly reduced regardless of the gas velocity. In contrast, the significantly higher steam concentrations of the lower temperature runs may have resulted in a greater sodium content forming in the coal ash, as indicated in Section 4.2.4. This would have the effect of increasing the amount of silicate melt phase in the ash (Kracek, 1939), causing an increased rate of sintering, and hence more extensive particle growth in the defluidised bed.

The assumption of greater sintering rate at higher steam conditions does not hold for defluidisation experiments under high steam gasification experiments. Where agglomeration has occurred, approximately one third of the amount of agglomerates are obtained in the high steam cases in comparison to beds from typical gasification experiments for any given bed temperature. The likely reason for this observation appears to be due to the temperature excursions that occur under typical steam-in-air gasification conditions following defluidisation, which are not seen with the high steam gasification cases. These elevated temperatures – which are not taken into account in maximum bed temperature calculations – would undoubtedly decrease the viscosity of ash during the formation of agglomerates, while possibly increasing the rate of char consumption (and hence increasing the amount of ash released into the bed). Such occurrences would exacerbate the amount of agglomerated ash produced at the end of the run.

In the high steam gasification experiments, agglomeration was only found at bed temperatures above approximately 790°C. Interestingly, this temperature corresponds

closely with the melting point of the sodium disilicate-quartz eutectic mixture of 74.2% SiO_2 composition (Kracek, 1939). This gives a strong indication that the agglomeration observed in the spouted bed gasification experiments is a direct result of sodium disilicate formation, which is promoted in the steam environment, as concluded by Kosminski (2001). Further chemical analysis is required in order to determine whether sodium disilicate formation has occurred within the agglomerate structures.

4.3.2 High Temperature Defluidisation Limit

As identified in Chapter 2, bed temperature and superficial velocity of the gas primarily determines the state of fluidisation in a fluidised bed operated at temperatures exceeding the minimum 'sintering temperature' of the bed material. The line identifying the minimum fluidisation velocity as it varies with temperature is termed the 'high temperature defluidisation limit'. The position of this line varies based on the properties of the material being fluidised – in the case of coal, the properties of the inorganic portion of the ash. Thus, it can be expected that as the composition of the ash varies, so will the position of this high temperature minimum velocity limit.

Previous studies investigating the effect of bed temperature on minimum fluidising velocity (Gluckman et al., 1975; Basu, 1982; Siegell, 1984; Manzoori, 1990) have been conducted primarily under combustion conditions only. Under these conditions, the primary bed material used is non-combustible sand, which becomes coated in ash from the coal, causing the bed particles to cohere. Implicit in this mechanism is that for a given coal, the ash composition does not change significantly under combustion conditions, and as such the initial sintering temperature of the fluidising material does not change to any significant extent. However, the preliminary inorganic analysis of agglomerates conducted in Section 4.2.4 indicates that increased sodium content is present in agglomerates produced under high steam conditions. This may increase the amount of melt phase in the ash for a given temperature (Kracek, 1939), thus decreasing the minimum sintering temperature of the ash. Therefore, the minimum spouting velocity required to maintain fluidisation in the bed is expected to be higher for a given temperature under gasification conditions.

The behaviour exhibited in the spouted bed experiments appears to conform to the high temperature defluidisation limit trend as seen in the other studies mentioned in the preceding paragraph. Figure 4.24 shows a velocity-temperature plot, which includes all spouted bed experiments.

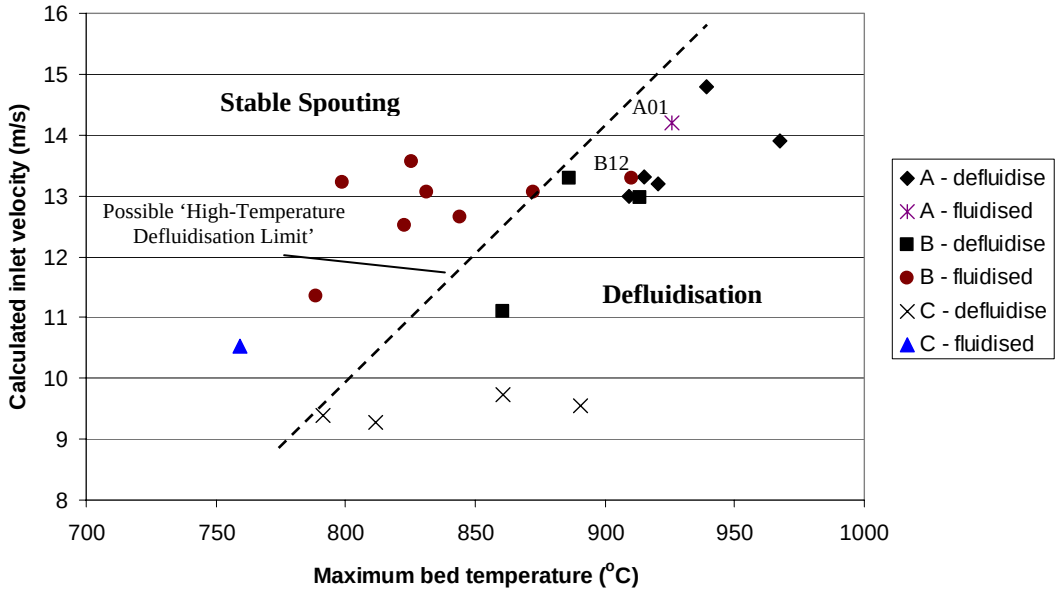

Figure 4.24. Calculated superficial velocity at the gas inlet to the bed versus maximum bed temperature. Dashed line indicates possible 'High Temperature Defluidisation Limit'.

In constructing the velocity – temperature plot, it was decided that the inlet velocity, rather than the cylindrical section superficial velocity would be used. This was decided based on a number of reasons, which include:

- Inlet gas velocities varied significantly more than superficial velocities measured at the cylindrical section diameter, given that experimental operating parameters were set based on a relatively constant cylindrical section superficial velocity;
- Based on bed monitoring and visual observations of the vessel following each run, agglomerates coalesce towards the bottom of the bed, where inlet velocity becomes more critical; and
- Superficial velocity in the cylindrical section, whilst the conventional method of characterising velocity in a spouted bed, does not adequately define the velocity of gas in the spout; the inlet velocity provides a more accurate identification of spout velocity.

Inlet velocity was calculated based on flow rate of gas and the gas temperature immediately prior to the gas inlet (i.e. TC 1). Appendix A details the calculation method employed. The calculated inlet velocities are shown in Table 4.8.

Table 4.8. Inlet gas temperature and corresponding velocity for all experiments. Terminal velocity calculation for a particle top size of 3.35 mm in the relevant density of the gas mixture used in each case is included for comparison.

Run	T_{inlet} (°C)	U_{inlet} (m/s)	$U_{t,\ 3.35mm}$ (m/s)
A01	386	14.2	9.43
A02	395	13.2	9.45
A03	390	14.8	9.39
A04	392	13.9	9.43
A05	367	13.3	9.25
A06	349	13.0	9.12
B01	338	13.1	9.13
B02	384	13.0	9.47
B03	347	12.7	9.23
B05	354	11.1	9.29
B06	313	11.4	8.98
B07	331	12.5	9.08
B08	350	13.3	9.22
B09	319	13.2	9.02
B10	367	13.1	9.35
B11	311	13.6	8.93
B12	374	13.3	9.43
C01	149	9.3	9.04
C02	146	9.4	9.01
C03	167	9.7	9.23
C04	153	10.5	9.08
C05	168	9.5	9.24

A possible ‘High Temperature Defluidised Limit’ is indicated in Figure 4.24, which divides runs that showed defluidisation behaviour from those that fluidised effectively. Note that no substantial conclusions can be derived from this estimated limit without further targeted experiments conducted specifically to define the limit. However, this line shows that two stable runs, A01 and B12 (marked in Figure 4.24), are included in the ‘defluidisation’ region to the right of the line. Each of these runs showed enlargement of particles in the bed following the experiments (refer to Section 4.2.3), which suggested that these experiments may have defluidised if run for longer than 4 hours.

Terminal velocities for 3.35 mm char particles (i.e. top size of the coal) were calculated based on the gas density at the inlet temperature and gas composition, shown in Table 4.8. The calculation method is shown in Appendix A. These terminal velocities were calculated to establish whether defluidisation encountered in the experiments was indeed due to particle growth in the bed, or whether the inlet velocity was insufficient to spout char particles at the inlet. The terminal velocity for 3.35 mm char particles does not vary substantially over the various conditions, at 9.22±0.17 m/s. In each experiment, the actual spout velocity exceeds the terminal velocity, indicating that all char particles should spout effectively without particles collecting at the base of the spout. Note that 90 wt% steam experiments (i.e. Runs C01-C05) possess inlet velocities only marginally above the calculated terminal velocities, suggesting the possibility that the largest char particles may not have been spouted effectively, contributing to agglomeration. However, the temperatures measured at TC 1 represent the gas temperature before it enters the bed, and may not have reflected the true temperature of the gas at the base of the bed. In comparison, the temperatures measured at TC 2 (35 mm above the gas inlet) varied between 640°C to 720°C for the high steam gasification experiments, showing that the gas heats rapidly once in the bed. Thus, it is probable that conditions within the bed would have ensured that all char particles (excluding agglomerates) would spout effectively regardless of the conditions.

4.3.3 Steam Concentration

Steam concentration of the fluidising gas is indicated as a major influence on ash behaviour in the preceding sections. In particular, evidence has been presented that indicates increasing steam content of the gasification environment results in a lowering of the temperature at which defluidisation occurs. This trend is reflected in a plot of temperature of defluidisation against the steam concentration used in each run, as shown in Figure 4.25. This shows that several maximum bed temperatures exist for each steam concentration, which is a result of the relative effects of A/F and T_f on bed temperature.

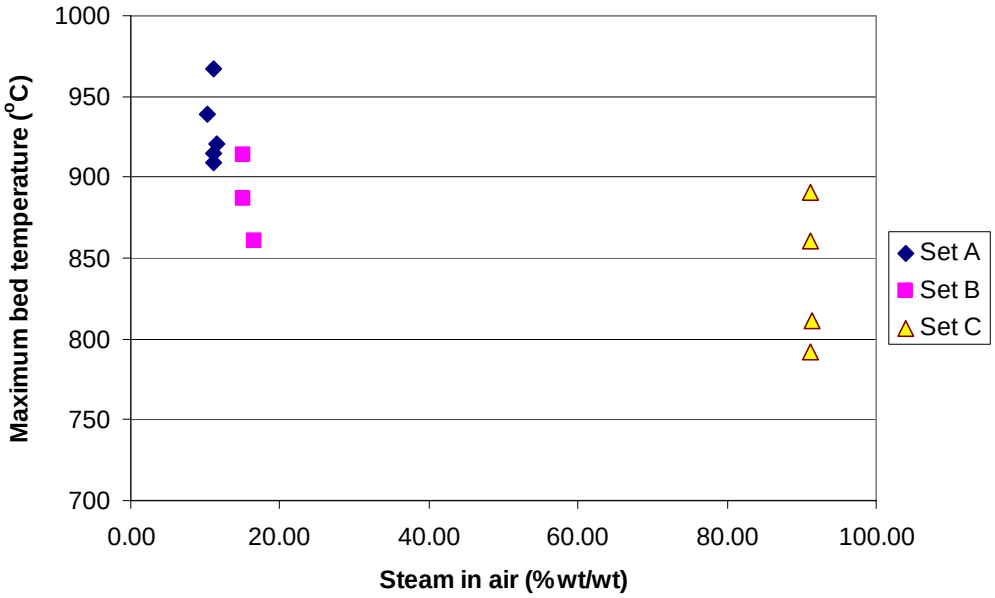

Figure 4.25. Maximum bed temperature of runs in which defluidisation was observed versus steam concentration of the fluidising gas.

The plot in Figure 4.25 shows that bed temperatures at which agglomeration and defluidisation occurs generally decrease as steam content of the fluidising gas increases. Taking the lowest temperature run for each steam concentration as the assumed 'minimum defluidisation temperature' in Figure 4.25, it is apparent that increasing the steam content results in a decrease in temperature required for defluidisation. The mechanism suggested by Kosminski (2001) involves steam lowering the melting point of sodium carbonate, which is a key product forming from organically bound sodium in the coal. Liquid sodium carbonate subsequently reacts with silica in the coal to produce sodium disilicate, which has a eutectic temperature of approximately 790°C. By increasing the steam content, more liquid sodium silicate may be expected to form in the ash, lowering the viscosity and increasing the likelihood of agglomeration. This effect may explain why less molten bonding phase was observed in agglomerates from 90 wt% steam conditions when compared with agglomerates from typical gasification conditions. Further analysis of chemical composition of the ash and agglomerates (presented in Chapter 5) is required to assess whether this is the case.

Commercially, the steam-to-fuel ratio (S/F) is more commonly referred to as a gasification operating parameter in preference to steam concentration in the fluidising gas, as it is easier, for control purposes, to associate the steam rate with coal feed rate. A plot of S/F

versus maximum bed temperature for both agglomeration and non-agglomeration runs is shown in Figure 4.26. Experiments are distinguished both by approximate S/F ratio used, and by whether agglomeration and/or defluidisation occurred. The results for typical gasification conditions are similar to those shown in Figure 4.25, namely that a wide span of maximum bed temperatures exists for each individual S/F $\leq$ 0.5. As S/F is increased beyond approximately 3.0 (i.e. high steam gasification conditions), maximum bed temperature is seen to decrease.

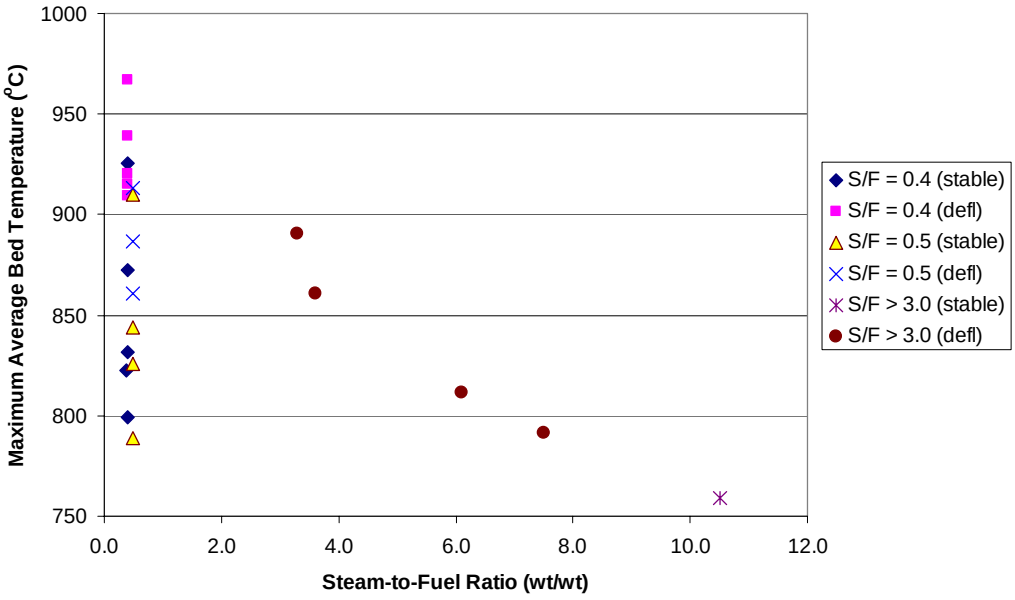

Figure 4.26. Maximum average bed temperature versus steam/fuel ratio of each experiment. Agglomeration and non-agglomeration runs are distinguished from one another.

Note that the bed temperatures referred to in Figure 4.26 do not represent the minimum temperature of defluidisation for each case, but rather is the temperature at which the run was operated at, which happened to coincide with defluidisation. In the case of high steam gasification runs, the results pertaining to effect of S/F on bed temperature is inconclusive, as T_f also decreases as S/F decreases. T_f was reduced primarily because coal feed rate (and hence S/F) was decreased in order to maintain constant bed height across the experiments in the set. While the true effect of S/F on bed temperature is difficult to interpret from the experiments that were conducted, Figure 4.26 does show that increasing S/F results in a decrease of minimum temperature at which defluidisation occurred for the relevant experiments. At S/F of 0.4, the minimum temperature at which defluidisation was observed was 909°C; at S/F of 0.5, the minimum temperature at which defluidisation occurred was

861°C; and at S/F of 7.5, the temperature of defluidisation was 791°C. Thus, evidence suggests that steam does promote sintering in the gasification environment, consistent with the suggestions in Section 4.3.1 regarding the impact of steam on ash sintering behaviour.

4.3.4 Ash content of bed

The literature review of Chapter 2 indicated that carbon content, or rather ash content of the bed, in a gasifier may contribute to agglomeration and defluidisation behaviour. This is because the higher the inorganic content in the bed, the more surface area is available for inorganic-inorganic interactions, and hence raise the possibility of particle collisions resulting in agglomeration. While not specifically a controlled variable in the spouted bed gasification experiments, given that no bed material is removed from the bed during operation, a commercial facility may enable better control of material removal and hence control of the amount of ash in the bed. The results of variation of bed ash content on agglomeration and defluidisation are investigated in the following section.

Inorganic elemental composition was measured in the bed material remaining at the completion of each experiment via X-ray Fluorescence (XRF) analysis. Addition of the individual elemental compositions, based on the initial weight of sample before preparation for XRF, results in a value for the total ash content of the sample. The bed samples analysed exclude any agglomerates exceeding 3.35 mm in size, which were easily removed via sieving. However, as 'free' ash in the bed (i.e. ash not bound within the char particles) and ash in char particle structures could not be separated readily using sieving methods, the ash content of the bed includes any smaller agglomerates, spherical ash particles, and ash remaining within char particle grains in the bed material.

Results from the bed inorganic content analysis are presented in Table 4.9. Inorganic content of the bed material is seen to vary over a wide range of values, from approximately 43 wt% up to 98 wt%. The lack of bed material removal from the spouted bed (other than by elutriation) during operation is the likely cause of the high inorganic contents, resulting in ash build up in the bed.

Table 4.9. Ash content of bed char for each experimental run, as analysed via X-Ray Fluorescence (XRF) analysis.

Run	Total %	Run	Total %	Run	Total %
A01	81.21	B01	43.22	C01	60.65
A02	88.15	B02	89.49	C02	74.17
A03	93.69	B03	97.93	C03	77.20
A04	85.88	B05	90.17	C04	51.41
A05	96.09	B06	55.76	C05	87.32
A06	92.08	B07	65.51		
		B08	96.97		
		B09	58.76		
		B10	65.38		
		B11	81.97		
		B12	84.39		

A plot of inorganic ash content of the bed at the completion of the run versus the maximum bed temperature is shown in Figure 4.27. Runs are distinguished by experimental set (i.e. steam concentration of the fluidising gas), and also by whether defluidisation occurred during the 4-hour operating period. This plot shows that all the typical steam gasification runs displaying defluidisation behaviour possessed inorganic contents exceeding approximately 85 wt%. This corresponds to results published by Hsieh and Roberts (1985) from their work with low-rank American coals, which indicates that agglomeration only occurs to a significant extent when carbon-conversion in a finite coal sample exceeds 80%. Carbon was seen to provide an inhibitory effect on ash sintering in the samples, such that ash could more readily sinter into larger agglomerates when a sufficient amount of carbon was removed. No agglomeration was observed below 860°C, indicating that defluidisation under typical steam gasification conditions may depend on both inorganic content of the bed and the bed temperature.

Runs that showed particle growth but no defluidisation were located close to the operating region identified above (i.e. bed temperature exceeding 860°C, inorganic content exceeding 85 wt%). Bed material from Runs A01 and B12 possessed ash contents just below the value of 85 wt%, at 81.2 wt% and 84.4 wt% respectively. This provides further evidence that the particle growth seen in these runs may have eventually succumbed to defluidisation if operated for sufficient time, with ash build-up eventually creating conditions favourable for defluidisation. Another run that exhibited particle growth – Run B03 – was seen to possess the highest inorganic content of all runs, at 97.9 wt% of the bed.

The bed temperature of this run however – approximately 844°C – may have been sufficiently low to prevent the ash from creating defluidisation conditions.

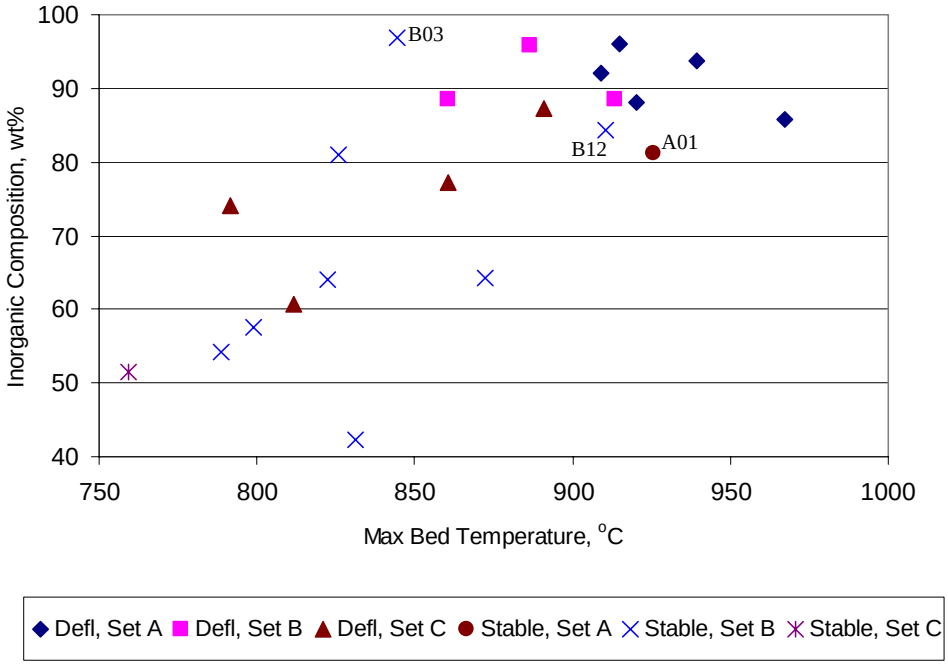

Figure 4.27. Inorganic content of bed material versus maximum bed temperature. Runs distinguished by experimental set and whether defluidisation occurred during the 4-hour operating period. Points which did not defluidise, yet showed significant particle growth, are identified

Defluidisation was observed at a substantially lower bed inorganic content under high steam conditions – as low as 60 wt% of the bed – with a minimum defluidisation temperature of approximately 790°C. This suggests that the operating limits for bed temperature and inorganic content identified in the preceding paragraphs are expanded from typical gasification conditions. Thus, as steam content of the fluidising gas is increased, more liquid phase may be expected in the ash, resulting in a lower inorganic content of the bed, and/or lower bed temperature, necessary to initiate agglomeration.

4.4 Physical Mechanism of Agglomeration and Defluidisation

Based on the results in the preceding sections, it may be concluded that the phenomena of agglomeration and defluidisation during gasification of high-sodium, high-sulphur lignite occurs due to the following mechanism:

- For a given fluidising gas composition, the combination of bed temperature and superficial velocity obeys the 'high temperature defluidisation limit' observed under combustion conditions. This indicates that defluidisation can be avoided by increasing superficial velocity for a given temperature to increase particle momentum, or decrease bed temperature to decrease the sintering propensity of the ash.
- Increasing steam content of the gasification environment tends to decrease the initial sintering temperature of the ash, resulting in defluidisation taking place at a reduced temperature for any given superficial velocity.
- Under bed temperature and gas velocity conditions at which the bed is susceptible to agglomeration and defluidisation, particle growth occurs during stable operation. This particle growth appears to arise mainly via coating of mineral particles from the coal with a molten silicate phase. In the case of the 77-mm spouted bed, with no bed material removal during operation, particle growth is coincident with an increase in total inorganic composition of the bed.
- In the experiments exhibiting particle growth, the total inorganic content of the bed material exceeded approximately 80 wt% under typical steam gasification conditions, and approximately 60 wt% under high steam gasification conditions.
- As particle growth reaches a critical limit, spouting becomes unstable, resulting in defluidisation. Defluidisation is manifested by particles in the annulus surrounding the spout effectively becoming stationary, with channelling through the centre of the bed.
- Under typical gasification conditions, the closely packed bed arising from defluidisation promotes the formation of hot spots. The temperature excursion accelerates sintering of the ash, resulting in the formation of multi-particle agglomerates in a molten silicate matrix.

The basic premise surrounding the above mechanism is the formation of an inorganic liquid phase in the bed during operation. Strong evidence points to steam being primarily responsible for promoting agglomeration and defluidisation at lower bed temperatures. Differences were observed in agglomerate structure from high to low steam conditions, indicating that less molten silicate phase was present in high steam agglomerates even though defluidisation was observed at significantly lower temperatures. This observation raises the possibility that the silicate ash matrix created under high steam conditions was

stickier than that of the low steam experiments. Thus, S/F is a critical parameter for controlling the phenomena of agglomeration and defluidisation when dealing with gasification of high sodium lignite, and should be the focus of control strategies for mitigating these ash-related problems.

4.5 Summary

The influence of agglomeration and defluidisation on stable spouting of a high-sodium, high-ash lignite (i.e. Lochiel coal) was investigated in a 77-mm I.D. spouted bed gasifier. Three sets of experiments were conducted, investigating spouting behaviour under three different fluidising gas compositions (i.e. low, medium, and high steam environments). The high steam-to-fuel ratios used in the 'high' steam gasification experiments are not practical for use in commercial fluidised bed gasification processes, but were used in experiments for the purpose of providing a basis for identifying the effect of steam on agglomeration and defluidisation during fluidised bed gasification of high-sodium lignite.

Results show that agglomeration and defluidisation is an issue with Lochiel coal. Bed operation appeared to be governed by the 'high-temperature defluidisation limit' as observed under combustion conditions in previous studies, suggesting that defluidisation could be controlled by simply operating the bed at high superficial velocity and/or relatively low bed temperatures. However, this operating map was complicated by steam content in the fluidising gas, which suggested that initial sintering temperature of the ash was reduced under increased steam content.

Experiments outside the approximated high-temperature defluidisation limit on the associated plot – whether agglomeration was observed or not – showed overall particle growth had taken place in comparison to runs which were inside the defluidisation limit. This particle growth was attributed mainly to coating of mineral particles by a silicate mixture. These coated particles were observed to be more prevalent in defluidisation runs. Particle growth was seen to coincide with increased inorganic content of the bed compared to stable runs, at approximately 80 wt% under typical gasification conditions, and approximately 60 wt% under high steam conditions. This suggests that defluidisation occurs only when the inorganic content of the bed exceeds a certain proportion of the bed,

which agrees with a previous laboratory study (Hsieh and Roberts, 1985). It also indicates that less inorganic phase is required for agglomeration to occur under high steam conditions.

The evidence presented points to steam being the major influence on agglomeration and defluidisation, with agglomeration observed as low as 860°C under typical steam gasification conditions, and as low as approximately 790°C under high steam gasification conditions. The minimum temperature under the latter conditions corresponds to the eutectic temperature of sodium disilicate-quartz mixture, agreeing with findings in a previous study that sodium disilicate formation is responsible for agglomeration in high sodium content lignite (Kosminski, 2001). Further analysis of ash composition is required in order to determine whether this stickiness is indeed a result of increased sodium silicate formation in the ash.